1999

Investigation and visualization of the stability boundary for stressed power systems

Rong Qi
Iowa State University

INFORMATION TO USERS

This manuscript has been reproduced from the microfilm master. UMI films the text directly from the original or copy submitted. Thus, some thesis and dissertation copies are in typewriter face, while others may be from any type of computer printer.

The quality of this reproduction is dependent upon the quality of the copy submitted. Broken or indistinct print, colored or poor quality illustrations and photographs, print bleedthrough, substandard margins, and improper alignment can adversely affect reproduction.

In the unlikely event that the author did not send UMI a complete manuscript and there are missing pages, these will be noted. Also, if unauthorized copyright material had to be removed, a note will indicate the deletion.

Oversize materials (e.g., maps, drawings, charts) are reproduced by sectioning the original, beginning at the upper left-hand corner and continuing from left to right in equal sections with small overlaps. Each original is also photographed in one exposure and is included in reduced form at the back of the book.

Photographs included in the original manuscript have been reproduced xerographically in this copy. Higher quality 6" x 9" black and white photographic prints are available for any photographs or illustrations appearing in this copy for an additional charge. Contact UMI directly to order.

UMI

A Bell & Howell Information Company
300 North Zeeb Road, Ann Arbor MI 48106-1346 USA
313/761-4700 800/521-0600

Investigation and visualization of the stability boundary for stressed power systems

by

Rong Qi

A dissertation submitted to the graduate faculty

in partial fulfillment of the requirements for the degree of

DOCTOR OF PHILOSOPHY

Major: Electrical Engineering (Electric Power)

Major Professor: Dr. Vijay Vittal

Iowa State University

Ames, Iowa

1999

Graduate College
Iowa State University

This is to certify that the Doctoral dissertation of

Rong Qi

has met the dissertation requirements of Iowa State University

Signature was redacted for privacy.

Major Professor

Signature was redacted for privacy.

For the Major Program

Signature was redacted for privacy.

For the Graduate College

TABLE OF CONTENTS

LIST OF TABLES

LIST OF FIGURES

ACKNOWLEDGMENTS

I would like to thank my advisor, Dr. Vijay Vittal for the time, effort and advice that he generously provided throughout this work. His professional enthusiasm and constant guidance were of immense help during the course of this endeavor.

My sincere thanks to Dr. V. Ajjarapu, Dr. J. D. McCalley and Dr. D. Chen for their valuable comments on this work and for serving on my committee. I am especially thankful to Dr. W. Kliemann and Dr. Y. Ni, for their great help and warm encouragement throughout the whole work.

I would like to thank my fellow students, Songzhe Zhu, Vincent Van Acker, Nagaraj Balijepalli and Chuanjiang Zhu for their friendship and assistance. Thanks are also due to all my friends at Iowa State University and those in China for the wonderful times we shared together.

I have no words that can do justice in expressing what my parents and grandparents have meant to me from the time I was born. To my wonderful husband Zhaobin and to my dear daughter Clare, whose gorgeous smiles gave me endless strength, I offer a sincere 'thank you' from the depths of my heart.

1 INTRODUCTION

Present interconnected power systems are being pushed to their limits due to heavier loading of the transmission network and delay in facility construction. The resultant vulnerability in withstanding system disturbances requires a more accurate understanding of system stability behavior. In analyzing system stability behavior, it is important to characterize and determine the stability boundary of the system. This provides a measure of the capability of the system to handle large disturbance and also provides a means to develop preventive and corrective control schemes. Several nonlinear mathematical tools are being exploited along with the existing tools to investigate this nonlinear phenomenon in stressed power systems. These results are of great interests.

This dissertation presents the use of real normal form of vector fields [1, 2], a comparatively new analysis tool in the area of power systems [3, 4, 5], combined with the use of XGobi [6, 7], an effective graphic package for multi-dimensional visualization, to investigate and visualize the stability boundary of the stressed system. It also depicts the structural characteristics for the stressed power system corresponding to specific fault scenarios by computing the participation factors and the nonlinear indices along the actual fault trajectory which is obtained from time simulation of the equations governing system dynamics. The objective of this research is to analyze and explain the nonlinear phenomena in stressed power systems and characterize the stability boundary of the power system when subjected to large disturbances. The structural information provided by the method of normal forms will also be utilized in explaining the mechanism of instability near the stability boundary and will be used to determine the critical

interactions involved.

The main thrust of this dissertation is to characterize the stability boundary of the stressed power system by obtaining the nonlinear structural information through the visualization of the stability boundary in multiple dimensions, and by utilizing the analytical measures of nonlinear interaction indices and nonlinear participation factors obtained using the method of normal forms.

The characterization of the stability boundary includes the following steps:

- First approximate the stable manifold of the controlling unstable equilibrium point (UEP) using the real normal form method and display the manifold using XGobi to obtain the visualization of the stability boundary of the system.

The original second order nonlinear system is transformed to a linear system by using a similarity transformation and a nonlinear coordinate transformation around the controlling unstable equilibrium point (UEP). The definition of the controlling UEP can be found in chapter 2. In the linear space, the stable manifold of the system is constructed by spanning all stable directions. The stable manifold of the transformed linear system is transformed back to the original system variables to approximate the stability boundary. XGobi is then used to visualize the approximated stability boundary. Since the exact stability boundary for a practical sized power system is difficult to obtain, it is meaningful to approximate the stability boundary using the proper approaches.

- Then compute the nonlinear participation factors and the nonlinear indices for the system at each point along the actual fault trajectory.

The nonlinear interaction indices provide the sequence of the dominant modes of the system along the fault trajectory, and the participation factors corresponding to the dominant mode provide the critical machines involved in the interaction for each fault scenario.

Combining the results of these two steps, the characterization of the stability boundary for the stressed system can be effectively derived.

In this research work, we also approximate the stability boundary of the system using the transient energy function (TEF) method and compare this approximation with the approximation of the stable manifold obtained using the real normal form approach.

XGobi, a high dimensional graphics package, is used to visualize the high dimensional approximations of the stability boundary of the stressed power system. It allows us to visualize the entire picture in all the dimensions and not only in 3-dimensions as is conventionally done. By viewing in N-dimensions, a global perspective and the structure of the stability boundary can be visualized. Since the stable manifolds and the actual system trajectories are dependent on N-states of the system, and not dependent only on some states of the system, using the conventional 3-dimensional visualization package may result in the loss of information, or just present some local information. XGobi provides a valuable and effective way to study the structure of stressed power system.

The proposed approach has been tested on the IEEE 4-generator system [38] and 11-generator system [4].

1.1 Review of Previous Work

Efforts have been made earlier to approximate the stability boundary of a power system. Some of them are essential and establish the foundation for future research.

Among these previous works, a huge body of them exists in the application of Lyapunov function method to power system. These were largely used for transient stability assessment and a detailed review of these approaches are given in [8, 9, 10]. In this review of previous work, we will concentrate on aspects of previous work which are specifically related to the characterization of the stable manifolds of the controlling UEP.

In the 70s, Kakimoto, et.al. [11] and Athay, et.al. [12] first developed the Potential

Energy Boundary Surface (PEBS) method. This method avoids computing the controlling UEP and only requires a quick fault-on system trajectory integration to compute the critical energy, which is defined as the maximum value of the potential energy along the fault-on trajectory of the system. This method is simple to implement and received wide attention. In multi-machine systems, the PEBS is quite complex to visualize in the rotor-angle space. It constitutes a multi-dimensional surface passing through the UEP's around the post-fault stable equilibrium point (SEP) corresponding to a specific fault. The traditional way to display the PEBS consists of showing the equi-potential contours in 2-dimension, which is known as a potential "well". Later, Chiang, et.al. have provided a theoretical foundation for the PEBS method in [13] and for the Boundary Controlling Unstable Equilibrium Point (BCU) method for power system transient stability analysis in [14]. It has been shown in [14] that the region of attraction of the post-fault system is the union of the stable manifolds of UEP's lying on the stability boundary. The BCU method suggests the use of the region employing the value of the energy function at the controlling UEP as the stable manifold, which is a local approximation of the stability boundary. Meanwhile, Zaborsky et.al. [16] have also developed a valuable foundation for analytical techniques toward stability boundary characterization. In [16] the authors proved that under some basic assumptions, the quasi-stability boundary is the union of the closures of $(N-1)$-dimensional stable manifolds associated with equilibria on the stability boundary. However, the stable manifold for a practical size power system is extremely difficult to compute. A good solution to this problem is to approximate the stability boundary near that UEP by a constant energy surface of the critical energy through the UEP of interest. In addition to this approximation, a clear understanding of the relative geometry of the constant energy surface and the stability boundary is provided. It is shown that the constant energy surface is not smooth in the vicinity of $(N-1)$-dimensional UEP and a component of it is locally inside the stability boundary.

The above mentioned efforts are based on Lyapunov's direct method [17] and use

the energy function to approximate the stable manifold and deal with the relationship between the energy surface and the stability boundary.

Yee and Spalding [18] have developed a method of hyper-planes which is quite different from Lyapunov's method to analyze multi-machine power systems. The hyper-planes are tangent to the stability boundary in the state space of angles and speed deviations and are indeed a first order approximation to the stability boundary. Based on this work, Cook, et.al. [19] have proposed a method to approximate the stability boundary using second order hyper-surfaces. However, these techniques have been applied to small scale systems and have not been tested on realistic power systems, which are usually larger in size.

Related to the construction of stable manifolds for differential equations in terms of dynamical systems, there are a number of mathematical tools, see [1, 20, 21, 22]. Most of them approximate the local stable and unstable manifold by the corresponding invariant linear manifolds, which are relatively easy to calculate. However, the simple linearization may lose important nonlinear information and is not practical and applicable to stressed power systems. There are two rigious mathematical techniques named center manifold theorem [23, 24], and the normal form technique [25, 26] that allow for simplification of the dynamical systems. The center manifold theorem approach provides a means of obtaining the invariant manifolds in nonautonomous systems [27].

Since the early 1990s, the normal form technique [28] has been used as a useful tool to study the dynamic behavior of stressed power systems by researchers at Iowa State University. A series of results [29, 3, 30, 31, 32, 33, 4, 5] have appeared by applying this technique to stressed power systems. Starrett used this technique to characterize the mode-state participation and investigated the relationship between the stressed system and nonlinearity in her dissertation in 1994 [29]. In 1995, Lin presented the study of modal interaction and its effects on control performance in stressed power systems by using the normal forms of vector fields [3]. Ni, et.al. applied the normal form of vector

fields to the ac/dc system in [30]. In 1996, Thapar, et.al. [31], developed nonlinear indices using normal form of vector fields to predict interarea separation in power systems. Jang, et.al. [32, 33] analyzed the effect of nonlinear modal interaction on control performance by using the normal forms technique in control design in 1997. In all these works, the analysis was done around the stable equilibrium point (SEP).

Saha, et.al. [4, 5] have proposed a methodology to approximate the stable manifold of a UEP using normal form theory. The nonlinear system is transformed into a linear system by a nonlinear coordinate transformation. The stable eigenspace of the transformed linear space, formed by each stable eigenvector in the linear space, is transformed back to the original coordinates using the inverse nonlinear transformation, which results in an approximated stable manifold. The approximated stable manifold is displayed in 3 dimensions corresponding to only the angle variables of the system.

In this dissertation, the stability boundary of the system is approximated by the stable manifold of the controlling UEP. The normal form technique is applied again to transform the system into a linear system, and the stable eigenspace of the transformed linear space formed by spanning all the stable directions around the controlling UEP is transformed back to the original coordinates using the inverse nonlinear transformation to approximate the stable manifold. The computation of the constant energy surface near the controlling UEP also provides an approximation of the stability boundary. The graphic package XGobi is used to visualize both approximations of the stability boundary in N dimensions corresponding to all independent state variables of the system.

1.2 Problem Statement

Consider a type-1 UEP, in this case there is only one eigenvalue with positive real part. The entire eigenspace is of N-dimension. Therefore, we get $(N-1)$-dimensional stable manifolds and a 1-dimensional unstable manifold. Suppose the system is trans-

formed to the linear space, and the i-th eigenvalue has positive real part, then the i-th direction is the unstable direction. The earlier work [4] represented the $N-1$ stable manifolds simply by $N-1$ straight lines corresponding to each stable eigenvector in the eigenspace. The accurate approximation of the stable manifolds, denoted by E^s, is provided by spanning all $N-1$ stable directions around the controlling UEP.

The approximated stable manifold E^s can be transformed back to the original coordinates, i.e., the machine coordinates, using the real normal form transformation.

The objective of this work is to obtain the second order manifolds and to develop a procedure to find a better approximation for the stability boundary.

In this work, normal forms of vector fields are used to compute the manifolds. The equi-energy surface around the controlling UEP is also computed. The behavior of the trajectory near the manifolds is studied. Also, a multi-dimensional visualization package, XGobi [6, 7], is used to present the characteristics of the approximation of the stability boundary for both the manifold and the energy surface. In order to make more sense of the approximations of the stability boundary, the trajectories near the approximations are shown on the same picture along with the manifold and energy surface. Meanwhile the exit points of the trajectory, which is related to a certain fault scenario, from the manifold and from the energy surface are computed respectively and compared with the critical clearing time to judge the accuracy of the approximations. Also this work aims at obtaining the structural information for the system related to some specific fault scenarios. By computing the participation factors and nonlinear indices along the trajectory, the nonlinear structural information can be analyzed to characterize the stability boundary.

1.3 Outline of the Dissertation

The organization of this dissertation is as follows:

This introduction gives the motivation and background for this research, and provides the general overview of the proposed method. Chapter 2 describes the mathematical model, analytical formulation, and visualization tools. It also contains the motivation for the visualization package–XGobi and the description of the grand tour, a salient feature of XGobi which helps us to display the multi-dimensional surface effectively. Chapter 3 provides two methods of approximating the stability boundary. The first one is the approximation of the stable manifold which is obtained from the real normal form technique. The second one is the approximation of the equi-energy surface which is obtained from the transient energy function. The exit point of the approximated stability boundary is computed, followed by the corresponding time instant. Comparing the time instant corresponding to the exit points along the fault trajectory from the two approximated stability boundaries with the critical clearing time provides an estimate of the accuracy of the approximation. It also provides a criteria to judge which approximation is better, i.e., less conservative. After computing the approximation of the stability boundary, the visualizations of these two approximations are described in chapter 4. In order to obtain the structural information, both linear participation factors and nonlinear participation factors are computed in chapter 5, along with the nonlinear indices. The numerical examples of the proposed method on both the IEEE 4-generator system and the 11-generator system, including the eigen-analysis, approximations of the stability boundary, and the structural information for the system are described in chapter 6. Finally, the conclusions and the scope of the future work are given in chapter 7.

2 MATHEMATICAL MODEL, ANALYTICAL FORMULATION, AND VISUALIZATION TOOLS

2.1 Power System Model

In the multi-machine system model considered, the generators of the system are represented by the classical model [34]. Each machine is represented by a constant voltage behind transient reactance, and loads are represented as constant impedances. After reduction of the system to the internal generator nodes, the swing equation for the i-th machine can be written as

$$\begin{aligned} \dot{\delta}_i &= \omega_i - \omega_0 \\ M_i\dot{\omega}_i &= P_{mi} - E_i^2 G_{ii} - \sum_{j=1}^{n} (C_{ij}cos\delta_{ij} + D_{ij}sin\delta_{ij}) \end{aligned} \tag{2.1}$$

where,

δ_i: i-th rotor angle in radian

ω_i: i-th rotor speed in rad/sec, ω_0: $2\pi f_0$, $f_0 = 60Hz$

$M_i = 2H_i/\omega_0$: i-th rotor inertia, P_{mi}: i-th mechanical power

$C_{ij} = E_iE_jG_{ij}$, $D_{ij} = E_iE_jB_{ij}$

$E\angle\delta$: generator internal voltage, $\delta_{ij} = \delta_i - \delta_j$

$G_{ij} + B_{ij} = Y_{ij}$: element of bus admittance matrix reduced to generator internal bus

Equation (2.1) can be put into a general form as

$$\dot{x} = F(x) \tag{2.2}$$

where

$$x = [\delta_1, \omega_1, \delta_2, \omega_2, \ldots, \delta_N, \omega_N]^T$$

and F is an analytic vector field that maps R^N into R^N and is continuously differentiable. We assume that the total order of the system described by equation (2.1) is N.

A point, x_{eq}, is called an equilibrium point if $F(x_{eq}) = 0$. A stable equilibrium point is represented as SEP and the unstable equilibrium point is represented as UEP.

2.2 Similarity Transformation and Real Normal Form

The derivation of the second-order real transformation is shown below.

Equation (2.2) is expanded as a Taylor's series about an equilibrium point (EP) x_{eq}. In this work the EP chosen is the controlling UEP, and the equations for the postfault system are obtained as

$$\dot{x} = Ax + F_2(x) + \sum_{i=3}^{\infty} F_i(x) \tag{2.3}$$

where

$$A = D_x F(x)$$

$$F_{2i}(x) = \tfrac{1}{2} x^T H_i x, \quad i = 1 \ldots N$$

A is the Jacobian matrix given by the derivative of $F(x)$ and evaluated at the controlling UEP. $H_i = \frac{\partial^2 F_i}{\partial x_j \partial x_k}(x)$ is the i-th Hessian matrix at x obtained by evaluating the second order derivative of $F(x)$. The detailed information on computing the Jacobian matrix A and Hessian matrix H of a power system for the model considered can be found in Appendix A of [4].

With the similarity transformation $x = Uy$, where U is the matrix of right eigenvectors of A, we are able to obtain the Jordan canonical form of A. Applying this transformation to the Taylor's series expansion (2.3) yields:

$$\dot{y} = Jy + G_2(y) + \sum_{i=3}^{\infty} G_i(y) \tag{2.4}$$

where J is the Jordan canonical form of A, and

$$G_{2i}(y) = \sum_{k=1}^{N} \sum_{l=1}^{N} \alpha_{kl}^{i} y_k y_l, \quad i = 1 \ldots N$$

G_{2i} is the i-th matrix corresponding to the second term on the right hand side of equation (2.4) after the similarity transformation, and $(\alpha_{kl}^{i})_{k,l=1\ldots N}$ is given by

$$\tfrac{1}{2} \sum_{m=1}^{N} V_{im}^{T} [U^T H_m U], \; V = (V_{im})_{i,m=1\ldots N}.$$

where V is the matrix of left eigenvectors of A. The normal form technique [1, 36] transforms the system of equation (2.4) into its simplest linear representation along with a nonlinear coordinate transformation provided that the resonance condition $\lambda_i = \lambda_k + \lambda_l$ for $i, k, l = 1, 2, \ldots, N$ (pairwise distinct), is not satisfied. The second order polynomial transformation is given by

$$y = z + h_2(z) \tag{2.5}$$

where the coefficients of h_2 are given by

$$h_{2kl}^{i} = \frac{\alpha_{kl}^{i}}{\lambda_k + \lambda_l - \lambda_i} \tag{2.6}$$

with α_{kl}^{i} and $\lambda's$ defined as above.

Applying this transformation to (2.4) yields

$$\dot{z} = Jz + o(|\, z \,|^3) \tag{2.7}$$

The dynamical system (2.7) can be approximated up to second order simply by ignoring the terms in equation (2.7) higher than the second order. Therefore the system can be approximated by a linear differential equation of the form

$$\dot{z} = Jz \tag{2.8}$$

together with the second order polynomial transformation given by (2.5), if the corresponding resonance condition is not satisfied.

The procedure to obtain the second order transformation is shown in Figure 2.1 [4] (left figure) and can be repeatedly applied to yield higher order approximations.

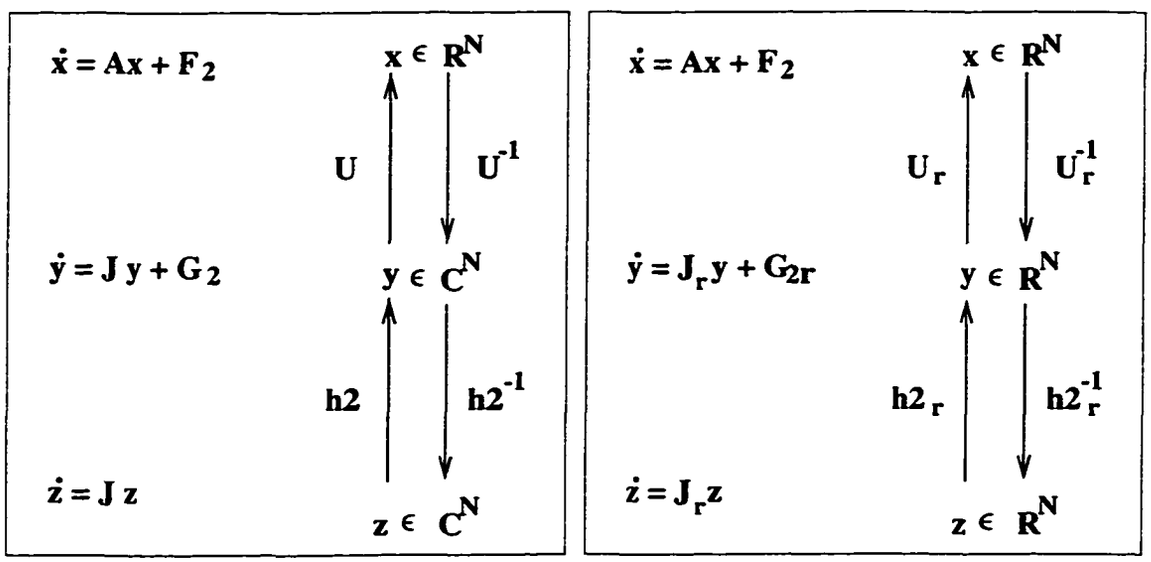

Figure 2.1 Normal form transformation (left) & real normal form transformation (right)

Note that the differential equations (2.4)-(2.8) are, in general, complex valued. This makes it difficult to interpret the resulting graphical figure in an intuitive manner. Therefore, the real Jordan form and the real normal form transformation is used in this work. The procedure shown in Figure 2.1 (right figure) is described below in 3 steps.

Step 1:

Apply the real Jordan form to equation (2.3) to obtain the real Jordan matrix J_r for matrix A. Denote by U_r, the real matrix of the right eigenvectors of A and by V_r, the real matrix of associated left eigenvectors.

Suppose the i-th and $(i+1)$-th eigenvalues of A are a complex conjugate pair of the form $\lambda_{i,i+1} = \alpha \pm j\beta$, the i-th and $(i+1)$-th block of J_r are obtained as

$$J_r^{i,i+1} = \begin{bmatrix} \alpha & \beta \\ -\beta & \alpha \end{bmatrix}$$

The real eigenvectors U_r can be derived by solving the equation $AU_r = U_r J_r$. It can be proved that the corresponding two columns in U_r are real and are formed from the original complex right eigenvectors of A. That is, in the complex conjugate pair of eigenvectors corresponding to $\lambda_{i,i+1} = \alpha \pm j\beta$, the real and imaginary components are taken separately to form two columns of U_r. The detailed proof can be found in [35].

Step 2:

The transformation

$$x = U_r y \tag{2.9}$$

applied to (2.3) yields the equivalent system

$$\dot{y} = J_r y + G_{2r}(y) + H.O.T. \tag{2.10}$$

where the i-th component of $G_{2r}(y)$ is given by

$$\sum_{k=1}^{N} \sum_{l=k}^{N} C_{kl}^{i} y_k y_l$$

with

$$[C_{kl}^{i}] = \tfrac{1}{2} \sum_{m=1}^{N} V_{rim}^{T} [U_r^T H_m U_r]$$

Step 3:

If the second order non-resonance condition holds, i.e., if $\lambda_i \neq \lambda_k + \lambda_l$ for all three tuples of eigenvalues of A, then the real normal form transformation of equation (2.10) is defined as

$$y = z + h2_r(z) \tag{2.11}$$

where the $h2_r$'s are obtained by solving the following homological equation, also see [1, 2]

$$Lah2_r = G_{2r} \tag{2.12}$$

La is known as the *Lie bracket*[1] of the vector fields $J_r y$ and $h2_r(y)$, and is given by

$$Lah2_r(y) = Dh2_r(y)J_r y - J_r h2_r(y) \tag{2.13}$$

where $Dh2_r(y)$ is the Jacobian matrix of the vector function $h2_r(y)$.

The computational steps for determining *La* can be found in an example listed below [4].

Example

We consider a two dimensional system which has the following Jordan system:

$$J_r = \begin{bmatrix} \alpha & \beta \\ -\beta & \alpha \end{bmatrix}$$

We consider the standard basis given by

$$\begin{pmatrix} 1 \\ 0 \end{pmatrix}, \begin{pmatrix} 0 \\ 1 \end{pmatrix}$$

and denote the coordinates with respect to this basis by $y = [y_1, y_2]^T$. Then we have

$$H_2 = span\left\{\begin{pmatrix} y_1^2 \\ 0 \end{pmatrix}, \begin{pmatrix} y_1 y_2 \\ 0 \end{pmatrix}, \begin{pmatrix} y_2^2 \\ 0 \end{pmatrix}, \begin{pmatrix} 0 \\ y_1^2 \end{pmatrix}, \begin{pmatrix} 0 \\ y_1 y_2 \end{pmatrix}, \begin{pmatrix} 0 \\ y_2^2 \end{pmatrix}\right\} \tag{2.14}$$

We compute each $La(.)$ using equation (2.13) as follows [20].

$$La\begin{pmatrix} y_1^2 \\ 0 \end{pmatrix} = \begin{pmatrix} 2y_1 & 0 \\ 0 & 0 \end{pmatrix}\begin{pmatrix} \alpha y_1 + \beta y_2 \\ -\beta y_1 + \alpha y_2 \end{pmatrix} - \begin{pmatrix} \alpha & \beta \\ -\beta & \alpha \end{pmatrix}\begin{pmatrix} y_1^2 \\ 0 \end{pmatrix}$$
$$= \begin{pmatrix} \alpha y_1^2 + 2\beta y_1 y_2 \\ \beta y_1^2 \end{pmatrix}$$

$$La\begin{pmatrix} y_1 y_2 \\ 0 \end{pmatrix} = \begin{pmatrix} y_2 & y_1 \\ 0 & 0 \end{pmatrix}\begin{pmatrix} \alpha y_1 + \beta y_2 \\ -\beta y_1 + \alpha y_2 \end{pmatrix} - \begin{pmatrix} \alpha & \beta \\ -\beta & \alpha \end{pmatrix}\begin{pmatrix} y_1 y_2 \\ 0 \end{pmatrix}$$
$$= \begin{pmatrix} \alpha y_1 y_2 - \beta y_1^2 + \beta y_2^2 \\ \beta y_1 y_2 \end{pmatrix}$$

$$La\begin{pmatrix} y_2^2 \\ 0 \end{pmatrix} = \begin{pmatrix} 0 & 2y_2 \\ 0 & 0 \end{pmatrix}\begin{pmatrix} \alpha y_1 + \beta y_2 \\ -\beta y_1 + \alpha y_2 \end{pmatrix} - \begin{pmatrix} \alpha & \beta \\ -\beta & \alpha \end{pmatrix}\begin{pmatrix} y_2^2 \\ 0 \end{pmatrix}$$
$$= \begin{pmatrix} -2\beta y_1 y_2 + \alpha y_2^2 \\ \beta y_2^2 \end{pmatrix}$$

$$La\begin{pmatrix} 0 \\ y_1^2 \end{pmatrix} = \begin{pmatrix} 0 & 0 \\ 2y_1 & 0 \end{pmatrix}\begin{pmatrix} \alpha y_1 + \beta y_2 \\ -\beta y_1 + \alpha y_2 \end{pmatrix} - \begin{pmatrix} \alpha & \beta \\ -\beta & \alpha \end{pmatrix}\begin{pmatrix} 0 \\ y_1^2 \end{pmatrix}$$
$$= \begin{pmatrix} -\beta y_1^2 \\ \alpha y_1^2 + 2\beta y_1 y_2 \end{pmatrix}$$

$$La\begin{pmatrix} 0 \\ y_1 y_2 \end{pmatrix} = \begin{pmatrix} 0 & 0 \\ y_2 & y_1 \end{pmatrix}\begin{pmatrix} \alpha y_1 + \beta y_2 \\ -\beta y_1 + \alpha y_2 \end{pmatrix} - \begin{pmatrix} \alpha & \beta \\ -\beta & \alpha \end{pmatrix}\begin{pmatrix} 0 \\ y_1 y_2 \end{pmatrix}$$
$$= \begin{pmatrix} -\beta y_1 y_2 \\ \alpha y_1 y_2 - \beta y_1^2 + \beta y_2^2 \end{pmatrix}$$

$$La\begin{pmatrix} 0 \\ y_2^2 \end{pmatrix} = \begin{pmatrix} 0 & 0 \\ 0 & 2y_2 \end{pmatrix}\begin{pmatrix} \alpha y_1 + \beta y_2 \\ -\beta y_1 + \alpha y_2 \end{pmatrix} - \begin{pmatrix} \alpha & \beta \\ -\beta & \alpha \end{pmatrix}\begin{pmatrix} 0 \\ y_2^2 \end{pmatrix}$$
$$= \begin{pmatrix} -\beta y_2^2 \\ -2\beta y_1 y_2 + \alpha y_2^2 \end{pmatrix}$$

Now we represent the linear operator $La(.)$ by a matrix representation. With respect to the standard basis given above, the columns of matrix $La(.)$ are constructed from the coefficients multiplying each basis element that are obtained when $La(.)$ acts individually on each basis element of H_2 given in (2.14)

$$La(.) = \begin{pmatrix} \alpha & -\beta & 0 & -\beta & 0 & 0 \\ 2\beta & \alpha & -2\beta & 0 & -\beta & 0 \\ 0 & \beta & \alpha & 0 & 0 & -\beta \\ \beta & 0 & 0 & \alpha & -\beta & 0 \\ 0 & \beta & 0 & 2\beta & \alpha & -2\beta \\ 0 & 0 & \beta & 0 & \beta & \alpha \end{pmatrix} \tag{2.15}$$

In our case, the computation of $h2_r$ involves the solution of a set of linear algebraic equations following equation (2.13). Here La is a two dimensional matrix, both $h2_r$ and G_{2r} are three dimensional. In order to solve equation (2.13), we convert both three dimensional matrices into one dimension respectively. For the i-th component of G_{2r}, which is a two dimensional matrix, pack the lower triangular portion of G_{2r} into a one dimensional matrix b. Solving the homological equation $La * x = b$, the result x is unpacked into a two dimensional matrix, which is the i-th component of h_{2r}. The detailed procedure of the computation of h_{2r} is presented below.

For each state variable or each pair of state variables corresponding to the real eigenvalue or the complex conjugate pair of eigenvalues respectively, repeatedly perform the following 4 steps to obtain $h2_r$:

1. Form the La matrices for the corresponding Jordan block following the example listed in Example.

2. Convert the three dimensional Hessian matrix G_{2r} after similarity transformation to a one dimensional matrix b.

3. Solve the homological equation $La * x = b$ and obtain the results x.

4. Convert back the one dimensional x into a three dimensional $h2_r$.

In the Z-space, the second order system equation (2.10) now has the form

$$\dot{z} = J_r z \tag{2.16}$$

For this system of linear differential equations, we can study the modes of oscillation of the system, and, furthermore, the stable manifold in the Z-space. Consider the case of a type-1 UEP. In this situation, there is only one mode i corresponding to the unstable eigenvalue. Therefore, we obtain the approximation of the stable manifold E^s by spanning all $N-1$ stable directions (assume N=6, i=3)

$$E^s = span\left\{\begin{bmatrix}1\\0\\0\\0\\0\\0\end{bmatrix}, \begin{bmatrix}0\\1\\0\\0\\0\\0\end{bmatrix}, \begin{bmatrix}0\\0\\0\\1\\0\\0\end{bmatrix}, \begin{bmatrix}0\\0\\0\\0\\1\\0\end{bmatrix}, \begin{bmatrix}0\\0\\0\\0\\0\\1\end{bmatrix}\right\} \tag{2.17}$$

Compared with the earlier work [4], which represented the $N-1$ stable manifolds simply by $N-1$ straight lines corresponding to each stable eigenvector in the eigenspace, the approach given in equation (2.17) is more accurate.

The stable manifold E^s, which is of $N-1$-dimension, is a hyper-plane in the Z-space. Using equations (2.11) and (2.9), each point on the hyper-plane in the Z-space can be mapped back to the Y-space and then to the X-space. By gridding the hyper-plane and applying the real transformation on each grid point, the hyper-plane can be mapped back to the X-space as a smooth hyper-surface. The curvature of this hyper-surface is

caused by the nonlinear transformation. Similarly, points in the X-space can be mapped to the Y-space and then to the Z-space by using the inverse transformation.

The detailed information about the construction of stable and unstable manifolds is provided in chapter 3.

2.3 Transient Energy Function

For a given disturbance trajectory, assuming t_{cl} is the fault clearing time, the dynamics of the power system can be described by a set of differential equations [37]:

$$\dot{x}(t) = f_1(x(t)) \qquad -\infty < t \leq 0 \tag{2.18}$$

$$\dot{x}(t) = f_2(x(t)) \qquad 0 < t \leq t_{cl} \tag{2.19}$$

$$\dot{x}(t) = f_3(x(t)) \qquad t_{cl} \leq t < \infty \tag{2.20}$$

$x(t)$ is the vector of state variables of the system at time t. The equations represent the pre-fault system, the faulted system and the post-fault system respectively. At $t = 0$, a fault occurs in the system and the dynamic equation changes from f_1 to f_2. During $0 < t \leq t_{cl}$, the system is governed by the fault-on dynamics f_2. The fault is cleared at time t_{cl} and the system topology may be changed due to the switching in the network, i.e., f_3 may be different from f_2. The largest value of t_{cl} for which the trajectory of (2.20) with the initial condition $x(t_{cl})$ will converge to the post-fault SEP as $t \to \infty$ is referred to as the critical clearing time.

For the given fault-on trajectory, if the exit point lies on the stable manifolds of the UEP x^{co}, then we call x^{co} the controlling UEP [8].

The equi-energy surface through the controlling UEP of the system describes an approximation of the stability boundary. The total energy surface is considered.

For the system governed by equation (2.1), the system transient energy $V(x)$ [38, 9] with

$$x = [\delta_1, \omega_1, \delta_2, \omega_2, \ldots, \delta_N, \omega_N]^T$$

is given by

$$V(x) = \sum_{i=1}^{n} \frac{1}{2} M_i {\omega_i}^2 - \sum_{i=1}^{n} P_i(\theta_i - \theta_i^s) - \sum_{i=1}^{n-1} \sum_{j=i+1}^{n} \left[C_{ij}(cos\theta_{ij} - cos\theta_{ij}^s) + \int_{\theta_i^s + \theta_j^s}^{\theta_i + \theta_j} D_{ij} cos(\theta_i + \theta_j) \right] \tag{2.21}$$

Where C_{ij} and D_{ij} are system constants depending on internal voltage and the transfer admittances; M_i's are inertia constants, and

$$\begin{aligned} \theta_i &= \delta_i - \delta_0 \\ \omega_i &= \dot{\delta}_i - \dot{\delta}_0 \end{aligned} \tag{2.22}$$

are the angles and speeds with respect to the inertial center.

Here δ_i's are the angles for generators; δ_0 is the angle of the inertial center, given by

$$\delta_0 = 1/M_0 \textstyle\sum_{i=1}^{n} M_i \delta_i \text{ and } M_0 = \textstyle\sum_{i=1}^{n} M_i.$$

In equation (2.21), the first term is defined as kinetic energy. The second term is the position energy. The third term is the magnetic energy, which is also part of the potential energy. The fourth term is the dissipation energy, which is the energy dissipated in the network transfer conductances. We will use the term "potential energy" to represent the last three components.

The critical transient energy is given by the potential energy at the controlling UEP for the particular disturbance under consideration. It is defined as

$$V_{cr} = V(x^{UEP}) - V(x^{SEP})$$

Here $V(x^{UEP})$ is the potential energy at the controlling UEP, and $V(x^{SEP})$ is the potential energy at the post-fault SEP.

In this dissertation, the equi-energy surface is formed by those points obtained by spanning all N directions around the controlling UEP in X-space, which have the total energy very close to the critical energy.

2.4 Visualization Package - XGobi

In this section we provide the background for the graphical tool XGobi [6, 7], which is used to visualize the stressed power system stability boundary.

The primary method for visualizing the system is called a grand tour. In addition, there are several other methods which are important: manual, user-controlled rotations through the high-dimensional space, and rendering the objects to be viewed, which are stable manifold, equi-energy surface and various trajectories.

2.4.1 Motivation for XGobi

The number of the minimum independent states for a N-generator system is $2*(N-1)$. Therefore, the approximated stability boundary is of $2*(N-1)$ dimensions. Even if N is equal to 4, i.e., a 4-generator system, the approximated stability boundary is of 6 dimensions, greater than 3 dimensions, which are the maximum dimensions displayed by conventional visualization tools. As a result, the problem of visualization in higher dimensions arises. We choose XGobi, a multi-dimension visualization package to display the multi-dimensional surfaces.

For dynamic projections higher than 3 dimensions, the usual intuitions trained on $3-D$ rotations break down. However, XGobi [39] works in arbitrary dimensions. It is

based on selecting sequences of projections and moving continuously from one projection to the next.

With one of the features of XGobi, *Grand Tour*, the shape of the stable manifold and energy surface can be observed by rotation from one projection to another continuously. We can observe the curvature of the surfaces. The trajectory related to a certain fault scenario and the unstable eigen-direction are shown in the same picture labeled by different colors, which enables analysis and comparison of the effect of the stability boundary approximation obtained by different methods (manifold and equi-energy surface).

The description of the grand tour feature is presented in the following.

2.4.2 Grand Tour [40] - A Feature of XGobi

The major method for visualizing the system in this dissertation is called grand tour [41, 42, 43]. An example is shown in Figure 2.2 [44]. The actual pictures with colors are shown in both chapter 4 and chapter 6.

In Figure 2.2, the axis tree at lower left describes the euclidean projection from 6-space. The first three axes (Var1, Var2, Var3) represent three relative angles, i.e., δ_{21}, δ_{31} and δ_{41}. The other three axes (Var4, Var5, Var6) represent three relative speeds, i.e., ω_{21}, ω_{31} and ω_{41}.

Intuitively, one can consider the grand tour to be a rotation through a high-dimensional space. It provides views of a high-dimensional object "from all possible sides", rather like taking a helicopter and flying around the object.

Technically, the grand tour algorithm consists of a sequence of projections of the object space $\mathbb{R}^N$ onto a viewing space $\mathbb{R}^2$. Once a projection plane is obtained the important visualization step is how to "render" the object - the grand tour simply provides the animation engine for obtaining projections of the high-dimensional object. Taking a projection is analogous to physically observing the shadow of an object, which would suggest rendering the view in the projection as a geometric shape using a convex

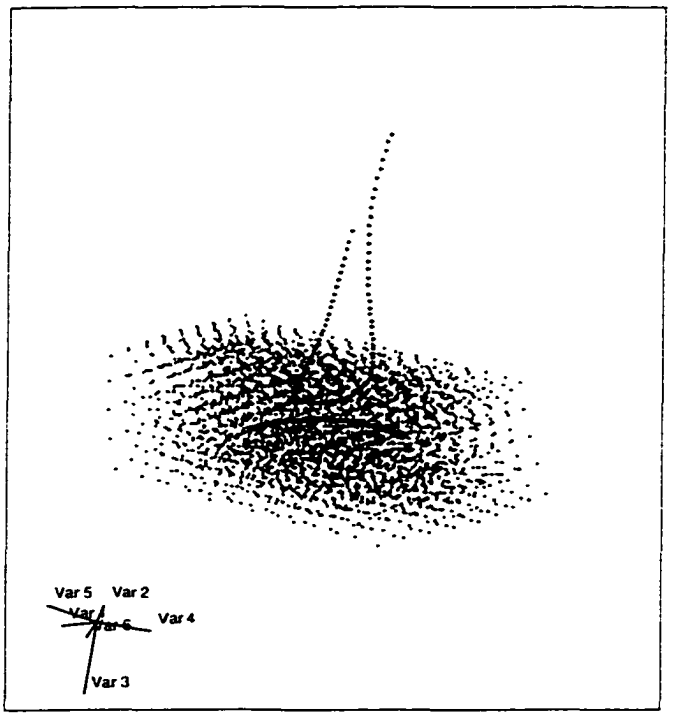

Figure 2.2 An example of grand tour

hull algorithm. However useful information, such as density of the features, and relative position of several features of the object can be lost by opaqueness. In practice rendering may be determined by the manner in which the high-dimensional object is defined, and the tools available in the software.

In XGobi, the primary visualization method is a scatterplot. The manifold is represented by a grid of points on the surface of the manifold, and the trajectories are represented by a string of points, corresponding to the time sequence in the dynamical system, in the N-dimensional space.

There is a modification to the grand tour algorithm which allows us to manually choose the path of views. The modification is described in [45]. The manual controls allow us to change the contribution of a variable to the current view: to increase or decrease the projection coefficient, which indicates the index of the variable to be manipulated. When there exists prior information or intuition about important features the

manual controls give us the ability to "cruise" smaller, but informative neighborhoods in the high-dimensional space.

As in Figure 2.2, the rotation of the axis tree can be automatic or manipulated in terms of the different visualization functions in grand tour. During regular grand tour, each axis moves automatically according to some algorithm. With manual control, one of the axes can be manipulated to move dramatically together with the trivial movements of the rest of the axes, which changes the contribution of a variable to the current view. By doing the manual control on each axis, a good spot for visualizing can be easily obtained.

3 APPROXIMATION OF THE STABILITY BOUNDARY

In this chapter, two methods for approximating the stability boundary around the controlling UEP are developed. One is the stable manifold derived by the normal form method in eigenspace, the other is the equi-energy surface around the controlling UEP.

We choose IEEE 4-generator system [38] and 11-generator system [4] as the test system for analyzing the procedure.

3.1 Approximation of the Stable Manifold

Consider the equation (2.2). The solution of (2.2) is called a trajectory and denoted by $\phi(t, x_0)$ with $t \in \mathbb{R}$, $x_0 \in \mathbb{R}^N$ (initial value), and $\phi(0, x_0) = x_0$.

Denote the fixed points set for the equation (2.2) by

$$E = \{x^* \in \mathbb{R}^N, F(x^*) = 0\} \tag{3.1}$$

For each $x^* \in E$ the stability region (domain of attraction) is given by

$$A(x^*) = \{x \in \mathbb{R}^N, \lim_{t \to \infty} \phi(t, x) = x^*\} \tag{3.2}$$

and its stability boundary is $\partial A(x^*)$. The set of fixed points on the stability boundary of $x^* \in E$ is

$$E(x^*) = \{x \in E, x \in \partial A(x^*)\} \tag{3.3}$$

A fixed point $x^* \in E$ is called hyperbolic, if its Jacobian matrix $D_x F(x^*)$ has no eigenvalues with zero real part. For a hyperbolic fixed point $x^* \in E$, its stable manifold is given by

$$W^s(x^*) = \{x \in \mathbb{R}^N, \lim_{t\to\infty} \phi(t,x) = x^*\} \tag{3.4}$$

and its unstable manifold is given by

$$W^u(x^*) = \{x \in \mathbb{R}^N, \lim_{t\to-\infty} \phi(t,x) = x^*\} \tag{3.5}$$

A hyperbolic fixed point $x^* \in E$ is called stable, if all eigenvalues of the Jacobian matrix $D_x F(x^*)$ have negative real parts. It is a type-k unstable equilibrium point, if $D_x F(x^*)$ has exactly k eigenvalues with positive real part. The following theorem describes the stability boundary of a stable equilibrium point. Here int A and cl A denote the interior and the closure respectively, of a set $A \subset \mathbb{R}^N$.

Theorem 1

Let $x^* \in E$ be a stable fixed point of the differential equation (2.2)

Assume

1. *$int(cl(A(x^*))) = A(x^*)$, and*

2. *For all $x \in E(x^*)$ the intersection of $W^s(x)$ with $W^u(x)$ is transversal.*

Then we have

$$\partial A(x^*) = \bigcup_{x \in E(x^*)} W^s(x) \tag{3.6}$$

Furthermore, concentrating on the type-1 unstable equilibrium points $E1(x^*)$, we have

$$\partial A(x^*) = \bigcup_{x \in E1(x^*)} cl(W^s(x)) \tag{3.7}$$

The proof of Theorem 1 can be found in [13, 16].

According to Theorem 1 it suffices to study the stable manifolds $W^s(x)$ of the type-1 UEP's $x \in E1(x^*)$ in order to obtain the stability region of an SEP $x^* \in \mathbb{R}^N$. If the dimension N of the system (2.2) is large, there is, in general, no reliable way to compute the stable manifolds. Therefore, we approximate $W^s(x)$ using normal forms of vector fields, expanded at the controlling UEP $x \in \mathbb{R}^N$. We concentrate on the case where all eigenvalues of the Jacobian matrix $D_x F(x)$ are simple, e.g., all limit sets are actually hyperbolic fixed points, which is the typical situation in power systems.

3.1.1 The Second Order Approximation

Applying the real transformations presented in chapter 2 allows us to obtain approximations of the stability boundary of an SEP $x^* \in \mathbb{R}^N$. Let $x \in E(x^*)$ be a fixed point on the stability boundary of x^* and assume that x is hyperbolic, consider the linear system (2.16), where J_r is the real Jordan form of $A = D_x F(x)$. Denote by E^s and E^u, the stable and unstable linear subspace of J respectively. Note that E^u is 1-dimensional, since x is a type-1 UEP. Define the manifolds as

$$V^s = U_r((z + h_{2r}(z))(E^s)), \quad V^u = U_r((z + h_{2r}(z))(E^u)) \tag{3.8}$$

These are second order approximations of the stable and unstable manifold $W^s(x)$ and $W^u(x)$ in terms of the system (2.2), i.e., centered at the UEP x. In our case, we choose the controlling UEP x^{UEP} as the EP x described above. The numerical computation of E^s, E^u is described below.

For a N-generator system, there are all together $2*(N-1)$ states including $N-1$ relative angles and $N-1$ relative speeds. After establishing the system state equation (2.2) corresponding to the post-fault scenario, by using the real transformations equation (2.8)-(2.11) described in chapter 2, we first obtain the transformations of the system, which transfer the system from the machine system space, i.e., X-space into the Y-space, then to the normal form space, i.e., Z-space. Note that the power system has been expanded about the controlling UEP, which results in the controlling UEP being the origin of coordinates of the Z-space. In the Z-space, which is a linear space, there is one eigenvalue which has a positive real part associated with the type-1 controlling UEP and it corresponds to the unstable direction[46]. Thus, by spanning the remaining $2*N-3$ eigen-directions around the origin, we get the stable manifold E^s in the Z-space. It is a hyper-plane in $2*(N-1)$-dimension obtained by gridding the eigenspace. The procedure is described as follows: Let $B^s = \{e_1, \ldots, e_{2N-3}\}$ be an orthonormal basis in E^s, and let $\Delta > 0$ be a gridding step length. The hyperplane E^s is approximated by the gridded eigenspace G^s as

$$G^s = \sum_{i=1}^{2N-3} d_i \Delta e_i, d_i \in \{-k, \ldots, 0, \ldots, k\} \tag{3.9}$$

where k is a parameter that determines the size of the hypercube G^s in E^s to be considered. G^s is exactly the hyperplane E^s under the condition that $\Delta \to 0$ and $k \to \infty$. Practically, the parameter k is small due to the limitations of the computation space. However, the information around the controlling UEP, is not likely to be affected by the small k. In the case of large sized power system, G^s is approximated by spanning some stable eigen-directions, which are related to the large values of $h2_r$. Here, the large values of $h2_r$ represents strong nonlinear interaction between the natural modes of oscillation involved with this $h2_r$. One also observes more curvature of the manifold in the directions corresponding to those modes. The details regarding the approach and

the analysis of results are described in chapter 4 and chapter 6 respectively.

The procedure to compute the unstable manifold E^u in the Z-space is very similar to the computation of E^s. Due to the type-1 UEP, the unstable eigenvector in the linear space is equal to E^u. Hence E^u is approximated by the gridded eigenspace G^u as

$$G^u = d\Delta e_u, d \in \{-k, \ldots, 0, \ldots, k\} \tag{3.10}$$

where Δ and k have the same definitions as before. e_u is the vector showing the unstable direction, whose elements are all zeros except for the i-th element , which is equal to 1. Here we assume that the i-th direction is unstable.

Using equation (2.11) and equation (2.9) results in the stable manifold E^s and unstable manifold E^u first in the Y-space, i.e., $(z+h2_r(z))(G^s)$ and $(z+h2_r(z))(G^u)$, and then in the X-space, i.e., $V^s = U_r((z + h2_r(z))(G^s))$ and $V^u = U_r((z + h2_r(z))(G^u))$, using (3.8). The numerical results of V^s and V^u are obtained in two steps: First, applying the nonlinear transformation $y = (z + h2_r(z))$ to each point z of G^s and G^u respectively in the Z-space results in the corresponding y. Then applying the similarity transformation $x = U_r y$ to each y results in the corresponding x. The set of the resulting x's constitutes the approximated manifolds V^s and V^u respectively. Obviously the manifolds V^s and V^u are no longer a plane and a straight line in the machine space, i.e., the X-space, but a curved surface and curved line respectively due to the nonlinearity. We describe the curvature of the manifolds in terms of a two-dimensional system in Figure 3.1.

Since the transformations are about the second order system, both E^s and V^s are the second order approximation of the stability boundary. The computational steps to obtain E^s, E^u, V^s and V^u are described in Figure 3.2.

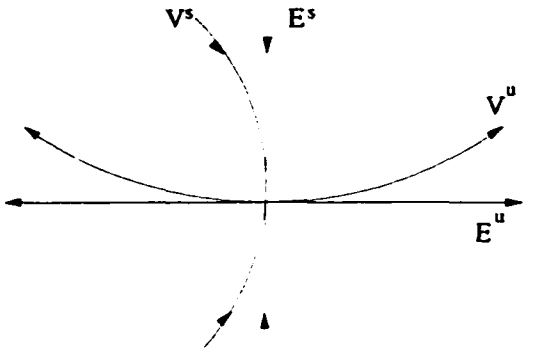

Figure 3.1 Curvature of the manifolds

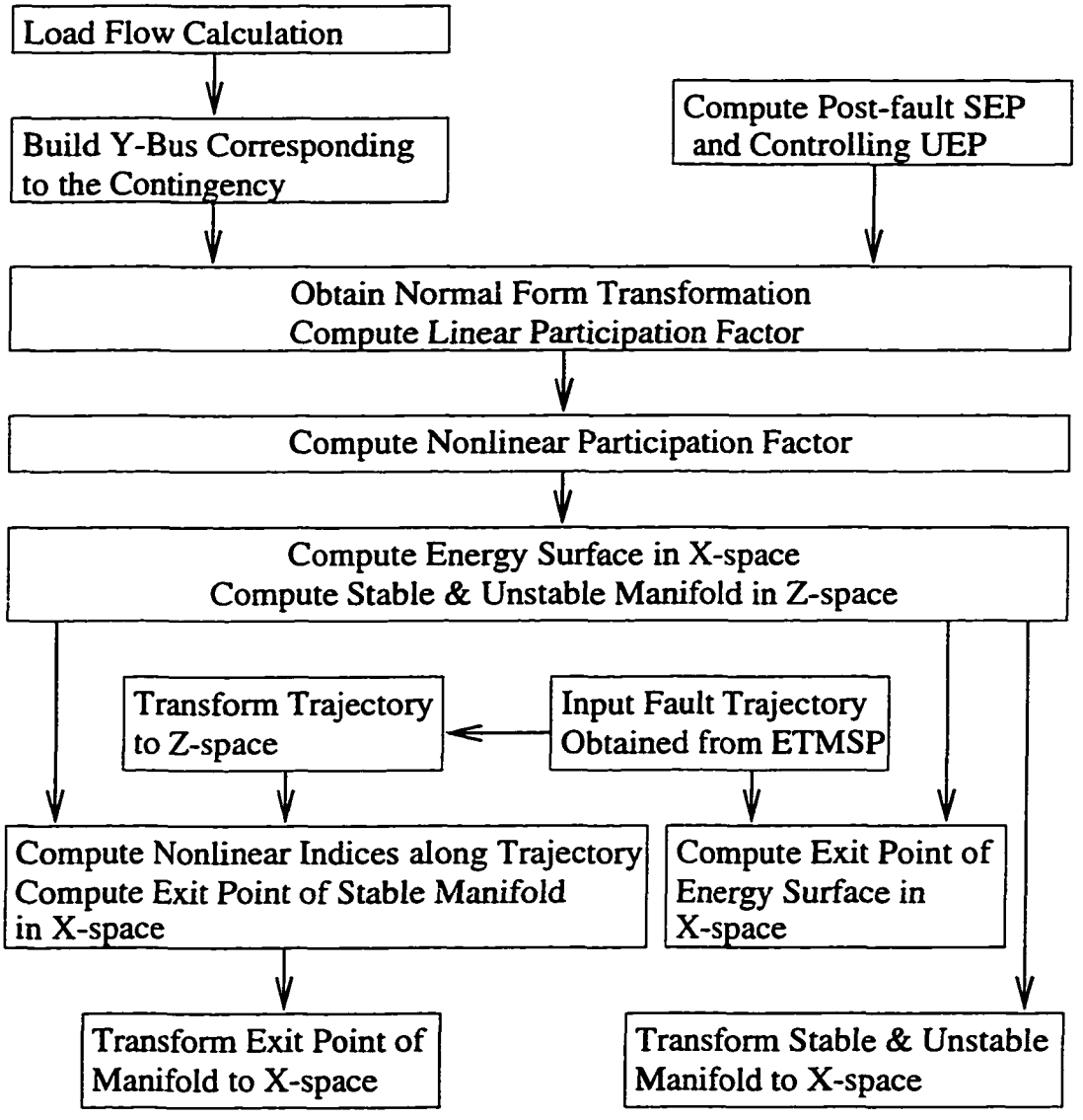

Figure 3.2 Flow charter of the computation

3.1.2 Computation of the Exit Point From the Stable Manifold

The exit point of the trajectory $\phi(t, x_0)$ from the manifold V^s related to a certain fault scenario is hard to obtain due to the nonlinearity. It is very difficult to find the intersection point mathematically between a curved line, in this case $\phi(t, x_0)$, and a curved surface V^s in multi-dimensions. See Figure 3.3.

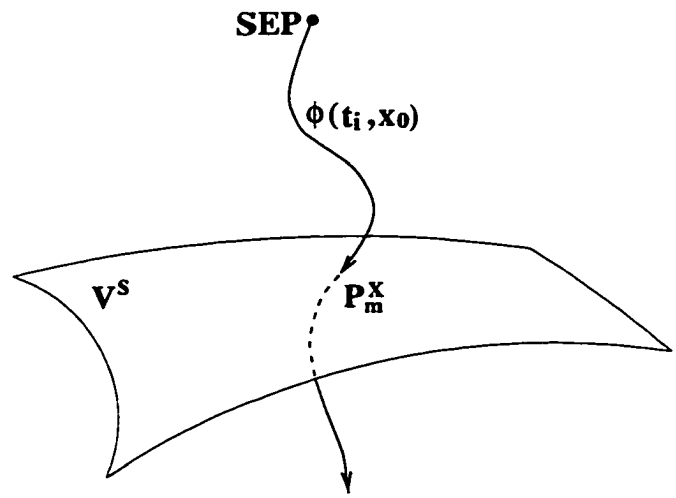

Figure 3.3 Exit point from manifold in the X-space

In order to present the problem intuitively, we simplify the problem by taking a 2-dimensional system. The actual case is multi-dimensional, which is more complicated than the one shown in Figure 3.3.

An effective method to tackle this problem is to compute the exit point in the transformed linear space first, which is denoted by P_m^Z, then transform P_m^Z to the machine space to obtain P_m^X. Since the manifold is a hyper-plane in linear space, it is relatively easy to compute P_m^Z in this space first. See Figure 3.4.

Note that the clearing time t_{cl} is greater than the critical clearing time t_{cr} for the trajectory, otherwise there will be no exit point on the manifold. The procedure to compute P_m^X is described below in 4 steps:

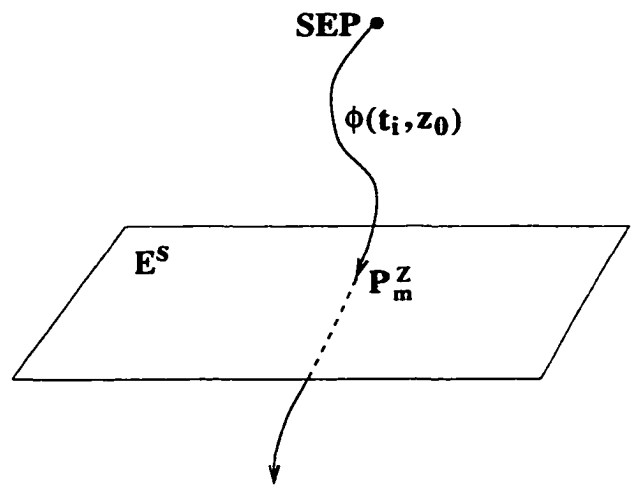

Figure 3.4 Exit point from manifold in the Z-space

Step 1:

Select a simple normal vector for E^s. Suppose the i-th mode is the only unstable direction for this type-1 N-dimensional system. In this case, the normal vector is chosen as

$$z_m = \begin{bmatrix} 0 & 1 \\ \vdots & \vdots \\ 1 & i \\ 0 & i+1 \\ \vdots & \vdots \\ 0 & N \end{bmatrix}$$

Step 2:

Applying the inverse real transformation described in chapter 2 to the fault trajectory $\phi(t, x_0)$ obtained from ETMSP [47] leads to $\phi(t, z_0)$ in the Z-space.

Step3:

Compute the dot product of z_m and each point on the trajectory, which is denoted

by $\phi(t_i, z_0)$. t_i stands for the corresponding time instant during the time simulation:

$$Q = z_m \cdot \phi(t_i, z_0) \tag{3.11}$$

Note that Q is equal to zero at the exit point. By tracing the change of sign of Q, the accurate exit point P_m^Z can be obtained by interpolation at the point at which Q is equal to zero.

Step 4:

Using the real transformation equations (2.11) and (2.9), we can transform P_m^Z into the X-space:

$$P_m^X = U_r((z + h_{2r}(z))(P_m^Z)) \tag{3.12}$$

After computing the exit point P_m^X, the time instant t_m corresponding to P_m^X can be easily obtained. By comparing the exit time t_m and the critical clearing time t_{cr}, we can conclude whether the approximation is optimistic or conservative.

3.2 Approximation of the Energy Surface

Another approximation to the stability boundary used in practice is based on the transient energy function $V(x)$. The idea is based on Lyapunov functions and leads to an energy function described in equation (2.21) [9]. A point $x \in \mathbb{R}^N$ lies within the stability region of x^* of the post-fault system, if $V(x) < V(x^{UEP})$ where x^{UEP} denotes all the UEP's on $\partial A(x^*)$. This observation leads to a conservative stability criterion for a given fault trajectory $\phi(t, x_0)$, because only the energy level for the UEP close to $\phi(t_{cl}, x_0)$ is crucial for stability assessment. Hence the concept of a controlling UEP on $\partial A(x^*)$ was introduced. See chapter 2. The controlling UEP is the UEP determining the stability of the fault trajectory within the framework of stability analysis via transient energy functions.

3.2.1 The Equi-energy Surface

An approximation of the stable manifold $W^s(x), x \in \partial A(x^*)$ around the controlling UEP x^{UEP} is obtained as

$$V^e(x) = \{x \in \mathbb{R}^N, V(x) = V(x^{UEP})\} \tag{3.13}$$

which is the energy surface of the function V through the controlling UEP x^{UEP}. Both sets V^s in (3.8) and V^e in (3.13) are approximations to the true stability boundary of the post-fault system around the controlling UEP $x^{UEP} \in \partial A(x^*)$. The following sections are concerned with the visualization of these approximations in higher dimensions, with the comparison of V^s and V^e, and with a visual assessment of the quality of the approximations via comparison with actual system trajectories in the neighborhood of the controlling UEP.

3.2.2 Computation of the Exit Point From the Energy Surface

The computation of the exit point of the fault trajectory $\phi(t, x_0)$ corresponding to a specific scenario from the equi-energy surface is presented in the following:

Compute the total energy (compare equation (2.21)) of each point along the trajectory and find out the point P_e which has the energy closest to the critical energy V_{cr}, i.e., the energy at the controlling UEP. The interpolation technique is applied again to get the accurate exit point while the time instant t_e corresponding to P_e is obtained. By comparing the exit time t_e and the critical clearing time t_{cr}, we can conclude whether the approximation is optimistic or conservative. Also comparing t_e, t_m and t_{cr} provides a comparison of the effectiveness of the approximation.

4 VISUALIZATION OF THE APPROXIMATION OF THE STABILITY BOUNDARY

After computing the second order stable manifold and the equi-energy surface to approximate the stability boundary, the important issue is to display them in all the dimensions. For a N-generator power system, they are $2(N-1)$ dimensions, which corresponds to $N-1$ relative angles and $N-1$ relative speeds.

As introduced in chapter 2, a multi-dimensional visualization package XGobi [6, 7] is used to display the surfaces. With *Grand Tour*, the shape of the stable manifold and energy surface can be observed by rotation from one projection to another continuously. The curvature of the surfaces can be detected. In order to obtain the nonlinear structural information of the system effectively, the trajectory related to a certain fault scenario and the unstable eigen-direction are shown in the same picture labeled by different colors along with the approximations of the stability boundary. It enables analysis and comparison of the effect of the stability boundary approximation using different methods (manifold and equi-energy surface).

In this chapter, we will present some results related to the IEEE 4-generator 11-bus system, which is considered as the base test system for this dissertation, to describe the visualizations.

4.1 Visualization of the Stable Manifold

In chapter 3, section 3.1.1, we have presented the method to approximate the stability boundary of the power system by computing the approximated stable manifold V^s.

For the 4-generator system shown in Figure 4.1, we choose generator 1 as the reference, which leads to a 6-dimensional state space with 3 states of relative angles and 3 states of relative speeds. In our example the controlling UEP is of type-1, and hence the system (2.1) has a 5-dimensional stable subspace E^s, and a 1-dimensional unstable subspace E^u in the machine space. By using normal form transformation equations (2.12) and (2.10), E^s and E^u are transformed to V^s and V^u respectively in the original (i.e., machine) space.

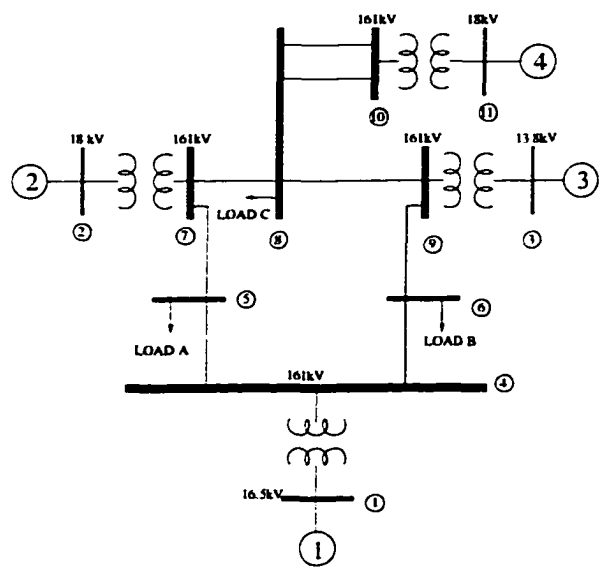

Figure 4.1 4-generator system

To obtain the graphical representation of the approximated stable and unstable manifolds, $V^s(x)$ and $V^u(x)$, at the controlling UEP x in the original coordinates, we proceed as follows: Let $B^s = \{e_1, \ldots, e_5\}$ be an orthonormal basis in E^s, and let $\Delta > 0$ be a discretization parameter. The hyperplane E^s is discretized as $D^s = \{\sum_{i=1}^{5} d_i \Delta e_i, d_i \in \{-k, \ldots, 0, \ldots, k\}, i = 1 \ldots 5\}$, where k is a parameter that determines the size of the

hypercube D^s in E^s to be considered. The transformed set $U((z+h_2(z))(D^s))$, which is denoted by V^s in chapter 3, is an approximation of the stable manifold $W^s(x)$, given by equation (3.8). It constitutes a second order approximation to the stability boundary of the power system (2.1). Similarly, we discretize the unstable subspace E^u of system (2.1) as a set D^u, which is then transformed into an approximation of the unstable manifold $W^u(x)$, denoted by V^u in chapter 3.

Two fault trajectories $\phi_1(t, x_0)$ and $\phi_2(t, x_0)$ of the system with the clearing times $t_{cl1} < t_{cr}$ and $t_{cl2} > t_{cr}$ are computed by the time simulation package ETMSP (Extended transient-midterm stability program) [47]. They are both displayed together with stable and unstable manifolds in Figure 4.2. Figure 4.2 depicts the approximated stability boundary, the unstable manifold and the fault trajectory labeled in different colors, which enables us to understand how the trajectory approaches the manifold. For both pictures in Figure 4.2, the collection of blue dots represent the second order approximation V^s, the red dots depict the trajectories ϕ_1 and ϕ_2, the green dots denote the unstable manifold. For each picture in Figure 4.2 and Figure 4.3, the first three axes (Var1, Var2, Var3) represent three relative angles, i.e., δ_{21}, δ_{31} and δ_{41}. The other three axes (Var4, Var5, Var6) represent three relative speeds, i.e., ω_{21}, ω_{31} and ω_{41}.

It is easy to see the curvature of V^s due to the nonlinearity of the system structure, and the behavior of two fault trajectories. For the stable case, see the top picture in Figure 4.2, the trajectory $\phi_1(t, x_0)$ starting from the initial point x_0 labeled in green, which is indeed the prefault SEP, goes toward the stable manifold and converges to the postfault SEP, which is the isolated point labeled in pink, without going through the manifold.

For the unstable case with clearing time greater than t_{cr}, see in the bottom picture in Figure 4.2, the fault trajectory $\phi_2(t, x_0)$ starting from the initial point x_0 labeled in green, passes through the second order approximation V^s for $t_{cl2} < t_{cr}$. After clearing, i.e., for $t > t_{cr}$, the trajectory "follows" V^s in the direction of the UEP for a while, until

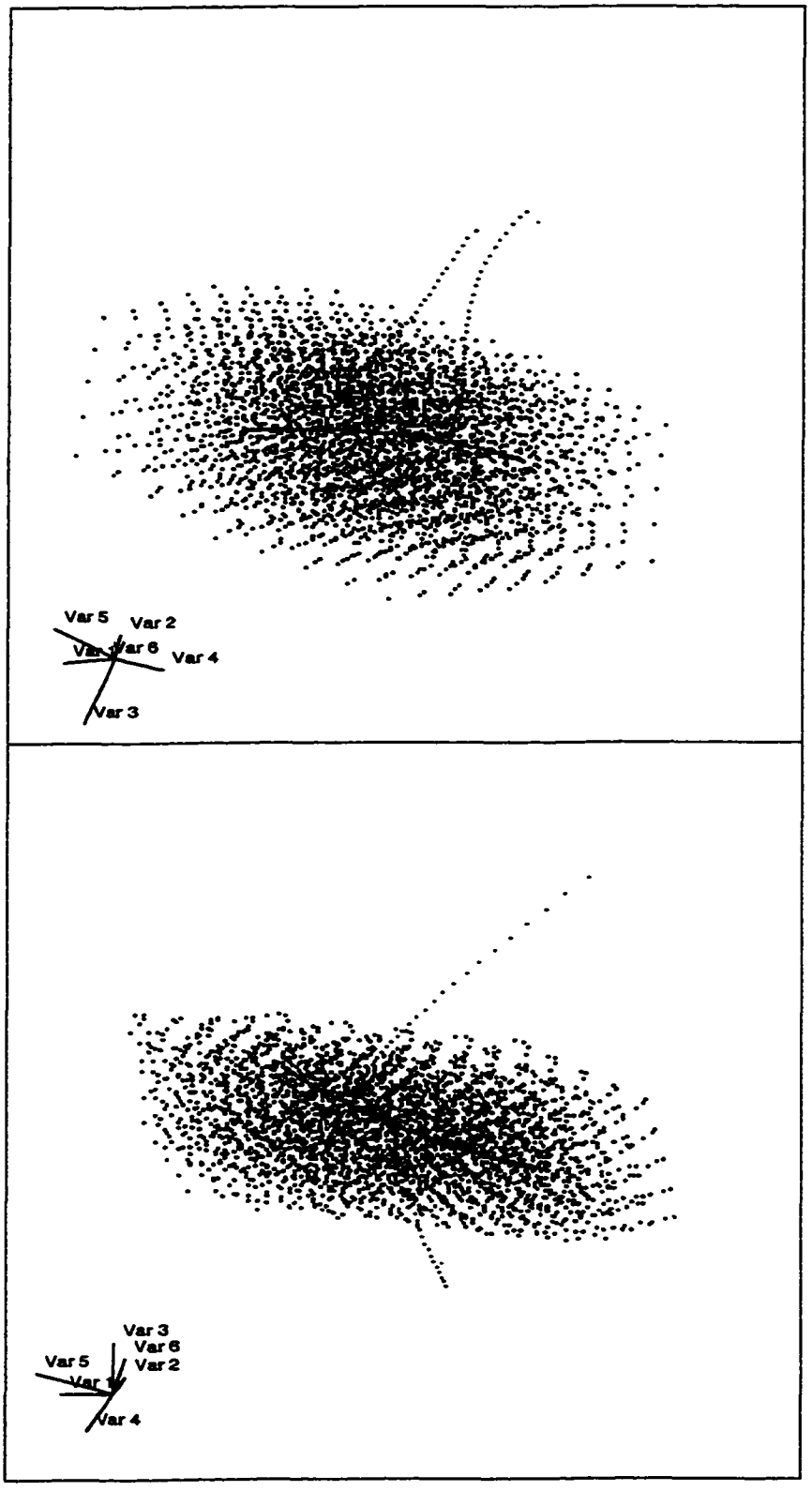

Figure 4.2 Second order approximation (top: stable case and bottom: unstable case)

it becomes unstable in the direction of V^u, the approximation of the unstable manifold, and leaves.

To visualize the approximated stable manifold effectively, a series of the rotating pictures obtained in grand tour are presented in chapter 6.

4.2 Visualization of the Energy Surface

In chapter 3, we have introduced a second approximation to the stability boundary in a power system, namely the energy surface V^e at the controlling UEP. The total energy is computed for the system as in equation (2.1). To find the energy surface, we compute the energy function V around the controlling UEP (see 2.22) and discretize the stable space in machine coordinates. The energy surface is "made up" of those grid points, whose energy level is close to the energy at the controlling UEP.

For the same fault scenarios $\phi_1(t, x_0)$ and $\phi_2(t, x_0)$ as in Figure 4.2, we show in Figure 4.3, the energy surface approximation V^e (yellow), the second order approximation V^u of the unstable manifold (green), and the trajectories (red) $\phi_1(t, x_0)$ in the top picture (stable case), and $\phi_2(t, x_0)$ in the bottom picture (unstable case). We can see in the top picture in Figure 4.3 (stable case), the trajectory ϕ_1 starting from the prefault SEP (the initial point labeled in green), approaches the energy surface in the direction of the controlling UEP and returns to the postfault SEP (the isolated point labeled in pink) without passing through the surface. For the unstable case, see in the bottom picture in Figure 4.3, the trajectory ϕ_2 starting from the prefault SEP (the initial point labeled in green), approaches the energy surface, stays in the direction of the unstable manifold (green curve in picture) for a while and passes through the surface and takes off. Thus, becoming unstable.

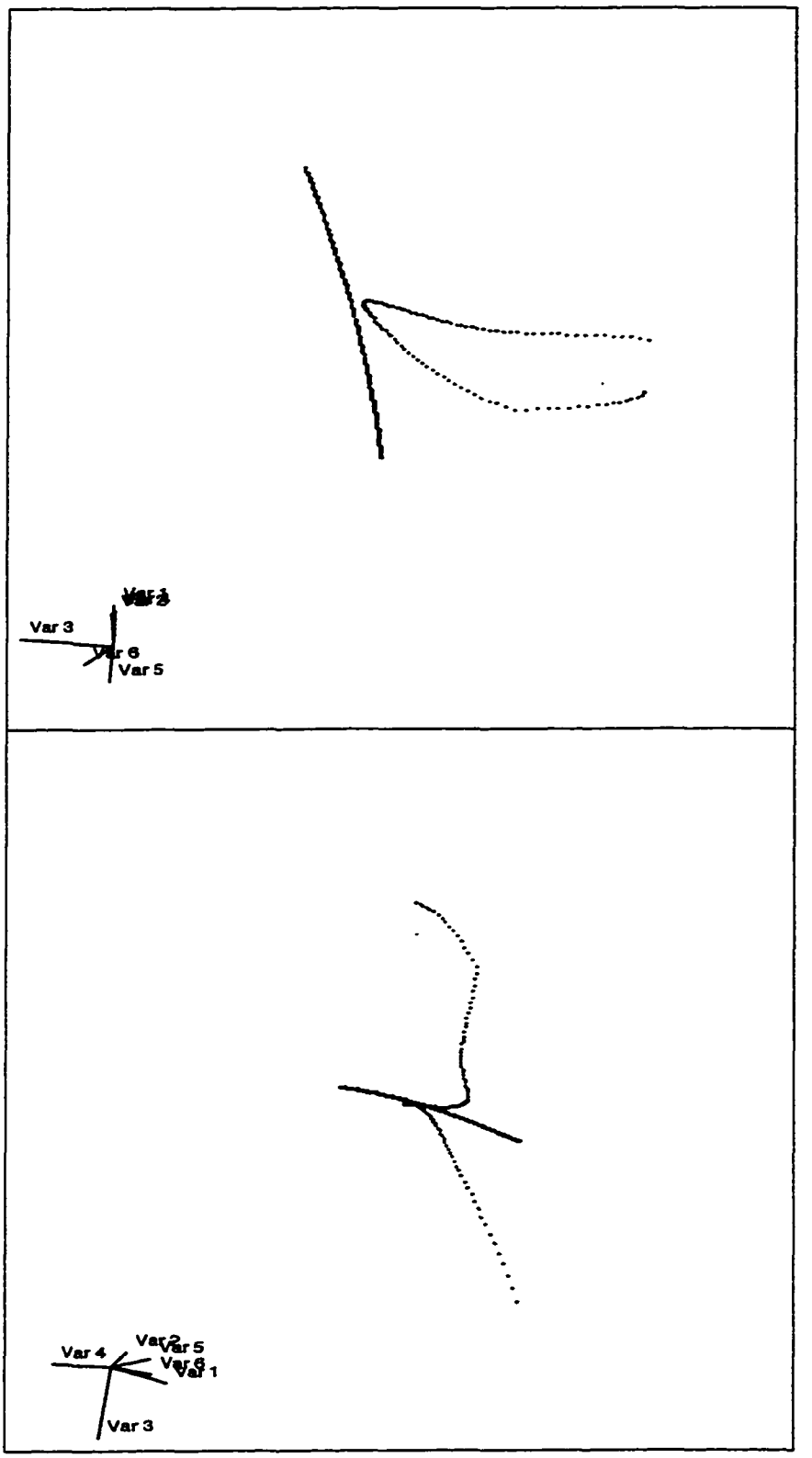

Figure 4.3 Energy surface (top: stable case and bottom: unstable case)

4.3 The Whole Picture

In order to compare the different methods (stable manifold and energy surface) described in the previous section to approximate the stability boundary, the two approximation surfaces, V^s and V^u, together with the actual fault trajectory $\phi_1(t, x_0)$ or $\phi_2(t, x_0)$, and the unstable manifold V^u are visualized in the same picture. See the top picture (stable case) and the bottom picture (unstable case) in Figure 4.4.

Figure 4.4 shows that the trajectories ϕ_1 and ϕ_2 of the full nonlinear system (2.1) follow the manifolds V^s and V^u more closely than they follow the energy surface V^e. Furthermore, the visualizations allows for a better impression of the curvature of V^s and V^u than for the curvature of V^e. This is to be expected, because the energy surface consists of two nonlinear "cones" that meet at the UEP and are not directly linked to the behavior of the system trajectories close to the stability boundary.

Similarly, a series of the rotating pictures obtained in grand tour are presented in chapter 6 in order to effectively visualize the complete picture with both approximations.

4.4 Visualization of Large Sized Power Systems

For large sized power systems, which are the standard situation in practical power systems, the computation and visualization of the stability boundary in all the dimensions are difficult, and even impossible due to the large computing resources and computation time. To solve this problem, an extension of the approach described in the previous sections is developed. The main idea of this extension is to construct the stable manifold or the energy surface to approximate the stability boundary by spanning only those stable eigen-directions which are related to the large values of $h2_rs$, instead of spanning all stable directions. Here the large values of $h2_rs$ represent strong nonlinear interaction between the natural modes of oscillation involved with these $h2_rs$ and one also observes more curvature of the manifold in the directions corresponding to those

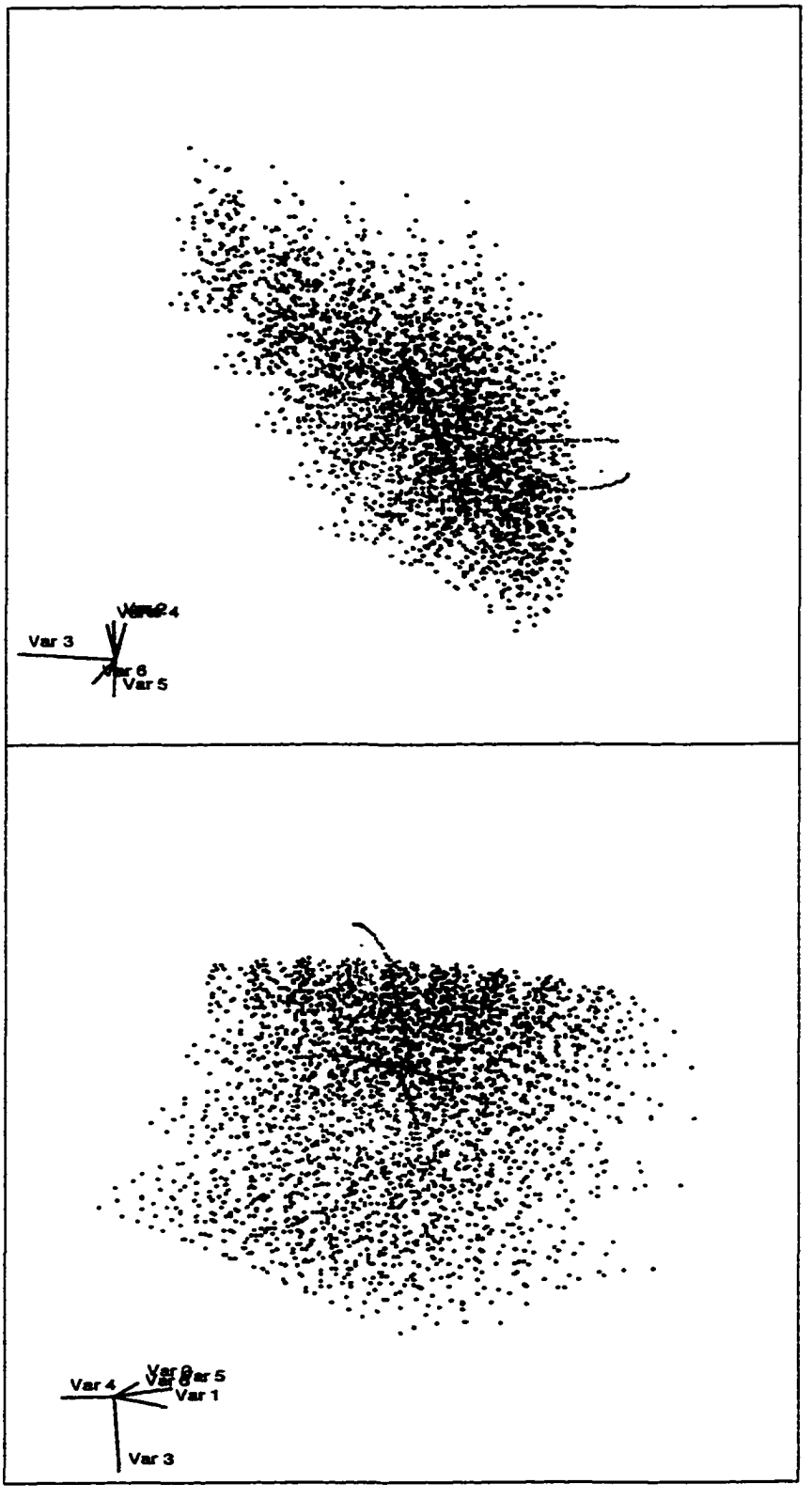

Figure 4.4 Stable manifold and energy surface (top: stable case and bottom: unstable case)

modes. By performing this kind of approximation, the important information regarding the nonlinearity caused by the stress won't be lost. The detailed procedure is described as follows:

Consider the 11-generator system, see the one-line diagram shown in Figure 4.5. We consider the type-1 UEP. For the classical power system model considered, there are all together 20 minimum independent states including 10 relative angles and 10 relative speeds. If we approximate the stable manifold or the energy surface by spanning all the stable directions, which is equal to 20-1=19 for this case, and assume k is equal to 1, which is the minimum value. Then each surface consists of $3^{19} = 1.16 * 10^9$ vectors. Each vector contains 20 elements. The minimum storage of each approximated surface is around $200GB$. It is a huge number and the computation time is huge as well. These numbers become larger for systems bigger than 11-generator system, which is very common in practical power systems. It makes the computation very time-consuming and requires a large amount of computing resources. As a matter of fact, for a specific contingency, most modes in the large system have little effect on the system dynamic behavior and only a few modes are critical to the contingency. It is not important to span all the stable directions. Thus, the selection of modes to be spanned is very important. We select those modes which are related to the large values of $h2_r s$. In this case, we select 6 major modes which are associated with large values of $h2_r s$, including the unstable direction. Denote the stable modes as the i-th, j-th, k-th, l-th, m-th mode, and the unstable mode as the u-th mode. Spanning 5 stable directions as we did in the previous chapter to obtain the stable manifold E^s in the Z-space:

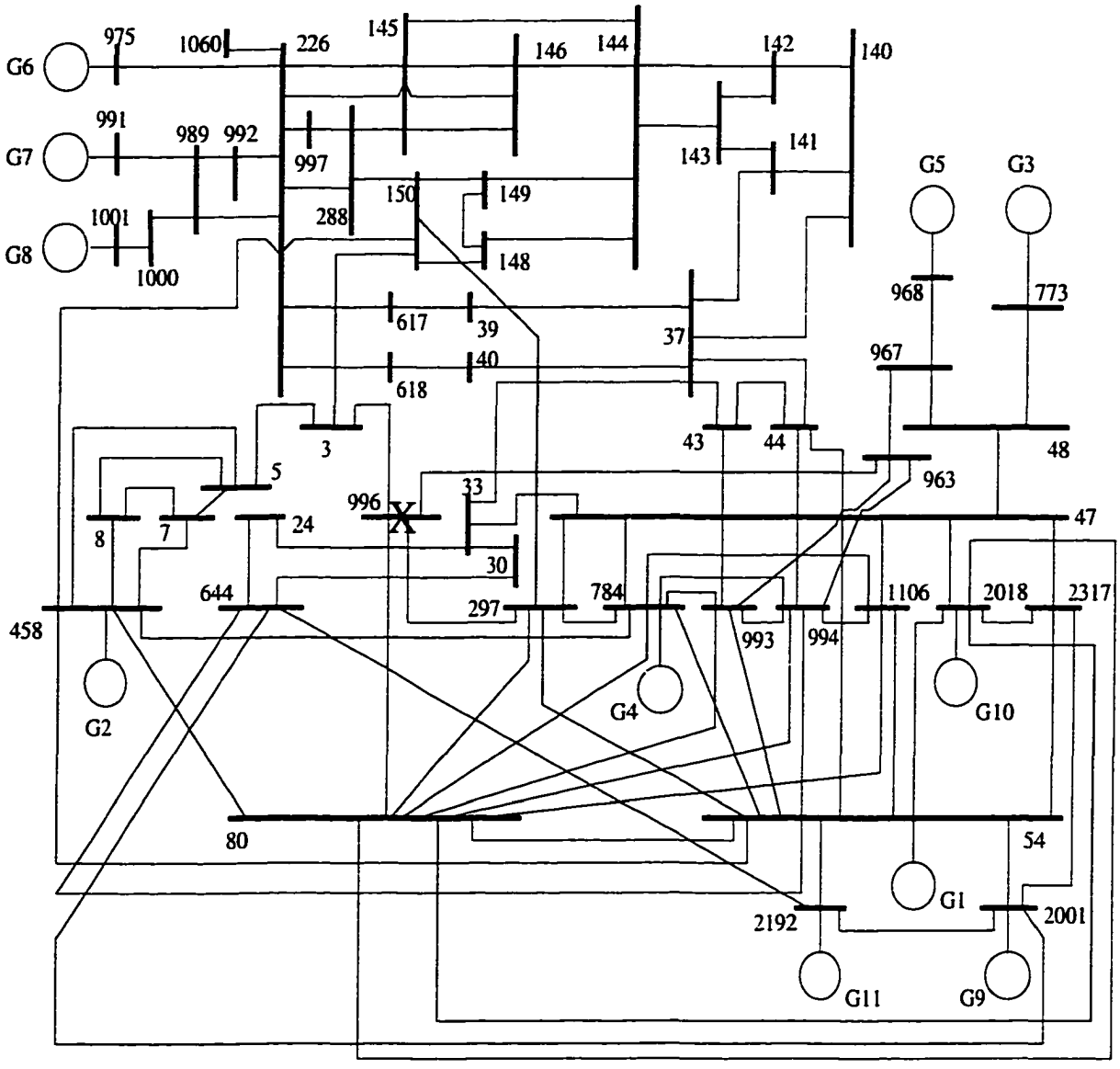

Figure 4.5 11-generator system

$$E^s = span\left\{ \begin{bmatrix} 0 \\ \vdots \\ 1 \\ 0 \\ \vdots \\ 0 \end{bmatrix} \begin{matrix} 1 \\ \vdots \\ i \\ i+1 \\ \vdots \\ 20 \end{matrix}, \begin{bmatrix} 0 \\ \vdots \\ 1 \\ 0 \\ \vdots \\ 0 \end{bmatrix} \begin{matrix} 1 \\ \vdots \\ j \\ j+1 \\ \vdots \\ 20 \end{matrix}, \begin{bmatrix} 0 \\ \vdots \\ 1 \\ 0 \\ \vdots \\ 0 \end{bmatrix} \begin{matrix} 1 \\ \vdots \\ k \\ k+1 \\ \vdots \\ 20 \end{matrix}, \begin{bmatrix} 0 \\ \vdots \\ 1 \\ 0 \\ \vdots \\ 0 \end{bmatrix} \begin{matrix} 1 \\ \vdots \\ l \\ l+1 \\ \vdots \\ 20 \end{matrix}, \begin{bmatrix} 0 \\ \vdots \\ 1 \\ 0 \\ \vdots \\ 0 \end{bmatrix} \begin{matrix} 1 \\ \vdots \\ m \\ m+1 \\ \vdots \\ 20 \end{matrix} \right\}$$

E^s can be transformed to V^s in the X-space by normal form transformations, using equation (2.11) and equation (2.9). The energy surface V^e in the X-space is constructed by spanning these 6 directions (5 stable modes and 1 unstable mode) and selecting those points whose energy is close to the critical energy.

For the visualization, one can select any of the interesting dimensions to plot pictures. To obtain the best effect of visualization, one can observe the picture in some dimensions at one time, instead of all dimensions. Using the structural information provided by nonlinear indices and participation factors based on the real normal form transformations, one can select the critical machines corresponding to the specific contingency for viewing. The principle of selecting the critical machines with respect to specific cases can be found in the next chapter. In our case, we select the angles and speeds of 3 critical machines at one time. Nevertheless, using XGobi, it is very easy to select the different dimensions for viewing, as long as the data points include all the elements corresponding to all the dimensions.

5 NONLINEARITY INDICES AND PARTICIPATION FACTORS

5.1 Nonlinear Indices

The presence of the nonlinear modal interaction plays a critical role in system dynamic performance. Therefore the quantification of nonlinear modal interaction is needed to understand the interactions. There are several ways to compute nonlinearity indices [49, 50].

Let us start from the real Jordan variable space $y \in \mathbb{R}^n$, where n is the number of dimensions for the system. The h_{2r} real transformation maps the Z-space into the Y-space via (5.1)

$$y_j(t) = z_j(t) + h^j_{2r}(z(t)) \qquad j = 1, 2, ..., n \tag{5.1}$$

Assuming the second order resonance condition is not satisfied, i.e., $\lambda_k + \lambda_l - \lambda_j \neq 0$ for all k, l, and j, the system in the Z-space is linear, i.e.,

$$\dot{z} = J_r z \tag{5.2}$$

where, J_r is the real Jordan form of the linear terms of the system equations as shown in (2.10), i.e., J_r is a real diagonal or block diagonal $n \times n$ matrix. Equation (5.2) is solved as

$$z_j(t) = z_{j,o} e^{\lambda_j t} \qquad \forall \lambda_j \in \mathbb{R}$$

$$z_j(t) = \sqrt{z^2_{j,o} + z^2_{j+1,o}}\, e^{\alpha_j t} cos(\omega_j t + \phi_j)$$

$$z_{j+1}(t) = \sqrt{z_{j,o}^2 + z_{j+1,o}^2} e^{\alpha_j t} cos(\omega_j t + \phi_j + \frac{\pi}{2}) \qquad \forall \lambda_{j,j+1} = \alpha_j \pm j\omega_j$$

where $z_{j,o}, z_{j+1,o}$ are the initial values and $\phi_j = tan^{-1}(\frac{-z_{j+1,o}}{z_{j,o}})$. The initial conditions are defined as the conditions at fault clearing with respect to the controlling UEP.

The corresponding solutions of (5.1) are given by

$$y_j(t) = z_j(t) + \sum_{k=1}^{n} \sum_{l=k}^{n} h2r_{kl}^j z_k(t) z_l(t) \qquad j = 1, 2, ..., n \tag{5.3}$$

which contains all second order terms corresponding to the normal form (5.1) and (5.2). Note that the r.h.s. of (5.3) contains influences of the nonlinearity in both terms: In the first term the nonlinear coordinate transformation (5.1) is reflected only in the initial value, in the second term the second order correction of the solution due to nonlinear modal interaction is represented. The linear system in the Y-space is

$$\dot{y} = J_r y \tag{5.4}$$

with solution

$$\bar{y}_j(t) = y_{j,o} e^{\lambda_j t} \qquad \forall \lambda_j \in \mathbb{R}$$

$$\bar{y}_j(t) = \sqrt{y_{j,o}^2 + y_{j+1,o}^2} e^{\alpha_j t} cos(\omega_j t + \phi_j)$$

$$\bar{y}_{j+1}(t) = \sqrt{y_{j,o}^2 + y_{j+1,o}^2} e^{\alpha_j t} cos(\omega_j t + \phi_j + \frac{\pi}{2}) \qquad \forall \lambda_{j,j+1} = \alpha_j \pm j\omega_j$$

which corresponds to the linearization of the original system. The comparison of the solutions $z_j(t)$, $\bar{y}_j(t)$ and (5.3) yields various indices. Note first of all that $h2r_{kl}^j$ is large, and it contributes to the second term in (5.3), if

a) C_{kl}^j is large.

b) $\lambda_k + \lambda_l - \lambda_j$ is small, i.e. $\lambda_j \approx \lambda_k + \lambda_l$.

Comparing the solutions $z_j(t)$ and $\bar{y}_j(t)$ described above, and denoting

$$\tilde{z}_{j,o} = z_{j,o} \qquad \forall \lambda_j \in \mathbb{R}$$

$$\tilde{z}_{j,o} = \sqrt{z_{j,o}^2 + z_{j+1,o}^2} \qquad \forall \lambda_{j,j+1} = \alpha_j \pm j\omega_j$$

$$\tilde{y}_{j,o} = y_{j,o} \qquad \forall \lambda_j \in \mathbb{R}$$

$$\tilde{y}_{j,o} = \sqrt{y_{j,o}^2 + y_{j+1,o}^2} \qquad \forall \lambda_{j,j+1} = \alpha_j \pm j\omega_j$$

we can assess the influence of the nonlinear effect on the initial value by considering

$$|\bar{y}_j(t) - z_j(t)| = |\tilde{y}_{j,o} - \tilde{z}_{j,o}|e^{\alpha_j t} \qquad \forall \lambda_j \in \mathbb{R}$$

$$|\bar{y}_j(t) - z_j(t)| = |\tilde{y}_{j,o} - \tilde{z}_{j,o}|cos(\omega_j t + \phi_j)$$

$$|\bar{y}_{j+1}(t) - z_{j+1}(t)| = |\tilde{y}_{j+1,o} - \tilde{z}_{j+1,o}|cos(\omega_j t + \phi_j + \frac{\pi}{2}) \qquad \forall \lambda_{j,j+1} = \alpha_j \pm j\omega_j$$

To this term which represents the difference in the linear part of the approximate solution and the linear solution, we add the second order terms to capture the effect of the nonlinearities on the difference between the terms. Hence we obtain the corresponding index as

$$I1(j) = |(\bar{y}_j(t) - z_j(t)) + \sum_{k=1}^{n}\sum_{l=k}^{n} h2r_{kl}^{j} z_k(t) z_l(t)| \qquad j = 1, 2, ..., n \qquad (5.5)$$

$I1$ for mode j identifies the dominant modal interaction. The biggest $I1$ corresponds to the most dominant mode. We can use $I1$ to find the most dominant mode of the system. For large sized systems, large computing resources and computation time are required to calculate the nonlinear indices of each mode for each time instant. A simplified approach to solve this problem is to obtain the dominant modes at fault clearing time and compute the nonlinear indices of the modes by taking into consideration only the second order terms which are related to those dominant modes, ignoring the insignificant modes.

The numerical results related to the nonlinear interactive indices of the system are presented in chapter 6.

5.2 Participation Factors

For large sized power systems, it is necessary to determine the state variables that have significant participation in the selected modes of oscillation for dynamic stability

analysis. Participation factors [48] are a well-known and effective method to find out which state variables significantly participate in the selected modes. In our work, we consider both linear participation factors and nonlinear participation factors.

5.2.1 Linear Participation Factors

Linear participation factors provide a simple method to find out mode-machine interactions [48]. For the linear term of system (2.3), suppose the initial condition vector is $x_0 = e_k$, (e_k represents the vector whose elements are all zeros except for the k-th element, which is equal to 1), and ignore the terms with the order equal to or higher than second order in (2.3). The time solution for the k-th state variable x_k is:

$$x_k(t) = \sum_{i=1}^{n} p_{ki} f(\lambda_i, t) = \sum_{i=1}^{n} (U_r^{ki} * V_r^{ki}) f(\lambda_i, t) \tag{5.6}$$

where

$$f(\lambda_i, t) = e^{\lambda_i t} \qquad \forall \lambda_i \in \mathbb{R}$$

$$f(\lambda_i, t) = e^{\alpha_i t} cos(\omega_i t + \phi_i)$$

$$f(\lambda_{i+1}, t) = e^{\alpha_i t} cos(\omega_i t + \phi_i + \frac{\pi}{2}) \qquad \forall \lambda_{i,i+1} = \alpha_i \pm j\omega_i$$

Here U_r is denoted for the real right eigenvector and V_r, the real left eigenvector of system (2.3).

The participation factor p_{ki} represents a sensitivity measure of the participation of the k-th machine state in the trajectory of the i-th mode. It is given by the following equation

$$p_{ki} = U_r^{ki} * V_r^{ki} \tag{5.7}$$

Linear participation factors p_{ki}s are functions of both the left and right eigenvectors, they are independent of eigenvector scaling. We will use them to find out the critical machines corresponding to certain fundamental modes of oscillation and compare the results with those obtained by computing the nonlinear participation factors of the system. This is described in the next section.

5.2.2 Nonlinear Participation Factors

For the nonlinear system (2.3), we extend the above concept to include second order terms in the participation factors [29]. We refer to these as nonlinear participation factors.

Again, we assume the initial condition vector of the system is $x_0 = e_k$. The normal form initial conditions z_0 can be obtained by first applying the inverse similarity transformation $y = V_r^{\wedge} x$ to the initial vector x_0 to obtain y_0, and then the second-order approximation of the inverse transformation $z = y - h_{2r}(y)$ to y_0. The solution z_0 obtained in linear space can be used by the normal form transformation equation (2.11) and (2.9) to express the solution for k-th machine state variable as

$$x_k(t) = \sum_{i=1}^{N} U_r^{ki}(V_r^{ik} + v_{2ikk}) f(\lambda_i, t) + \sum_{p=1}^{N} \sum_{q=p}^{N} u2_{kpq}(V_r^{pk} + v2_{pkk})(V_r^{qk} + v2_{qkk}) f(\lambda_p, t) f(\lambda_q, t) \tag{5.8}$$

where $f(\lambda_i, t)$ was defined in the previous section and

$$v2_{ipp} = -\sum_{k=1}^{N} \sum_{l=1}^{N} h2r_{kl}^{i} V_r^{kp} V_r^{lp}$$

$$u2_{ikl} = \sum_{j=1}^{N} U_r^{ij} h2r_{kl}^{j}$$

Using the approach given in [29], one can define second-order participation factors as

$$x_k(t) = \sum_{i=1}^{N} p2_{ki} f(\lambda_i, t) + \sum_{p=1}^{N} \sum_{q=p}^{N} p2_{kpq} f(\lambda_p, t) f(\lambda_q, t) \tag{5.9}$$

where,

$$p2_{ki} = U_r^{ki}(V_r^{ik} + v_{2ikk}) \tag{5.10}$$

$$p2_{kpq} = u2_{kpq}(V_r^{pk} + v2_{pkk})(V_r^{qk} + v2_{qkk}) \tag{5.11}$$

Note that there are two types of second-order participation factors. The $p2_{ki}$ represents the second-order participation of the k-th machine state in the i-th single-eigenvalue

mode. In fact, the linear participation factor, p_{ki}, is one term in the expression for $p2_{ki}$ which includes the second-order corrections. The $p2_{kpq}$ represents the second-order participation of the k-th machine state in the 'mode' formed by the combination of the p and q modes. In our work, we will focus on $p2_{ki}$, which provides the information of the second-order participation of the k-th machine state in the i-th single-eigenvalue mode. The numerical results are discussed in chapter 6.

5.3 Structural Information

As described above, the nonlinear indices provide the information of which mode is dominant for a specific contingency, while both the linear and nonlinear participation factors show which machines play a significant role in the selected modes. Combining these two nonlinear indices, we can obtain structural information regarding system dynamic performance. At each instant in time along the trajectory, the dominant modes in terms of nonlinear interaction can be determined using the index $I1$. The linear and nonlinear participation factors can then be used to determine the critical machines in these dominant modes. This analysis can be conducted at various time instants during the progress of the system trajectory in the vicinity of the stability boundary constructed and one can determine which synchronous machines and modes that dominate system dynamic behavior. This eventually can be used to device appropriate corrective and preventive control. With this information and those obtained from the pictures through XGobi, a global structural characterization can be easily obtained. The results related to the 11-generator system and the 4-generator system are described in chapter 6.

6 NUMERICAL RESULTS

This chapter contains the numerical results for the different issues presented in preceding chapters for the IEEE 4-generator system and the 11-generator system. The results address the following aspects:

1. Eigen-analysis of the systems. The linear participation factors of the system corresponding to specific contingencies.

2. Display of the second order approximations of the stability boundary as a surface in all states of the system by using *grand tour* feature of XGobi. The shape of the manifold, the directions of high and low curvature and the influence of speed components.

3. Display of the fault trajectory obtained from ETMSP in figures from 2. Observation of the behavior close to the stability boundary and the exit from the manifold in the unstable case.

4. The numerical results of the exit points of the fault trajectory from the approximations to the stability boundary (stable manifold and energy surface).

5. Nonlinear indices for each point along the actual fault trajectory and nonlinear participation factors of the system. The characterization of the system structure at the UEP, relative to different fault scenarios.

6. The equi-energy surface at the UEP, relative (also graphically) to the second order approximations of the stability boundary. Comparison of the two approximations, and the structural information provided.

6.1 IEEE 4-Generator Test System

For the IEEE 4-generator system (see the one-line diagram in Figure 4.1), there are all together 6 minimum independent states including 3 relative angles and 3 relative speeds. The machine data are listed in Table A.1. We choose generator 1 as the reference machine. The physical meaning for each state in the X-space, i.e., the machine space, is listed in Table 6.1.

Table 6.1 Physical meaning for each state (4gen.)

State Number	Physical Meaning
1	relative angle δ_{31}
2	relative angle δ_{21}
3	relative angle δ_{41}
4	relative speed ω_{31}
5	relative speed ω_{21}
6	relative speed ω_{41}

We study the following 3 cases:

- A three-phase fault at bus 10, cleared at 0.1575s by opening one line 8-10. The critical clearing time is 0.1576s.
- A three-phase fault at bus 10, cleared at 0.1578s by opening one line 8-10. The critical clearing time is 0.1576s.
- A three-phase fault at bus 7, cleared at 0.2018s by opening one line 5-7. The critical clearing time is 0.2010s.

6.1.1 Base Case Study (case I & II) - Three-phase Fault at Bus 10, cleared at 0.1575s and 0.1578s

For both cases I & II, the controlling UEP is presented in Table 6.2. Consider generator 1 as the reference machine, there is only one advanced machine, i.e., generator 4, at the controlling UEP. This is seen by observing state 3 which corresponds to the variable δ_{41}.

Table 6.2 Controlling UEP for 4-generator system (case I & II)

Machine	State	Relative Angles (deg.) and Relative Speeds (rad./s)
δ_{21}	2	22.2166
δ_{31}	1	16.4114
δ_{41}	3	140.9611
ω_{21}	5	0.0000
ω_{31}	4	0.0000
ω_{41}	6	0.0000

6.1.1.1 Eigen-analysis and Linear Participation Factors

Applying the real similarity transformation to the system corresponding to cases I and II, we obtain the eigenvalues and the linear participation factors. They are listed in Table 6.3 and Table 6.4.

From Table 6.3, we see that the 3rd mode corresponds to the unstable eigenvalue. We also observe that the UEP is a type-1 UEP.

Table 6.3 Eigenvalues for 4-generator system (case I & II)

Mode	Eigenvalue
1	$0.0000 + j11.3338$
2	$0.0000 - j11.3338$
3	$6.7197 + j0.0000$
4	$-6.7197 + j0.0000$
5	$0.0000 + j6.9010$
6	$0.0000 - j6.9010$

Table 6.4 Linear Participation Factors (4gen.)(case I & II)

Mode	State1	State2	State3	State4	State5	State6
1	.000000	.000000	.000000	.824480	.172702	.002819
2	.824480	.172702	.002819	.000000	.000000	.000000
3	.006986	.008776	.484237	.006986	.008776	.484237
4	.006986	.008776	.484237	.006986	.008776	.484237
5	.000000	.000000	.000000	.161548	.809746	.028707
6	.161548	.809746	.028707	.000000	.000000	.000000

6.1.1.2 Normal Form and Nonlinear Participation Factors

Using the proposed real normal form technique, we transform the system into a linear system and then obtain the stable manifold by spanning all the stable directions (all 6 modes except for the mode 3). The unstable manifold corresponds to the unstable direction (mode 3). Both manifolds are transformed back to the machine space. The nonlinear participation factors are computed using equation (5.10). The results are listed in Table 6.5. The interaction coefficients $h2_r$ are presented in Table 6.6.

Table 6.5 Nonlinear Participation Factors (4gen.)(case I & case II)

Mode	State1	State2	State3	State4	State5	State6
1	.000000	.000000	.000000	1.015592	.173003	.013650
2	.824709	.187775	.003737	.000000	.000000	.000000
3	.006846	.009477	.417336	.041819	.008820	.447037
4	.007463	.009199	.504554	.020478	.008821	.524940
5	.000000	.000000	.000000	.257564	.808679	.000128
6	.162211	.661566	.032153	.000000	.000000	.000000

There are some differences between linear participation factors and nonlinear participation factors, as seen in Table 6.4 and Table 6.5. For each mode, the participation factor of each state is different. Although the difference is not great, it reflects the effect of the nonlinearity. The large changes indicate more stress in the corresponding directions for the particular mode.

The actual trajectories $\phi_1(t, x_0)$ and $\phi_2(t, x_0)$ with clearing time of 0.1575s and

Table 6.6 Real Transformation Matrix $h2_r$ (4gen.)(case I & II)

Mode		State1	State2	State3	State4	State5	State6
1	State1	.000000	.005091	.007163	.007163	.000000	-.004662
	State2	.005091	.000000	.028455	-.028455	-.011698	.000000
	State3	.007163	.028455	-.014194	.000000	-.000124	.000826
	State4	.007163	-.028455	.000000	.014194	-.000124	-.000826
	State5	.000000	-.011698	-.000124	-.000124	.000000	.004088
	State6	-.004662	.000000	.000826	-.000826	.004088	.000000
2	State1	-.010182	.000000	-.024217	.024217	.014663	.000000
	State2	.000000	-.005091	-.007163	-.007163	.000000	.004662
	State3	-.024217	-.007163	.011997	.028791	-.000599	-.000753
	State4	.024217	-.007163	.028791	.011997	.000599	-.000753
	State5	.014663	.000000	-.000599	.000599	-.005198	.000000
	State6	.000000	.004662	-.000753	-.000753	.000000	.001230
3	State1	-.000645	.000191	.003293	.001372	.000243	-.000305
	State2	.000191	-.000758	.000000	-.001623	.000050	.000335
	State3	.003293	.000000	-.077116	.077116	-.015350	.000000
	State4	.001372	-.001623	.077116	.025705	-.003440	.006401
	State5	.000243	.000050	-.015350	-.003440	-.001425	.000663
	State6	-.000305	.000335	.000000	.006401	.000663	-.002042
4	State1	-.000645	-.000191	-.001372	-.003293	.000243	.000305
	State2	-.000191	-.000758	-.001623	.000000	-.000050	.000335
	State3	-.001372	-.001623	.025705	.077116	.003440	.006401
	State4	-.003293	.000000	.077116	-.077116	.015350	.000000
	State5	.000243	-.000050	.003440	.015350	-.001425	-.000663
	State6	.000305	.000335	.006401	.000000	-.000663	-.002042
5	State1	.000000	-.005455	.000389	.000389	.000000	.001062
	State2	-.005455	.000000	.000427	-.000427	-.003528	.000000
	State3	.000389	.000427	.033871	.000000	.006736	.020748
	State4	.000389	-.000427	.000000	-.033871	.006736	-.020748
	State5	.000000	-.003528	.006736	.006736	.000000	-.016683
	State6	.001062	.000000	.020748	-.020748	-.016683	.000000
6	State1	.017157	.000000	-.000309	.000309	.004487	.000000
	State2	.000000	.013689	.000064	.000064	.000000	.003528
	State3	-.000309	.000064	-.018204	-.081225	-.014481	-.006736
	State4	.000309	.000064	-.081225	-.018204	.014481	-.006736
	State5	.004487	.000000	-.014481	.014481	.033366	.000000
	State6	.000000	.003528	-.006736	-.006736	.000000	.016683

0.1578s respectively have been computed by using ETMSP (Extended Transient-Midterm Stability Program). By definition of the critical clearing time, these two trajectories are stable and unstable, respectively. The results of generator relative angles are shown in Figure 6.1. We note that generator 4 loses synchronism with the rest of the system.

6.1.1.3 Stable Manifold

- Stable case – fault cleared at 0.1575s

For this case, the clearing time (0.1575s) is less than the critical clearing time (0.1576s). It is hence a stable case. The approximated stable manifold is displayed by XGobi, along with the unstable manifold and the stable trajectory. (see Figure 6.2)

In the pictures shown in Figure 6.2 and 6.3, the stable manifold is displayed in blue, the unstable manifold in green and the system trajectory in red. The axis tree at lower left describes the Euclidean projection from 6-space. The first three axes (Var1, Var2, Var3) represent three relative angles, i.e., δ_{31}, δ_{21} and δ_{41}. The other three axes (Var4, Var5, Var6) represent three relative speeds, i.e., ω_{31}, ω_{21} and ω_{41}.

It is easy to see the curvature of the stable manifold in Figure 6.2 due to the non-linearity of the system. In Figure 6.2, the series of the rotating pictures show that the trajectory $\phi_1(t, x_0)$ starting from the initial point x_0 labeled in green, which is indeed the prefault SEP, goes toward the stable manifold and converges to the postfault SEP, which is the isolated point labeled in pink, without going through the manifold. The trajectory stays on one side of the stable manifold.

- Unstable case – fault cleared at 0.1578s

For this case, the clearing time (0.1578s) is greater than the critical clearing time (0.1576s), it is an unstable case. The approximated stable manifold, unstable manifold and the unstable trajectory are shown in Figure 6.3.

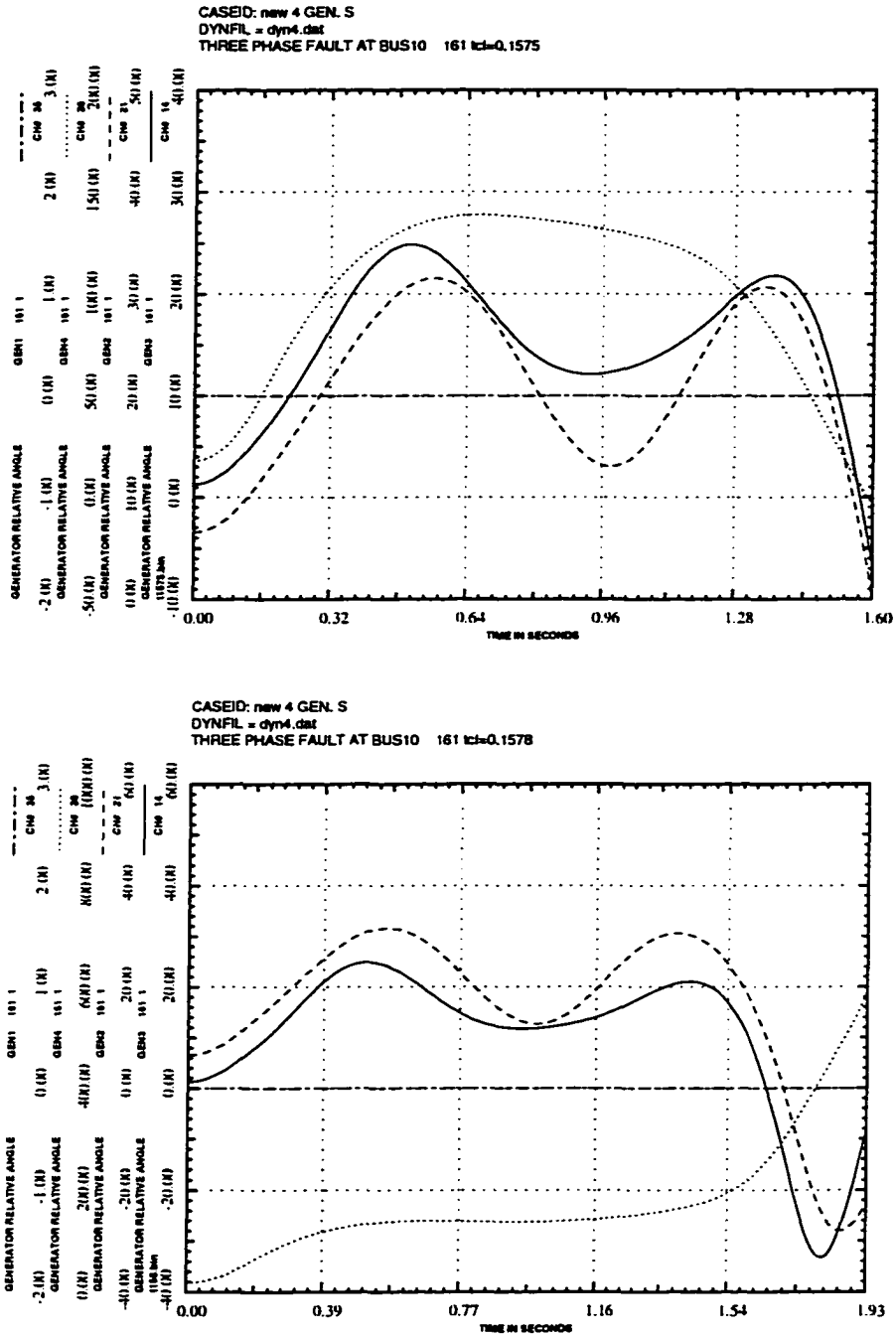

Figure 6.1 Fault trajectory (generator relative angle) (top: case I and bottom: case II) (4gen.)

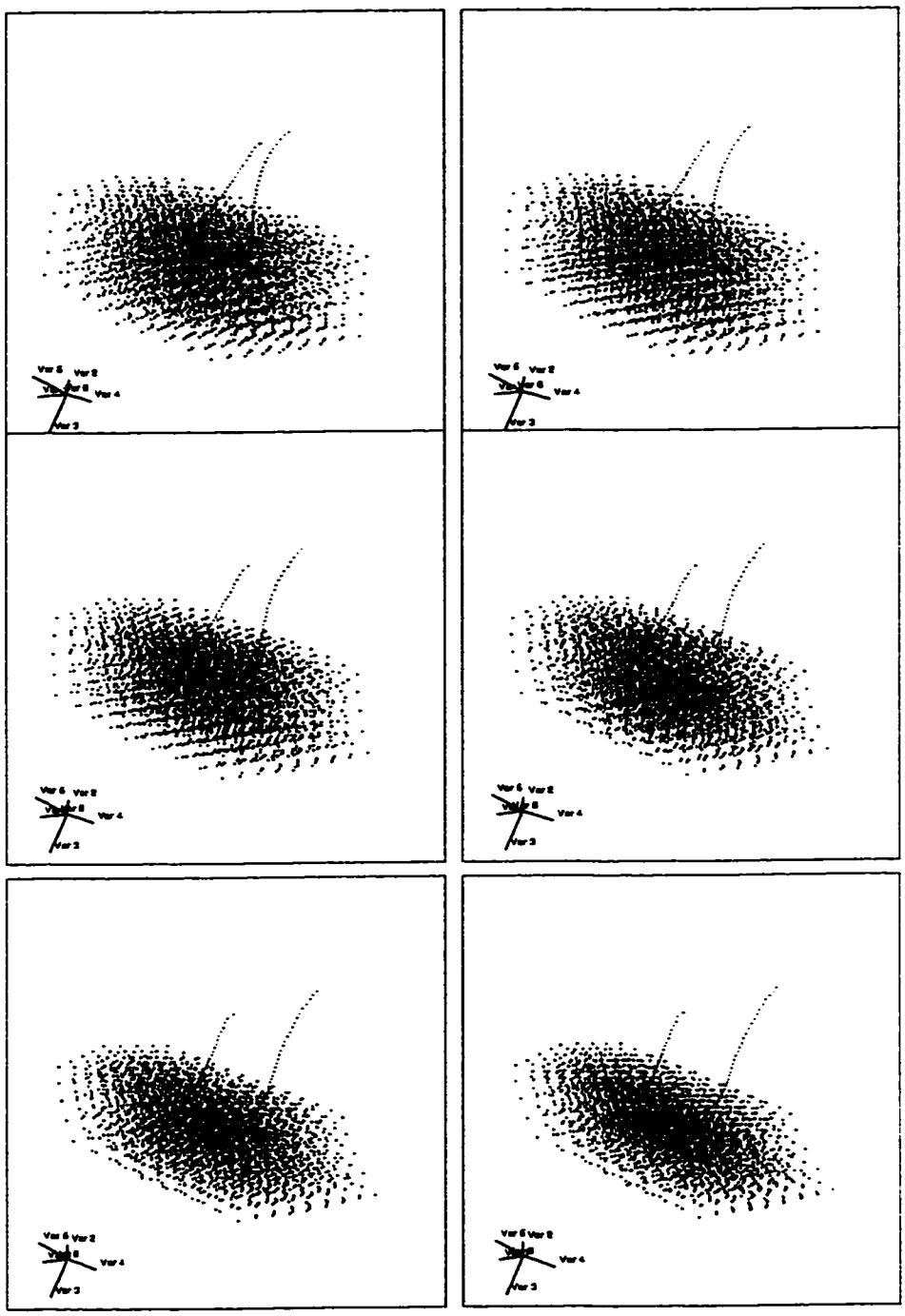

Figure 6.2 Second order approximation for the *stable* case (4gen.)

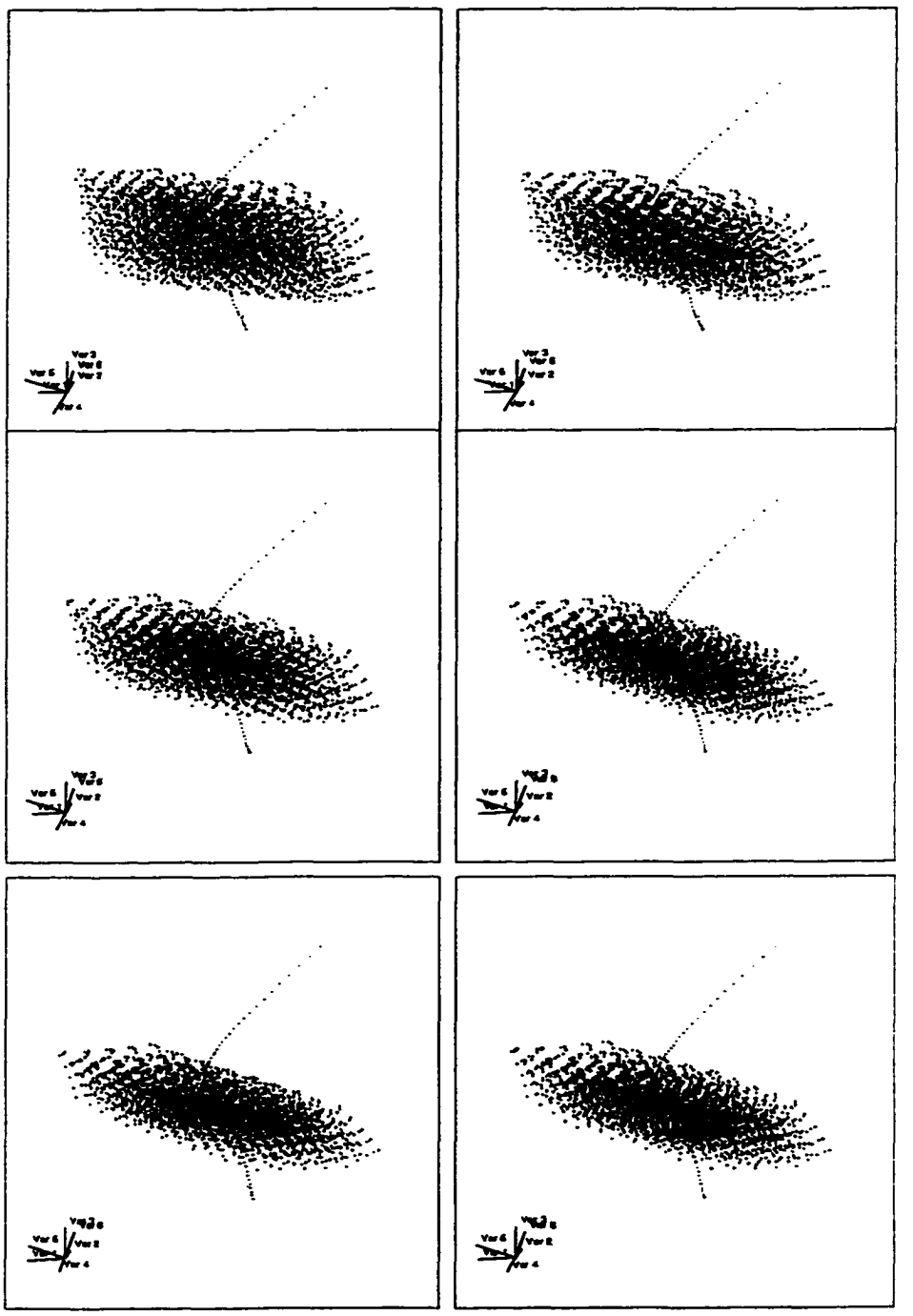

Figure 6.3 Second order approximation for the *unstable* case (4gen.)

In Figure 6.3, the series of the rotating pictures shows that the fault trajectory $\phi_2(t, x_0)$ starting from the initial point x_0 labeled in green, passes through the second order approximation of the stability boundary V^s. After clearing, i.e., for $t > t_{cr}$, the trajectory "follows" V^s in the direction of the UEP for a while, until it becomes unstable in the direction of V^u, the approximation of the unstable manifold, and leaves the stability boundary. The trajectory notably clings to the unstable manifold and then passes through the stable manifold.

6.1.1.4 Structural Information and Nonlinear Indices

- Stable case – fault cleared at 0.1575s

The nonlinear index $I1$ for each mode and the dot product Q (defined in chapter 3) computed at each time instant along the trajectory are shown in Table 6.7.

It is observed that from 0.0s-0.1112s, modes 6, 5, 4, 3 and 2 are the most dominant modes. Examining the nonlinear participation factors corresponding to these modes, we observe that the machines involved in these modes include generators 4, 3, and 2 which are electrically close to the fault. During this time period, Mode 6 remains the most dominant mode. From 0.1204s-0.5355s, mode 4 is the clearly dominant mode. This is the real stable mode, and the time period considered includes the clearing time 0.1575s. The dominant machine in this mode as indicated by the participation factors is generator 4. This happens to be the generator most significantly affected by the disturbance. We also observe that mode 3, the unstable real mode, never becomes the clearly dominant mode in the nonlinear interaction. The stable manifold is not intersected as indicated by the dot product Q and hence the system is stable.

- Unstable case – fault cleared at 0.1578s

The nonlinear index $I1$ for each mode and the dot product Q computed at each time instant along the trajectory for this unstable case are shown in Table 6.8. The

Table 6.7 Nonlinear Index and Q (4gen.)(case I)(stable case)

Time(s)	Mode1	Mode2	Mode3	Mode4	Mode5	Mode6	Q
.0000	.14836	2.33039	3.73307	3.73307	.38189	6.34940	4.6005
.0093	.20265	2.32412	3.86424	3.57139	.52629	6.33082	4.2446
.0185	.25859	2.30533	3.96415	3.38004	.67508	6.27513	3.8936
.0278	.31595	2.27417	4.03221	3.16034	.82763	6.18278	3.5478
.0371	.37454	2.23083	4.06803	2.91355	.98327	6.05434	3.2094
.0463	.43426	2.17550	4.07167	.31456	1.14200	5.89040	2.8785
.0556	.49463	2.10864	4.04289	.70675	1.30243	5.69238	2.5557
.0649	.55555	2.03056	3.98184	1.11827	1.46431	5.46110	2.2421
.0741	.61647	1.94184	3.88892	1.54609	1.62644	5.19849	1.9370
.0834	.67709	1.84302	3.76448	1.98857	1.78792	4.90607	1.6429
.0926	.73730	1.77550	3.60911	2.44500	1.94849	4.58530	1.3590
.1019	.79653	1.73956	3.52930	2.91180	2.10664	4.23870	1.0858
.1112	.85433	1.69872	3.52275	3.38677	2.26136	3.86837	.8245
.1204	.91033	1.65314	3.49433	3.86746	2.41156	3.64100	.7958
.1297	.96417	1.60292	3.44341	4.35192	2.55647	3.45506	.7753
.1390	1.01500	1.54805	3.36869	4.83508	2.69392	3.25595	.7613
.1482	1.06293	1.48899	3.27005	5.31704	2.82396	3.04445	.7541
.1575	1.10686	1.42565	3.14611	5.79131	2.94394	2.82116	.7526
.1674	1.04370	1.31276	2.89981	5.52458	2.77787	2.57346	.7560
.1774	.97943	1.20488	2.66231	5.23599	2.60766	2.34039	.7643
.1873	.91493	1.10236	2.43528	4.93214	2.43600	2.12249	.7768
.1973	.85124	1.00569	2.22006	4.62007	2.26559	1.91991	.7934
.2072	.78902	.91499	2.01755	4.30509	2.09844	1.73259	.8139
.2172	.72882	.83029	1.82827	3.99208	1.93627	1.56023	.8380
.2271	.67133	.75170	1.65260	3.68628	1.78089	1.40235	.8653
.2371	.61663	.67898	1.49038	3.38980	1.63288	1.25831	.8965
.2470	.56495	.61202	1.34126	3.10519	1.49286	1.12731	.9307
.2570	.51642	.55045	1.20492	2.83509	1.36160	1.00857	.9683
.2669	.47109	.49408	1.08077	2.58061	1.23921	.90124	1.0093
.2769	.42873	.44257	.96801	2.34135	1.12523	.80445	1.0543
.2868	.38953	.39572	.86605	2.11954	1.02021	.71732	1.1025
.2968	.35317	.35313	.77397	1.91393	.92339	.63901	1.1543
.3067	.31952	.31448	.69110	1.72420	.83447	.56879	1.2101
.3167	.28847	.27952	.61664	1.55004	.75308	.50587	1.2696
.3266	.25994	.24794	.54986	1.39145	.67904	.44951	1.3337
.3366	.23368	.21955	.49000	1.24657	.61146	.39913	1.4016
.3465	.20954	.19399	.43647	1.11472	.54998	.35412	1.4741
.3565	.18748	.17106	.38859	.99575	.49439	.31388	1.5510
.3664	.16728	.15057	.34580	.88778	.44392	.27800	1.6331

Table 6.7 (Continued)

Time(s)	Mode1	Mode2	Mode3	Mode4	Mode5	Mode6	Q
.3764	.14889	.13226	.30759	.79055	.39837	.24595	1.7201
.3863	.13219	.11597	.27348	.70299	.35728	.21736	1.8121
.3963	.11708	.10147	.24303	.62446	.32036	.19182	1.9097
.4062	.10343	.08860	.21586	.55375	.28711	.16905	2.0129
.4162	.09121	.07723	.19161	.49051	.25735	.14871	2.1220
.4261	.08027	.06713	.16998	.43399	.23075	.13051	2.2373
.4361	.07057	.05824	.15067	.38349	.20705	.11424	2.3585
.4460	.06198	.05038	.13346	.33832	.18593	.09966	2.4862
.4559	.05447	.04344	.11809	.29823	.16731	.08657	2.6210
.4659	.04787	.03730	.10439	.26244	.15079	.07479	2.7623
.4758	.04218	.03186	.09217	.23076	.13634	.06415	2.9105
.4858	.03721	.02704	.08128	.20242	.12614	.05454	3.0660
.4957	.03296	.02274	.07157	.17741	.11909	.04580	3.2286
.5057	.02932	.01893	.06292	.15524	.11257	.00108	3.3978
.5156	.02618	.01550	.05522	.13559	.10653	.00685	3.5755
.5256	.02350	.00588	.04837	.11829	.10100	.01215	3.7599
.5355	.02116	.00774	.04228	.10300	.09586	.01697	3.9514
.5455	.01914	.00926	.03687	.08959	.09115	.02138	4.1495
.5554	.01736	.01050	.03207	.07777	.08678	.02538	4.3548
.5654	.01574	.01152	.02781	.06737	.08269	.02900	4.5666
.5753	.01426	.01229	.02404	.05822	.07883	.03227	4.7844
.5853	.01286	.01291	.02071	.05030	.07521	.03522	5.0080
.5952	.01226	.01330	.01802	.04329	.07169	.03783	5.2368
.6052	.01231	.01356	.01567	.03716	.06828	.04016	5.4695
.6151	.01218	.01362	.01354	.03188	.06496	.04223	5.7059
.6251	.01188	.01359	.01160	.02733	.06292	.04409	5.9443
.6350	.01137	.01339	.00985	.02330	.06276	.04566	6.1846
.6450	.01068	.01344	.00826	.01984	.06211	.05137	6.4244
.6549	.00979	.01368	.00683	.01682	.06080	.05702	6.6638
.6649	.00873	.01441	.00554	.00417	.05891	.06258	6.8992
.6748	.00752	.01498	.00439	.00514	.05633	.06777	7.1315
.6848	.00618	.01538	.00335	.00585	.05316	.07272	7.3573
.6947	.00474	.01562	.00242	.00636	.04936	.07726	7.5747
.7047	.00323	.01568	.00159	.00667	.04498	.08129	7.7827
.7146	.01084	.01554	.00254	.00683	.04009	.08484	7.9796
.7246	.01173	.01523	.00297	.00685	.03471	.08775	8.1618
.7345	.01238	.01473	.00333	.00675	.02894	.08994	8.3290
.7444	.01276	.01408	.00364	.00656	.02288	.09147	8.4789

Table 6.7 (Continued)

Time(s)	Mode1	Mode2	Mode3	Mode4	Mode5	Mode6	Q
.7544	.01288	.01330	.00389	.00629	.01662	.09230	8.6102
.7643	.01274	.01237	.00410	.00597	.01026	.09251	8.7192
.7743	.01232	.01133	.00426	.00560	.00119	.09192	8.8076
.7842	.01167	.01018	.00437	.00519	.00235	.09053	8.8718
.7942	.01079	.00896	.00444	.00476	.00836	.08843	8.9112
.8041	.00975	.00771	.00448	.00432	.01405	.08588	8.9257
.8141	.00937	.00940	.00073	.00386	.01929	.08255	8.9137
.8240	.00960	.01041	.00080	.00340	.02400	.07869	8.8766
.8340	.00965	.01118	.00087	.00295	.02809	.07444	8.8127
.8439	.00951	.01168	.00094	.00251	.03147	.06971	8.7242
.8539	.00922	.01194	.00102	.00208	.03413	.06482	8.6104
.8638	.00875	.01196	.00110	.00167	.03598	.05967	8.4729
.8738	.00815	.01177	.00120	.00128	.03700	.05447	8.3129
.8837	.00740	.01136	.00130	.00092	.03716	.04918	8.1314
.8937	.00656	.01080	.00142	.00203	.03651	.04411	7.9314
.9036	.00561	.01012	.00468	.00227	.03507	.03925	7.7130
.9136	.00459	.00934	.00487	.00250	.03288	.03794	7.4793
.9235	.00350	.00849	.00504	.00269	.02995	.03689	7.2324
.9335	.00236	.00765	.00521	.00286	.02641	.03591	6.9739
.9434	.00120	.00771	.00537	.00300	.02233	.03502	6.7064
.9534	.00003	.00768	.00553	.00309	.01786	.03422	6.4318
.9633	.00444	.00757	.00570	.00314	.01352	.03351	6.1530
.9733	.00485	.00737	.00586	.00315	.01122	.03290	5.8711

pattern of the dominant modes is very similar to the stable case in Table 6.7 for the time 0.0s-0.7180s. However, in this case at 0.7280s, mode 3, the unstable mode becomes the most dominant mode in terms of the nonlinear interaction, and begins to increase its dominance. The nonlinear participation factors indicate that generator 4 is the most dominant machine in mode 3, and hence is the most affected. This generator loses synchronism with respect to the rest of the system. Examining the $h2_r$ matrix shown in Table 6.6, we observe that for mode 3, the only pair of the real states have strongest interaction between them are state 3 and 4, which indicates that the system has more stress along these two eigen-directions. This case demonstrates that the real stable eigen-direction plays an important role in a stable case while the real unstable eigen-direction

Table 6.8 Nonlinear Index and Q (4gen.)(case II)(unstable case)

Time(s)	Mode1	Mode2	Mode3	Mode4	Mode5	Mode6	Q
.0000	.14836	2.33039	3.73307	3.73307	.38189	6.34940	4.6005
.0093	.20694	2.32310	3.87316	3.55750	.53775	6.32779	4.2698
.0186	.26735	2.30130	3.97675	3.34783	.69846	6.26317	3.9432
.0278	.32958	2.26509	4.04355	3.10481	.86393	6.15589	3.6220
.0371	.39322	2.21479	4.07281	2.83054	1.03292	6.00681	3.3064
.0464	.45779	2.15078	4.06436	.46531	1.20448	5.81719	2.9965
.0557	.52305	2.07348	4.01832	.89687	1.37797	5.58825	2.6939
.0650	.58884	1.98343	3.93504	1.34985	1.55281	5.32155	2.3982
.0743	.65441	1.88129	3.81488	1.82101	1.72749	5.01926	2.1109
.0835	.71948	1.78526	3.65868	2.30779	1.90092	4.68375	1.8321
.0928	.78368	1.74792	3.52798	2.80849	2.07223	4.31706	1.5616
.1021	.84621	1.70481	3.52499	3.31886	2.23961	3.92236	1.3005
.1114	.90678	1.65619	3.49679	3.83638	2.40203	3.65246	1.0491
.1207	.96479	1.60217	3.44236	4.35794	2.55811	3.45234	.8074
.1300	1.01964	1.54289	3.36073	4.87978	2.70634	3.23706	.5756
.1392	1.07056	1.47844	3.25071	5.39766	2.84487	3.00733	.3546
.1485	1.11718	1.40933	3.11154	5.90815	2.97232	2.76412	.1435
.1578	1.05158	1.29503	2.86072	5.62592	2.79969	2.51470	-.0567
.1678	.98505	1.18603	2.61936	5.32295	2.62344	2.28040	-.0594
.1778	.91872	1.08273	2.38936	5.00694	2.44680	2.06182	-.0595
.1878	.85331	.98541	2.17178	4.68332	2.27183	1.85903	-.0576
.1978	.78970	.89436	1.96752	4.35845	2.10084	1.67187	-.0545
.2078	.72835	.80950	1.77706	4.03681	1.93545	1.50003	-.0506
.2178	.66973	.73080	1.60054	3.72264	1.77702	1.34290	-.0462
.2278	.61423	.65818	1.43789	3.41996	1.62679	1.19975	-.0420
.2378	.56198	.59139	1.28877	3.13064	1.48522	1.06985	-.0377
.2478	.51291	.53010	1.15259	2.85592	1.35245	.95229	-.0334
.2578	.46717	.47405	1.02880	2.59784	1.22897	.84620	-.0295
.2678	.42462	.42300	.91658	2.35643	1.11441	.75066	-.0261
.2678	.38522	.37649	.81525	2.13266	1.00893	.66481	-.0225
.2778	.34882	.33436	.72394	1.92594	.91200	.58777	-.0197
.2878	.31517	.29616	.64183	1.73544	.82306	.51877	-.0171
.2979	.28420	.26162	.56817	1.56123	.74194	.45701	-.0147
.3079	.25573	.23053	.50215	1.40205	.66796	.40182	-.0125
.3179	.22961	.20254	.44309	1.25739	.60077	.35251	-.0109
.3279	.20570	.17736	.39031	1.12634	.53989	.30846	-.0094
.3379	.18388	.15488	.34313	1.00784	.48481	.26917	-.0079
.3479	.16392	.13474	.30104	.90040	.43488	.23415	-.0070
.3579	.14586	.11678	.26347	.80415	.39007	.20288	-.0059

Table 6.8 (Continued)

Time(s)	Mode1	Mode2	Mode3	Mode4	Mode5	Mode6	Q
.3679	.12944	.10076	.22999	.71731	.34965	.17500	-.0051
.3779	.11469	.08655	.20010	.63966	.31349	.15011	-.0045
.3879	.10140	.07393	.17348	.56991	.28105	.12790	-.0041
.3979	.08954	.06274	.14973	.50755	.25213	.10806	-.0036
.4079	.07902	.05287	.12857	.45207	.22646	.09028	-.0033
.4179	.06969	.04409	.10971	.40247	.20368	.07436	-.0031
.4279	.06149	.03632	.09292	.35825	.18355	.06006	-.0031
.4379	.05430	.02945	.07798	.31879	.16580	.02282	-.0029
.4479	.04807	.02335	.06466	.28393	.15035	.03006	-.0031
.4579	.04267	.01794	.05281	.25302	.13691	.03678	-.0031
.4679	.03801	.01310	.04228	.22557	.12975	.04304	-.0035
.4779	.03401	.00879	.02517	.20139	.12360	.04895	-.0035
.4879	.03053	.00491	.03000	.17999	.11800	.05451	-.0038
.4979	.02752	.01984	.03435	.16112	.11295	.05981	-.0042
.5079	.02487	.02172	.03822	.14445	.10838	.06486	-.0044
.5179	.02251	.02346	.04172	.12983	.10428	.06976	-.0049
.5279	.02034	.02504	.04481	.11691	.10054	.07444	-.0052
.5379	.01830	.02645	.04757	.10556	.09713	.07899	-.0058
.5479	.01633	.02775	.05005	.09561	.09401	.08344	-.0064
.5580	.01438	.02889	.05237	.08799	.09114	.08788	-.0069
.5680	.01237	.02984	.05440	.08398	.08837	.09214	-.0074
.5780	.01149	.03064	.05634	.08053	.08573	.09640	-.0083
.5880	.01064	.03118	.05805	.07736	.08301	.10043	-.0088
.5980	.00950	.03155	.05977	.07462	.08032	.10451	-.0092
.6080	.00797	.03164	.06151	.07218	.07968	.10848	-.0100
.6180	.00610	.03148	.06320	.06987	.07983	.11225	-.0111
.6280	.00383	.03102	.06506	.06778	.07917	.11592	-.0117
.6380	.00123	.03023	.06699	.06570	.07767	.11940	-.0126
.6480	.00174	.02913	.06917	.06368	.07521	.12272	-.0133
.6580	.02208	.02765	.07173	.06167	.07168	.12579	-.0145
.6680	.02655	.02584	.07882	.05962	.06705	.12863	-.0154
.6780	.03111	.02363	.08725	.05737	.06128	.13110	-.0167
.6880	.03574	.02100	.09707	.05497	.01443	.13381	-.0176
.6980	.04037	.01802	.10843	.05225	.00526	.13777	-.0190
.7080	.04498	.01458	.12173	.04925	.00534	.14089	-.0204
.7180	.04947	.01072	.13714	.04579	.01749	.14320	-.0218
.7280	.05386	.01660	.15527	.04197	.03141	.14464	-.0234
.7380	.05849	.02292	.17637	.03759	.04727	.14498	-.0250

Table 6.8 (Continued)

Time(s)	Mode1	Mode2	Mode3	Mode4	Mode5	Mode6	Q
.7480	.06471	.02987	.20098	.03015	.06530	.14431	-.0268
.7580	.07130	.03752	.22962	.04037	.08574	.14241	-.0289
.7680	.07829	.04583	.26284	.05202	.10886	.13937	-.0307
.7780	.08584	.05490	.30181	.06522	.13511	.13822	-.0330
.7880	.09395	.06475	.34688	.08029	.16473	.13627	-.0352
.7980	.10279	.07539	.39925	.09739	.19825	.04108	-.0377
.8080	.11246	.08686	.46002	.11681	.23616	.02918	-.0405
.8180	.12319	.09934	.53047	.13880	.27905	.01561	-.0434
.8281	.13514	.11273	.61219	.16365	.32765	.00007	-.0463
.8381	.14856	.12717	.70672	.19170	.38267	.01753	-.0494
.8481	.16373	.14268	.81607	.22332	.44504	.03739	-.0529
.8581	.18100	.15941	.94250	.25884	.51576	.05963	-.0567
.8681	.20073	.17736	1.08804	.29876	.59588	.08434	-.0606
.8781	.22341	.19660	1.25622	.34334	.68686	.11155	-.0650
.8881	.24952	.21727	1.44926	.39325	.78988	.14157	-.0693
.8981	.27971	.23932	1.67125	.44875	.90671	.17418	-.0743
.9081	.31471	.26289	1.92597	.51035	1.03912	.20927	-.0795
.9181	.35525	.28788	2.21713	.57866	1.18887	.24701	-.0851
.9281	.40234	.31447	2.55008	.65399	1.35827	.28707	-.0910
.9381	.45694	.34235	2.92910	.73704	1.54947	.32932	-.0975
.9481	.52038	.37174	3.35993	.82820	1.76511	.37304	-.1042
.9581	.59396	.40268	3.84770	.92841	2.00770	.41843	-.1118
.9681	.67923	.43513	4.39780	1.03870	2.28010	.46532	-.1196

plays an important role in an unstable case.

The stable manifold is intersected at 0.1554s, which is obtained by interpolation at the point at which Q is equal to zero, and hence the fact that the system is unstable has been verified.

6.1.1.5 Comparison of Stability Boundary approximations

For the same fault scenarios $\phi_1(t, x_0)$ and $\phi_2(t, x_0)$ as in Figure 6.2 and 6.3, we show in Figure 6.4 and 6.5, the second order approximation V^s of the stability boundary (blue), its energy surface approximation V^e (yellow), the second order approximation V^u of the unstable manifold (green), and the trajectories (red) $\phi_1(t, x_0)$ (stable case,

Figure 6.4) and $\phi_2(t, x_0)$ (unstable case, Figure 6.5). The axis tree at lower left describes the Euclidean projection from 6-space. The first three axes (Var1, Var2, Var3) represent three relative angles, i.e., δ_{31}, δ_{21} and δ_{41}. The other three axes (Var4, Var5, Var6) represent three relative speeds, i.e., ω_{31}, ω_{21} and ω_{41}. The rotation sequences in Figure 6.4 and 6.5 are chosen for different projections in the *grand tour* than in Figure 6.2 and 6.3, because we want to draw attention to the differences in the approximations V^s and V^e. Both figures show that the trajectories ϕ_1 and ϕ_2 of the full nonlinear system follow the manifolds V^s and V^u more closely than they follow the energy surface V^e.

Applying the approaches described in section 3.2.2, the exit point from the energy surface is obtained. It happens at 0.1508s. Compared with the critical clearing time, i.e., 0.1576s, the exit point happens before the critical clearing time. It provides that the equi-energy surface is a conservative approximation. In addition to it, the exit point from the stable manifold happens at 0.1554s (Q=0) indicates that the second order stable manifold is also a conservative approximation to the stability boundary and it is less conservative than the energy surface approximation, because $0.1576s > 0.1554s > 0.1508s$.

6.1.2 Case III – Three-phase Fault at Bus 7, Cleared at 0.2018s

Table 6.9 shows the controlling UEP for case III. Consider generator 1 as the reference machine, three machines (gen. 2, gen. 3 and gen. 4) are all advanced at the controlling UEP. From the values of UEP, we see that gen. 4 and gen. 2 are more advanced than gen. 3. The fault trajectory including the generator relative angles obtained from ETMSP is presented in Figure 6.6. In Figure 6.6, the values of the three relative angles are not very big at the end of the simulation period because the simulation has been stopped by ETMSP due to the large relative speeds indicating that the system is unstable.

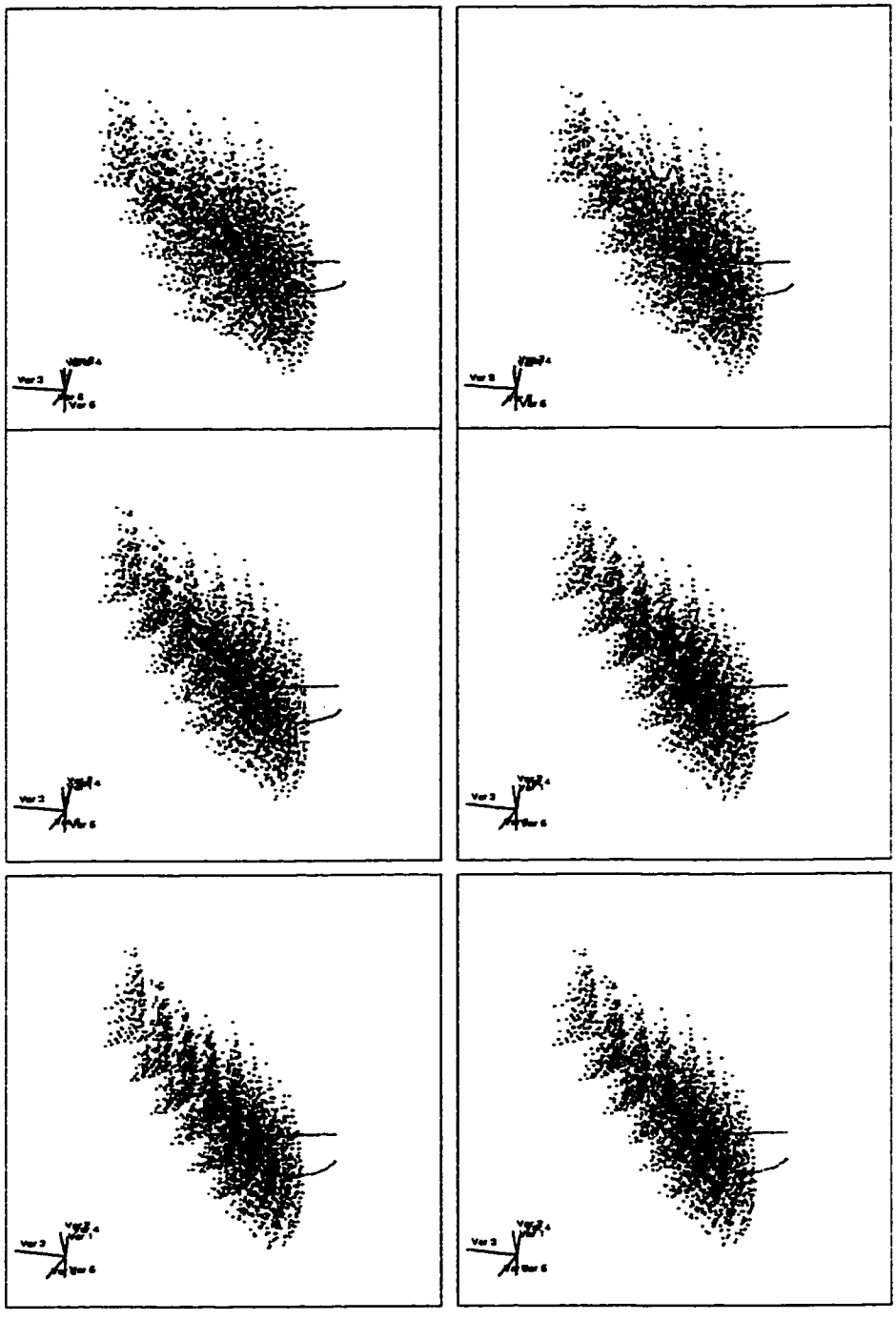

Figure 6.4 Energy surface approximation for the *stable* case (4gen.)

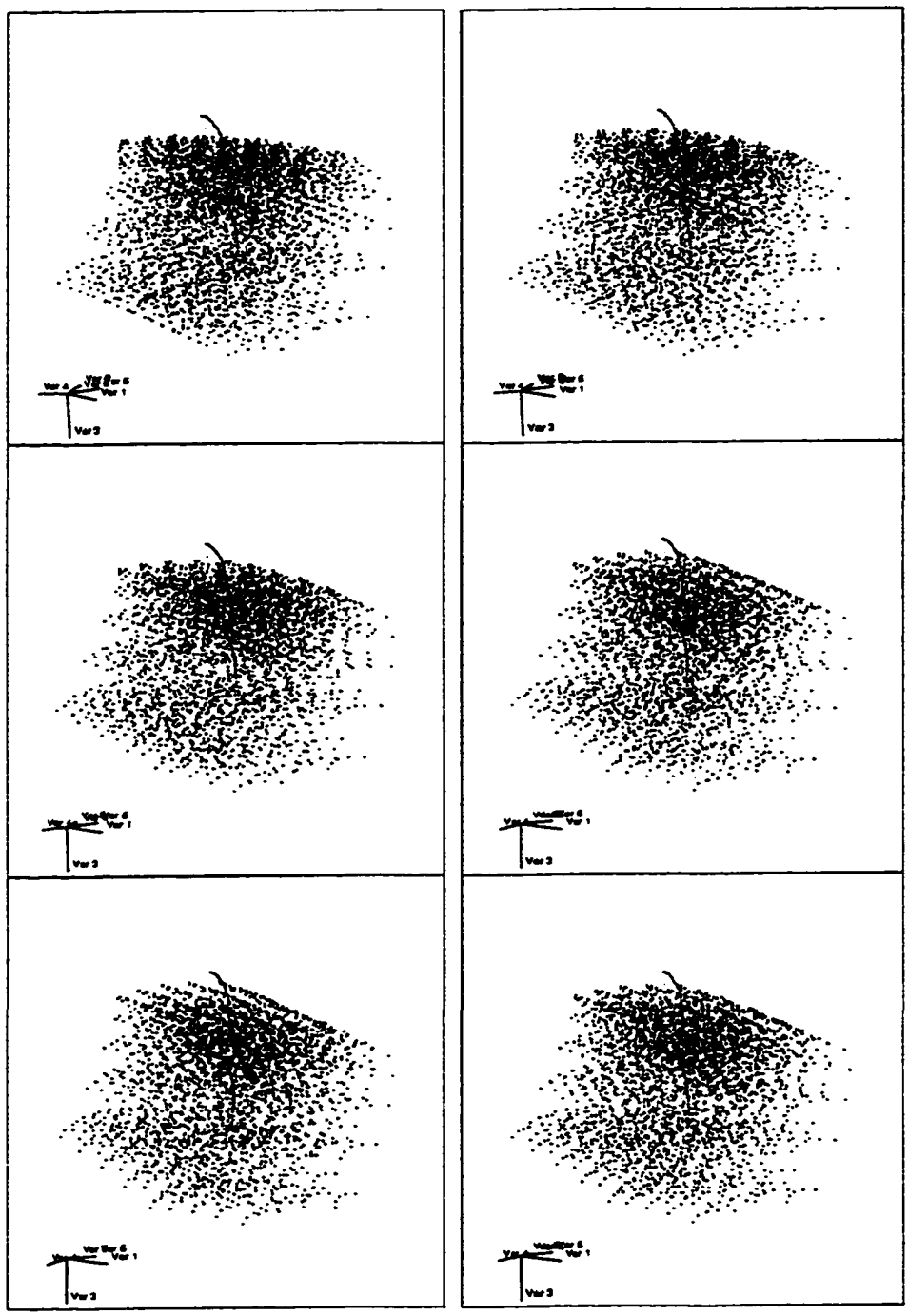

Figure 6.5 Energy surface approximation for the *unstable* case (4gen.)

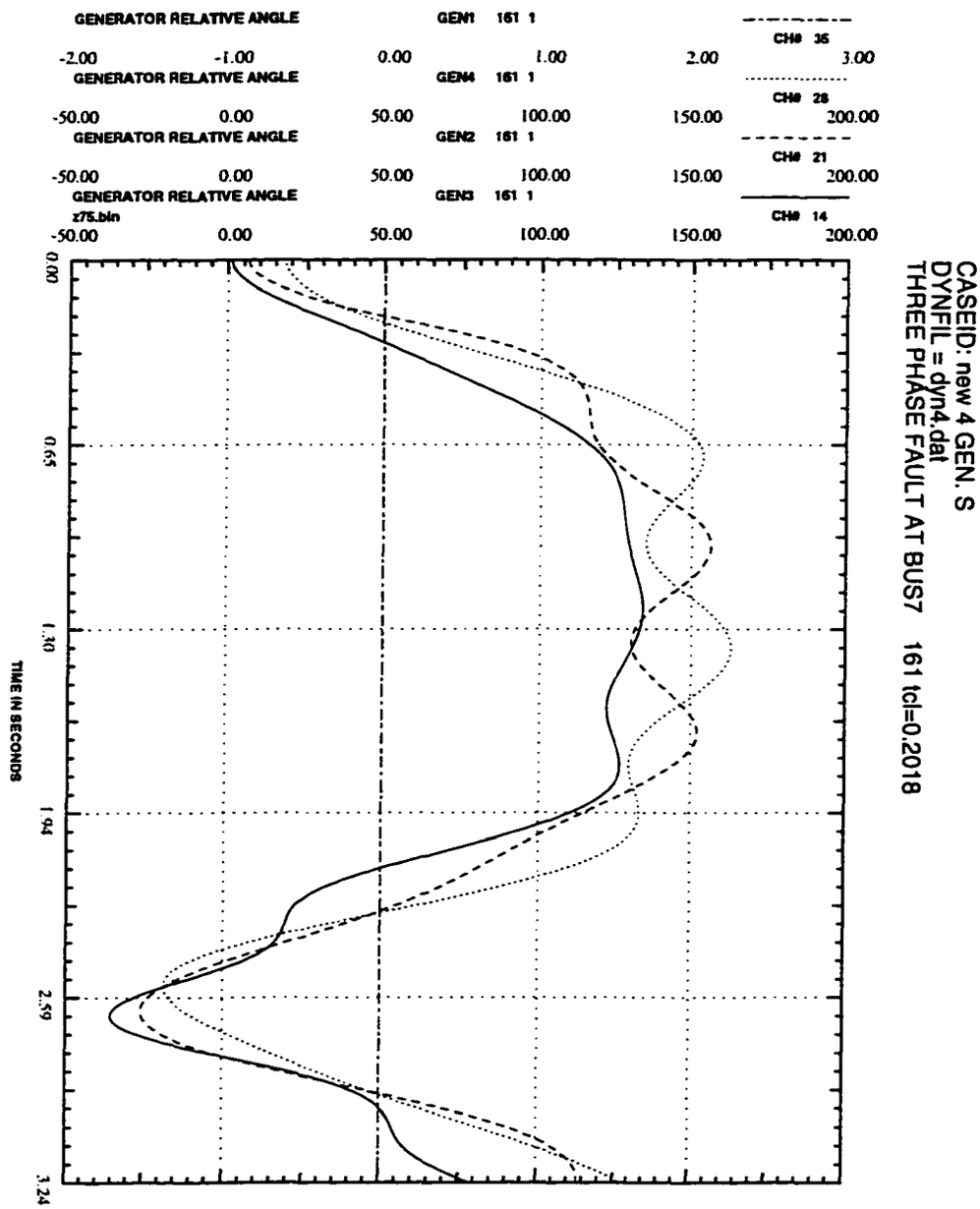

Figure 6.6 Fault trajectory (generator relative angle) (case III) (4gen.)

Table 6.9 Controlling UEP for 4-generator system (case III)

Machine	State	Relative Angles (deg.) and Relative Speeds (rad./s)
δ_{21}	2	145.6252
δ_{31}	1	134.0251
δ_{41}	3	151.3004
ω_{21}	5	0.0000
ω_{31}	4	0.0000
ω_{41}	6	0.0000

6.1.2.1 Eigen-analysis and Linear Participation Factors

The eigenvalues and the linear participation factors of case III are listed below in Table 6.10 and Table 6.11 respectively. According to Table 6.10, the 1st mode is the only mode corresponding to the unstable direction. Obviously the UEP of this system is a type-1 UEP.

Table 6.10 Eigenvalues for 4-generator system (case III)

Mode	Eigenvalue
1	$5.6666 + j0.0000$
2	$-5.6666 - j0.0000$
3	$0.0000 + j9.6260$
4	$0.0000 - j9.6260$
5	$0.0000 + j8.7071$
6	$0.0000 - j8.7071$

Table 6.11 Linear Participation Factors (4gen.)(case III)

Mode	State1	State2	State3	State4	State5	State6
1	.156471	.180429	.163100	.156471	.180429	.163100
2	.156471	.180429	.163100	.156471	.180429	.163100
3	.000000	.000000	.000000	.491900	.504554	.003546
4	.491900	.504554	.003546	.000000	.000000	.000000
5	.000000	.000000	.000000	.195159	.134587	.670254
6	.195159	.134587	.670254	.000000	.000000	.000000

6.1.2.2 Normal Form and Nonlinear Participation Factors

The proposed real normal form technique is applied to the system to obtain the stable manifold. Table 6.12 provides the interaction coefficients $h2_r$.

The nonlinear participation factors are listed in Table 6.13. We note that for mode 1 and 2, the participation factors corresponding to all the states are at the same level. This indicates that all three generators participate in the mode.

6.1.2.3 Structural Information and Nonlinear Indices

For this case, the fault clearing time (0.2018s) is greater than the critical clearing time (0.2010s). It is an unstable case. Table 6.14 provides the nonlinear indices and the dot product Q along the fault trajectory for this case.

It is observed that from 0.0s-0.6117s, mode 1 and 2 are the most dominant modes. Examining the nonlinear participation factors corresponding to these modes, we observe that the machines involved in these modes include generators 2, 4 and 3, which are electrically close to the fault. However, in this case at 0.6217s, Mode 1, the unstable mode becomes the most dominant mode in terms of the nonlinear interaction, and begins to increase its dominance. The nonlinear participation factors indicate that the generator 2, 4 and 3 are the most dominant machine in mode 1, and hence are the most affected. These generators lose synchronism with respect to generator 1 as seen in Figure 6.6. The $h2_r$ matrix shown in Table 6.12 provides that, for mode 1, only the pair of real states have strongest interaction between them. Once again this verifies that in this unstable case, the real unstable direction plays an important role in the system.

The stable manifold is intersected at 0.1965s, which is obtained by interpolation at the point at which Q is equal to zero, and hence the fact that the system is unstable has been verified. The stable manifold is a conservative second order approximation of the stability boundary because the exit point happens before the critical clearing time, i.e.,

Table 6.12 Real Transformation Matrix $h2_r$ (4gen.)(case III)

Mode		State1	State2	State3	State4	State5	State6
1	State1	-.02260	-.04520	-.01515	.00000	.01479	.00000
	State2	.00000	.00753	.00635	-.00748	-.00549	.00714
	State3	.00000	.00000	.01027	-.00605	-.00742	.00368
	State4	.00000	.00000	.00000	.01205	.00104	-.00888
	State5	.00000	.00000	.00000	.00000	.00890	-.00580
	State6	.00000	.00000	.00000	.00000	.00000	.01079
2	State1	-.00753	.04520	-.00635	-.00748	.00549	.00714
	State2	.00000	.02260	.01515	.00000	-.01479	.00000
	State3	.00000	.00000	-.01027	-.00605	.00742	.00368
	State4	.00000	.00000	.00000	-.01205	.00104	.00888
	State5	.00000	.00000	.00000	.00000	-.00890	-.00580
	State6	.00000	.00000	.00000	.00000	.00000	-.01079
3	State1	.00404	.00000	.00238	.00949	-.00094	-.00802
	State2	.00000	-.00404	-.00238	.00949	.00094	-.00802
	State3	.00000	.00000	.00000	-.00474	.00000	-.00110
	State4	.00000	.00000	.00000	.00000	-.00144	.00000
	State5	.00000	.00000	.00000	.00000	.00000	-.00019
	State6	.00000	.00000	.00000	.00000	.00000	.00000
4	State1	-.00343	.01638	-.00809	-.00238	.00670	.00332
	State2	.00000	-.00343	-.00809	.00238	.00670	-.00332
	State3	.00000	.00000	.00474	.00000	.00244	.00000
	State4	.00000	.00000	.00000	.00237	.00000	.00110
	State5	.00000	.00000	.00000	.00000	.00017	.00000
	State6	.00000	.00000	.00000	.00000	.00000	.00007
5	State1	-.00234	.00000	-.00252	-.00607	-.00008	-.00030
	State2	.00000	.00234	.00252	-.00607	.00008	-.00030
	State3	.00000	.00000	.00000	-.00238	.00000	-.00057
	State4	.00000	.00000	.00000	.00000	-.00081	.00000
	State5	.00000	.00000	.00000	.00000	.00000	.01366
	State6	.00000	.00000	.00000	.00000	.00000	.00000
6	State1	.00180	-.00970	.00507	.00071	.00024	.00008
	State2	.00000	.00180	.00507	-.00071	.00024	-.00008
	State3	.00000	.00000	.00263	.00000	.00146	.00000
	State4	.00000	.00000	.00000	.00155	.00000	.00081
	State5	.00000	.00000	.00000	.00000	-.01366	.00000
	State6	.00000	.00000	.00000	.00000	.00000	-.00683

Table 6.13 Nonlinear Participation Factors (4gen.)(case III)

Mode	State1	State2	State3	State4	State5	State6
1	.155303	.179601	.163194	.294801	.181294	.176138
2	.154057	.178639	.163195	.090400	.179804	.150898
3	.000000	.000000	.000000	.503841	.504547	.003568
4	.491883	.504671	.003546	.000000	.000000	.000000
5	.000000	.000000	.000000	.199341	.134414	.670542
6	.194977	.134498	.670165	.000000	.000000	.000000

0.2010s.

6.2 IEEE 11-Generator System

For the IEEE 11-generator system (see the one-line diagram in Figure 4.5), there are all together 20 minimum independent states including 10 relative angles and 10 relative speeds. The machine data are listed in Table B.1. Consider generator 1 as the reference machine. The physical meaning for each state in the X-space, i.e., the machine space, is listed in Table 6.15.

We study the following 2 cases:

- A three-phase fault occurs at Bus 996, it was cleared by opening lines 3-996 (2 lines) and lines 297-996 (3 lines) at 0.048 second.
- A three-phase fault occurs at Bus 996, it was cleared by opening lines 3-996 (2 lines) and lines 297-996 (3 lines) at 0.138s second.

6.2.1 Three-phase Fault at Bus 996, cleared at 0.048s & 0.138s

Table 6.16 presents the controlling UEP for this 11-generator system corresponding to both contingencies. Consider generator 11 as the reference machine, there are two advanced machines at the controlling UEP according to Table 6.16. They are generator 3 and generator 5. However, all the rest machines except for generator 9 have very similar

Table 6.14 Nonlinear Index and Q (4gen.)(case III)

Time(s)	Mode1	Mode2	Mode3	Mode4	Mode5	Mode6	Q
.0000	7.29021	7.29021	.25130	3.89424	.14564	2.50324	7.8856
.0096	7.48473	7.05685	.30603	3.88714	.18335	2.49882	7.3956
.0192	7.63994	6.78524	.36310	3.86586	.22248	2.48558	6.9117
.0288	7.75470	6.47783	.42217	3.83067	.26286	2.46368	6.4372
.0384	7.82967	6.13489	.48338	3.78180	.30468	2.43327	5.9709
.0480	7.86469	5.75859	.54648	3.71970	.34785	2.39462	5.5143
.0577	7.86022	.17167	.61136	3.64487	.39235	2.34806	5.0681
.0673	7.81677	.40563	.67762	3.55810	.43797	2.29409	4.6345
.0769	7.73545	1.00439	.74520	3.45994	.48482	2.23304	4.2125
.0865	7.61732	1.62075	.81380	3.35127	.53273	2.16549	3.8030
.0961	7.46374	2.25261	.88324	3.23286	.58171	2.09192	3.4059
.1057	7.27627	2.89428	.95299	3.10579	.63146	2.01307	3.0226
.1153	7.05656	3.54395	1.02291	3.02344	.68201	1.92944	2.6522
.1249	6.85351	4.19761	1.09264	2.98792	.73322	1.88885	2.2948
.1345	6.85113	4.85222	1.16199	2.94883	.78506	1.85916	1.9497
.1441	6.82672	5.50321	1.23045	2.90628	.83732	1.82761	1.6171
.1538	6.78013	6.14534	1.29753	2.86030	.88974	1.79441	1.2969
.1634	6.71209	6.77524	1.36298	2.81119	.94232	1.75985	.9882
.1730	6.62269	7.38874	1.42638	2.75897	.99487	1.72416	.6903
.1826	6.51318	7.98517	1.48781	2.70404	1.04757	1.68775	.4012
.1922	6.38293	8.55530	1.54622	2.64603	1.09985	1.65059	.1219
.2018	6.23338	9.09962	1.60182	2.58532	1.15197	1.61315	-.1502
.2118	5.90806	8.85963	1.54851	2.46043	1.13456	1.51691	-.1542
.2218	5.58693	8.58876	1.49281	2.33717	1.11399	1.42126	-.1544
.2318	5.27122	8.29064	1.43527	2.21574	1.09027	1.32652	-.1510
.2418	4.96248	7.97201	1.37680	2.09657	1.06370	1.23316	-.1454
.2518	4.66193	7.63826	1.31811	1.97993	1.03446	1.14163	-.1382
.2618	4.37045	7.29297	1.25960	1.86600	1.00264	1.05224	-.1300
.2718	4.08847	6.93843	1.20147	1.75477	.96820	.96530	-.1204
.2818	3.81700	6.58047	1.14433	1.64663	.93153	.88118	-.1106
.2918	3.55655	6.22169	1.08835	1.54170	.89275	.80018	-.1007
.3018	3.30757	5.86596	1.03386	1.44017	.85214	.72260	-.0915
.3118	3.06994	5.51399	.98071	1.34193	.80970	.64858	-.0823
.3218	2.84410	5.16863	.92907	1.24724	.76576	.57834	-.0736
.3318	2.63015	4.83221	.87902	1.15619	.72061	.51205	-.0658
.3418	2.42786	4.50539	.83042	1.06873	.67441	.44978	-.0586

Table 6.14 (Continued)

Time(s)	Mode1	Mode2	Mode3	Mode4	Mode5	Mode6	Q
.3518	2.23728	4.18974	.78327	.98499	.62750	.39168	-.0521
.3618	2.05831	3.88687	.73760	.90505	.58022	.33777	-.0468
.3717	1.89078	3.59686	.69326	.82894	.53285	.28804	-.0423
.3817	1.73431	3.32014	.65015	.75664	.48568	.24254	-.0386
.3917	1.58876	3.05744	.60826	.68824	.43908	.20115	-.0358
.4017	1.45375	2.80907	.56758	.62373	.39341	.16384	-.0341
.4117	1.32890	2.57435	.52795	.56311	.34891	.13056	-.0328
.4217	1.21391	2.35440	.48955	.50645	.30604	.10104	-.0327
.4317	1.10822	2.14816	.45225	.45359	.26498	.13647	-.0333
.4417	1.01147	1.95557	.41612	.40465	.22607	.15098	-.0345
.4517	.92314	1.77687	.38130	.35950	.18958	.16153	-.0368
.4617	.84271	1.61031	.34767	.31805	.15564	.16816	-.0390
.4717	.76971	1.45740	.31561	.28030	.12460	.17127	-.0428
.4817	.70349	1.31568	.28493	.24602	.09642	.17094	-.0464
.4917	.64360	1.18528	.25585	.21512	.07126	.16770	-.0506
.5017	.58952	1.06598	.22853	.18747	.04919	.16199	-.0555
.5117	.54063	.95642	.20296	.01623	.03018	.15406	-.0605
.5217	.49650	.85639	.17929	.02380	.01418	.14449	-.0660
.5317	.45655	.76511	.15758	.02899	.09842	.13359	-.0717
.5417	.42038	.68215	.13792	.03212	.10501	.12194	-.0779
.5517	.38752	.60664	.12030	.03355	.10790	.10994	-.0846
.5617	.35755	.53796	.11271	.03351	.10725	.09800	-.0914
.5717	.33008	.47523	.10563	.03228	.10327	.09503	-.0980
.5817	.30482	.41876	.09925	.03020	.09634	.09562	-.1056
.5917	.28147	.36720	.09351	.02748	.08678	.09588	-.1131
.6017	.26096	.32036	.08846	.04213	.08217	.09583	-.1208
.6117	.25177	.27794	.08414	.03583	.07634	.09543	-.1288
.6217	.24203	.23947	.08045	.03019	.06933	.09472	-.1371
.6317	.23159	.20483	.07738	.02517	.06143	.09369	-.1461
.6417	.22047	.17322	.07476	.02168	.05286	.09233	-.1548
.6517	.20861	.14498	.07257	.01812	.04398	.09068	-.1644
.6617	.19609	.11947	.02905	.01445	.03497	.08876	-.1742
.6717	.18302	.09667	.02447	.01062	.02608	.08661	-.1846
.6817	.16958	.07632	.01952	.00666	.04584	.08427	-.1952
.6916	.15593	.05839	.01445	.00254	.05763	.08180	-.2067

Table 6.14 (Continued)

Time(s)	Mode1	Mode2	Mode3	Mode4	Mode5	Mode6	Q
.7016	.14234	.04251	.00944	.03334	.06748	.07926	-.2183
.7116	.12902	.02879	.00470	.03750	.07508	.07749	-.2309
.7216	.11673	.01691	.00039	.04144	.08029	.08787	-.2440
.7316	.10602	.00678	.00336	.04510	.08293	.09873	-.2576
.7416	.09988	.00158	.00643	.04848	.08293	.09972	-.2722
.7516	.10249	.09791	.00876	.05156	.08033	.09552	-.2882
.7616	.10583	.10298	.01030	.05428	.07524	.08987	-.3048
.7716	.10964	.10766	.01105	.05661	.06780	.07740	-.3228
.7816	.11380	.11107	.01104	.05891	.05825	.06876	-.3413
.7916	.11811	.11323	.01032	.06267	.04691	.05580	-.3608
.8016	.12226	.11399	.02123	.06572	.03411	.04109	-.3817
.8116	.12610	.11350	.01604	.06795	.02027	.03458	-.4040
.8216	.12946	.11185	.01138	.06934	.01145	.02610	-.4280
.8316	.13212	.10918	.00663	.06981	.00870	.01555	-.4528
.8416	.13407	.10574	.00194	.06940	.02291	.02306	-.4787
.8516	.13495	.10145	.01225	.06812	.03629	.03848	-.5069

values in angles. The generator relative angles of both fault trajectories corresponding to the above two cases are shown in Figure 6.7 and 6.8 respectively. From Figure 6.8, we see that generator 3 (BUS #73322.0) and generator 5 (BUS #96822.0) become unstable as time increases.

6.2.1.1 Eigen-analysis and Linear Participation Factors

Table 6.17 provides the eigenvalues. From Table 6.17, we see that only mode 6 corresponds to the unstable eigenvalue. The UEP is a type-1 UEP.

6.2.1.2 Normal Form and Nonlinear Participation Factors

Applying the real normal form transformations to the system related to both contingencies, we obtain the nonlinear participation factors, which are shown in Table 6.18.

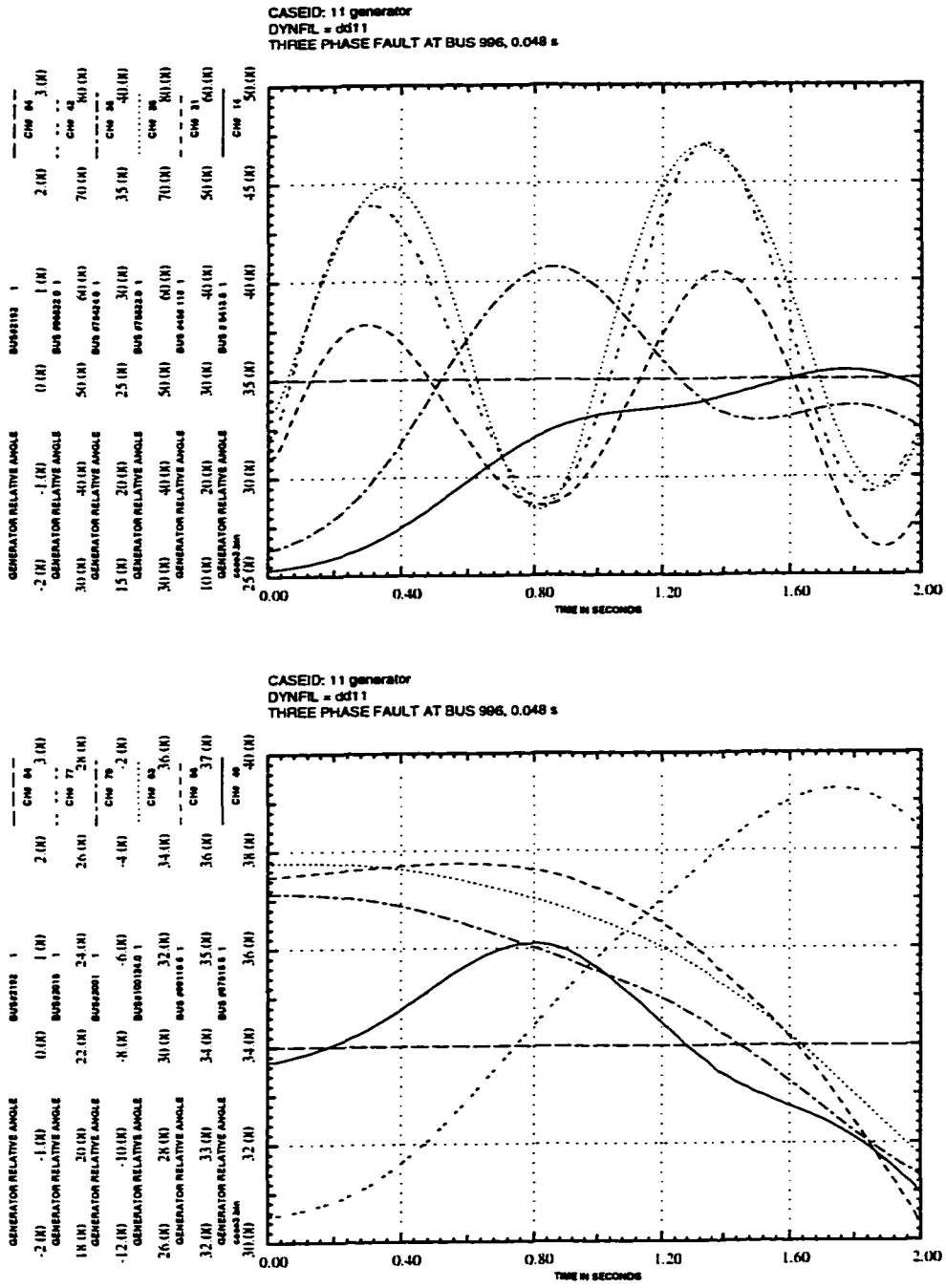

Figure 6.7 Fault Trajectory (generator relative angle) (top: gen.1-5 vs. gen.11 and bottom: gen.6-10 vs. gen.11) (case I) (11gen.)

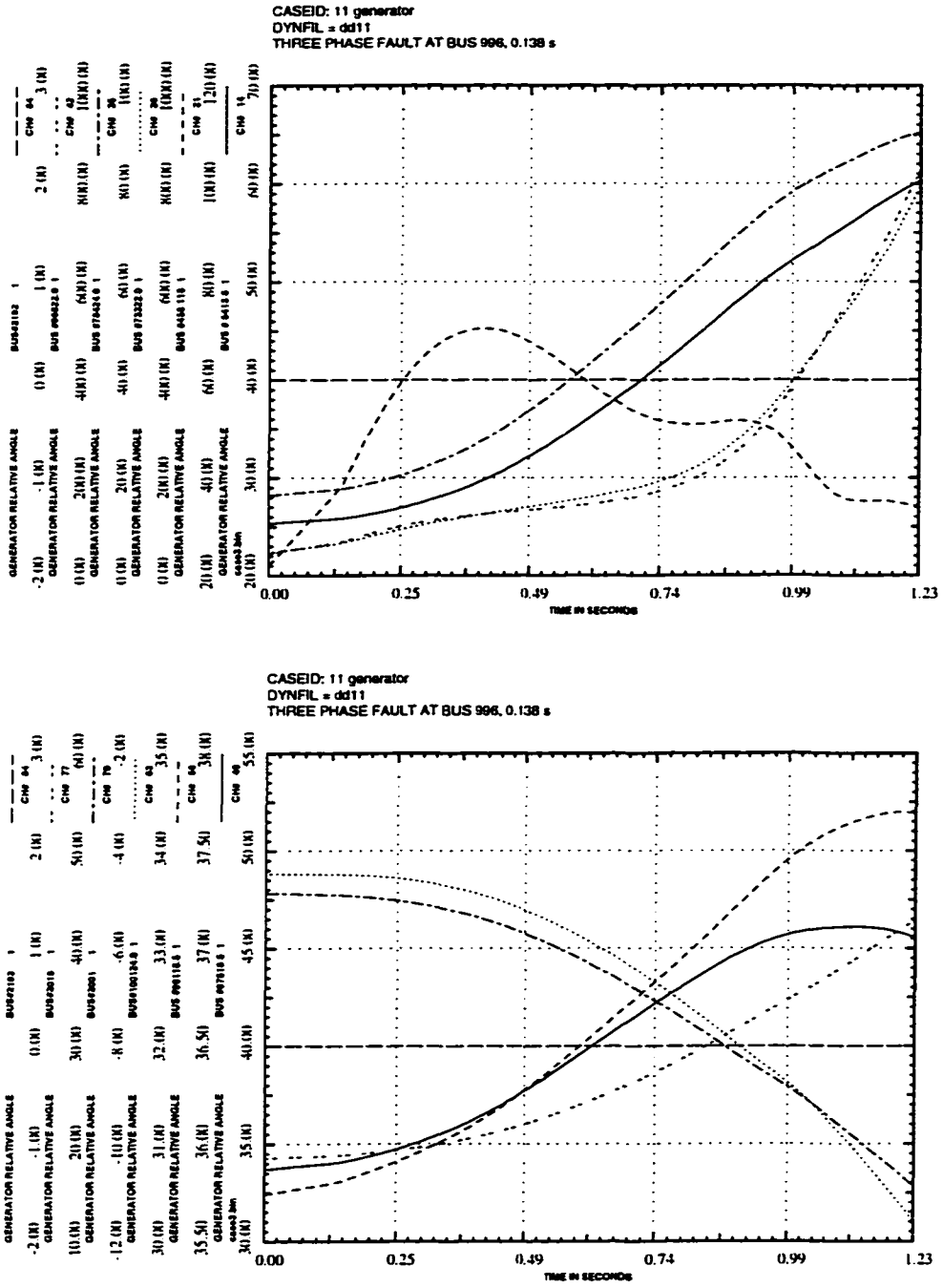

Figure 6.8 Fault trajectory (generator relative angle) (top: gen.1-5 vs. gen.11 and bottom: gen.6-10 vs. gen.11) (case II) (11gen.)

Table 6.15 Physical meaning for each state (11gen.)

State Number	Physical Meaning
1	relative angle δ_{4-11}
2	relative angle δ_{6-11}
3	relative angle δ_{3-11}
4	relative angle δ_{5-11}
5	relative angle δ_{2-11}
6	relative angle δ_{8-11}
7	relative angle δ_{9-11}
8	relative angle δ_{7-11}
9	relative angle δ_{10-11}
10	relative angle δ_{1-11}
11	relative speed ω_{4-11}
12	relative speed ω_{6-11}
13	relative speed ω_{3-11}
14	relative speed ω_{5-11}
15	relative speed ω_{2-11}
16	relative speed ω_{8-11}
17	relative speed ω_{9-11}
18	relative speed ω_{7-11}
19	relative speed ω_{10-11}
20	relative speed ω_{1-11}

6.2.1.3 Structural Information and Nonlinear Index

- Stable case – fault cleared at 0.048s

For this stable case, Table 6.19 shows the nonlinear indices and the dot product Q along the trajectory.

It is observed that from 0.0s-0.3337s, mode 6 the unstable mode is the most dominant mode. Examining the nonlinear participation factors corresponding to this mode, we observe that the machines involved in this mode include generators 3 and 5 which are electrically close to the fault. At 0.3456s, mode 5, the real stable mode becomes the clearly dominant mode and remains dominant for the rest of the time. The stable manifold is not intersected as indicated by the dot product Q and hence the system is stable. This is also verified by the fault trajectory obtained by ETMSP. (Figure 6.7)

Table 6.16 Controlling UEP for 11-generator system

Machine	State	Relative Angles (deg.) and Relative Speeds (rad./s)
δ_{1-11}	10	79.8606
δ_{2-11}	5	74.8615
δ_{3-11}	3	106.2877
δ_{4-11}	1	72.3726
δ_{5-11}	4	104.1500
δ_{6-11}	2	81.3749
δ_{7-11}	8	83.1683
δ_{8-11}	6	81.4884
δ_{9-11}	7	19.6920
δ_{10-11}	9	71.1717
ω_{1-11}	20	0.0000
ω_{2-11}	15	0.0000
ω_{3-11}	13	0.0000
ω_{4-11}	11	0.0000
ω_{5-11}	14	0.0000
ω_{6-11}	12	0.0000
ω_{7-11}	18	0.0000
ω_{8-11}	16	0.0000
ω_{9-11}	17	0.0000
ω_{10-11}	19	0.0000

Table 6.17 Eigenvalues for 11-generator system

Mode	Eigenvalue
1	0.0000+j10.2692
2	0.0000-j10.2692
3	0.0000+j9.5425
4	0.0000-j9.5425
5	-2.2167+j.0000
6	2.2167+j.0000
7	0.0000+j3.0873
8	0.0000-j3.0873
9	0.0000+j5.2285
10	0.0000-j5.2285
11	0.0000+j6.2441
12	0.0000-j6.2441
13	0.0000+j8.1740
14	0.0000-j8.1740
15	0.0000+j7.9122
16	0.0000-j7.9122
17	0.0000+j7.8107
18	0.0000-j7.8107
19	0.0000+j6.9519
20	0.0000-j6.9519

- Unstable case - fault cleared at 0.138s

The nonlinear indices and the dot product Q along the trajectory corresponding to this unstable case are shown in Table 6.20. It is observed that from 0.0s-0.4965s, the most dominant modes are some stable modes 4, 5, 8, 9, 10, 11 and the unstable mode 6 for a while, and at 0.5164s, mode 6 the unstable mode becomes the most dominant mode in terms of the nonlinear interaction, and begins to increase its dominance. The nonlinear participation factors indicate that generator 3 and 5 are the most dominant machines in mode 6, and hence are the most affected. These two generators lose synchronism with respect to the rest of the system. This characteristic is not clear from the information provided by the UEP. The angles corresponding to generators 3 and 5 are the most advanced. However, the other generators except generator 9 also have large angles at

Table 6.18 Nonlinear Participation Factors (11 gen.)(case I)

Mode	State1	State2	State3	State4	State5
	State6	State7	State8	State9	State10
	State11	State12	State13	State14	State15
	State16	State17	State18	State19	State20
1	.000000	.000000	.000000	.000000	.000000
	.000000	.000000	.000000	.000000	.000000
	.016773	.000085	.443588	.441144	.000086
	.000183	.000000	.000237	.000000	.000113
2	.016750	.000004	.443588	.382775	.000082
	.000004	.000000	.000002	.000001	.000004
	.000000	.000000	.000000	.000000	.000000
	.000000	.000000	.000000	.000000	.000000
3	.000000	.000000	.000000	.000000	.000000
	.000000	.000000	.000000	.000000	.000000
	.905154	.000373	.023356	.006199	.054378
	.000169	.000003	.001292	.000933	.016656
4	.905223	.000255	.023348	.000011	.054486
	.000101	.000005	.000023	.000544	.015799
	.000000	.000000	.000000	.000000	.000000
	.000000	.000000	.000000	.000000	.000000
5	.016844	.071964	.068241	.107998	.033572
	.028483	.001013	.043343	.233794	.148198
	.006359	.251818	.064154	.345387	.025533
	.812671	.004190	.826094	.109019	.186434
6	.018058	.086948	.368248	.343338	.034752
	.029169	.001025	.020592	.243309	.147476
	.018862	.295144	.868275	.780416	.036685
	.131127	.000301	.275680	.119105	.457473
7	.000000	.000000	.000000	.000000	.000000
	.000000	.000000	.000000	.000000	.000000
	.000951	.512755	.003789	.030070	.001225
	1.164020	.006277	.534100	.122231	.076122
8	.000639	.175970	.003511	.008055	.001127
	.293861	.006562	.379311	.112356	.052790
	.000000	.000000	.000000	.000000	.000000
	.000000	.000000	.000000	.000000	.000000
9	.016767	.016536	.199238	.024150	.037903
	.015311	.120520	.022883	.396480	.000750
	.000000	.000000	.000000	.000000	.000000
	.000000	.000000	.000000	.000000	.000000

Table 6.18 (Continued)

Mode	State1	State2	State3	State4	State5
	State6	State7	State8	State9	State10
	State11	State12	State13	State14	State15
	State16	State17	State18	State19	State20
10	.000000	.000000	.000000	.000000	.000000
	.000000	.000000	.000000	.000000	.000000
	.017127	.033580	.197648	.201386	.041044
	.133604	.121681	.164385	.394248	.000217
11	.000000	.000000	.000000	.000000	.000000
	.000000	.000000	.000000	.000000	.000000
	.001448	.004558	.029127	.142993	.005065
	.000057	.871904	.001501	.057774	.007049
12	.001461	.000194	.028784	.016883	.004652
	.000045	.871962	.000848	.062705	.007834
	.000000	.000000	.000000	.000000	.000000
	.000000	.000000	.000000	.000000	.000000
13	.000000	.000000	.000000	.000000	.000000
	.000000	.000000	.000000	.000000	.000000
	.001343	.024330	.011708	.030321	.277176
	.035589	.003134	.006748	.151507	.541932
14	.001388	.000392	.011620	.009679	.275588
	.007227	.003072	.000774	.142303	.533775
	.000000	.000000	.000000	.000000	.000000
	.000000	.000000	.000000	.000000	.000000
15	.000000	.000000	.000000	.000000	.000000
	.000000	.000000	.000000	.000000	.000000
	.004494	.003031	.019913	.004652	.053953
	.560130	.000308	.310035	.011327	.027657
16	.004602	.028303	.019888	.008662	.054152
	.558582	.000290	.283068	.011838	.028390
	.000000	.000000	.000000	.000000	.000000
	.000000	.000000	.000000	.000000	.000000
17	.000000	.000000	.000000	.000000	.000000
	.000000	.000000	.000000	.000000	.000000
	.026594	.082805	.138589	.011136	.504993
	.063453	.000792	.012237	.033839	.069395
18	.027022	.018257	.138330	.060607	.506132
	.058250	.000911	.055141	.036815	.073247
	.000000	.000000	.000000	.000000	.000000
	.000000	.000000	.000000	.000000	.000000

Table 6.18 (Continued)

Mode	State1	State2	State3	State4	State5
	State6	State7	State8	State9	State10
	State11	State12	State13	State14	State15
	State16	State17	State18	State19	State20
19	.000000	.000000	.000000	.000000	.000000
	.000000	.000000	.000000	.000000	.000000
	.000000	.725693	.000482	.000242	.000585
	.013605	.000011	.208558	.000039	.000026
20	.000000	.762453	.000523	.000246	.000591
	.014817	.000012	.222243	.000033	.000021
	.000000	.000000	.000000	.000000	.000000
	.000000	.000000	.000000	.000000	.000000

the UEP. Hence, a clear picture of the machines losing synchronism is not provided. The structural information provided by the method of normal forms clearly indicates the mechanism of instability and the machines which will lose synchronism.

The stable manifold is intersected at 0.0607s, which is obtained by interpolation at the point at which Q is equal to zero, and hence the fact that the system is unstable has been verified. Once again, the exit point from the equi-energy surface happens at 0.0539s, which is smaller than 0.0607s. It provides that the energy surface is more conservative than the stable manifold. The unstable phenomena can also be verified by the bottom picture in Figure 6.9.

6.2.1.4 Stable Manifold

Since this time the system is of large size, it is not easy to construct the manifold by spanning all the stable directions. Therefore, we select 5 stable directions and 1 unstable direction to approximate the stability boundary. It is chosen based on the large values of the $h2_r s$, see Table 6.21.

According to the values of $h2_r s$ shown in Table 6.21, in this case, we select 5 major stable modes as the mode 5, 9, 10, 11, 12 and one unstable mode as mode 6. The stable

Table 6.19 Nonlinear Index and Q (11gen.)(case I)

Time(s)	Mode1 Mode2 Mode3 Mode4 Mode5 Mode6 Mode7 Mode8 Mode9 Mode10 Mode11 Mode12 Mode13 Mode14 Mode15 Mode16 Mode17 Mode18 Mode19 Mode20	Q
.0000	.0062 .0450 .0064 .1247 2.0504	2.0212
	2.0504 .0915 1.6807 .5407 .0379	
	.0925 .1571 .0155 .1267 .0041	
	.0288 .0123 .0830 .0006 .0001	
.0120	.0035 .0446 .0141 .1259 1.8387	1.6097
	2.1922 .2008 1.6514 .5467 .0476	
	.0238 .1685 .0890 .1365 .0009	
	.0298 .0110 .0859 .0037 .0026	
.0240	.0136 .0504 .0230 .0766 .1871	1.2055
	2.2635 .3162 1.5637 .7019 .0616	
	.0592 .2847 .1663 .1609 .0057	
	.0199 .0104 .0567 .0077 .0045	
.0360	.0237 .0550 .0329 .0616 .2484	.8048
	2.2661 .4374 1.4175 .9517 .0820	
	.1623 .4320 .2495 .1911 .0237	
	.0202 .0119 .0587 .0120 .0068	
.0480	.0402 .0584 .0438 .0453 .7201	.4110
	2.3385 .5618 1.2806 1.2590 .1281	
	.4224 .6072 .3399 .2269 .0309	
	.0218 .0163 .1832 .0168 .0094	
.0599	.0366 .0569 .0494 .0425 .7273	.4112
	2.3133 .5526 1.2575 1.2816 .1478	
	.4250 .5901 .3544 .2098 .0314	
	.0218 .0180 .0555 .0169 .0108	
.0718	.0394 .0547 .0547 .0402 .7198	.4182
	2.2842 .5401 1.2331 1.2946 .2128	
	.2508 .5676 .3667 .1917 .0316	
	.0201 .0155 .0468 .0169 .0120	
.0837	.0419 .0519 .0596 .0381 .7037	.4291
	2.2530 .5257 1.2081 1.3000 .2751	
	.2291 .5407 .3768 .1727 .0317	
	.0185 .0464 .0381 .0169 .0132	
.0956	.0440 .0486 .0642 .0362 .6743	.4462
	2.2185 .5087 1.1820 1.2971 .3335	
	.4745 .5087 .3844 .1530 .0315	
	.0169 .0572 .0298 .0167 .0143	

Table 6.19 (Continued)

Time(s)	Mode1 Mode2 Mode3 Mode4 Mode5 Mode6 Mode7 Mode8 Mode9 Mode10 Mode11 Mode12 Mode13 Mode14 Mode15 Mode16 Mode17 Mode18 Mode19 Mode20	Q
.1075	.0457 .0448 .0682 .0346 .6346 2.1817 .4897 1.1553 1.2867 .3874 .5096 .4731 .3895 .1328 .0312 .0155 .0669 .0217 .0078 .0153	.4682
.1194	.0471 .0407 .0720 .0332 .5890 2.1439 .4697 1.1285 1.2704 .4372 .5401 .4353 .3923 .1123 .0308 .0140 .0753 .0139 .0071 .0161	.4932
.1313	.0481 .0361 .0752 .0323 .5317 2.1033 .4477 1.1012 1.2475 .4815 .5653 .3942 .3925 .0915 .0302 .0128 .0823 .0068 .0064 .0169	.5243
.1432	.0486 .0313 .0779 .0315 .4679 2.0630 .4247 1.0784 1.2192 .5206 .5851 .3508 .3902 .0708 .0296 .0116 .0876 .0001 .0057 .0176	.5596
.1551	.0488 .0263 .0803 .0310 .3982 2.0507 .4010 1.0674 1.1866 .5545 .5997 .3060 .3854 .0503 .0289 .0106 .0913 .0060 .0050 .0184	.5991
.1670	.0486 .0213 .0821 .0308 .3209 2.0387 .3762 1.0576 1.1497 .5824 .6087 .2596 .3781 .0303 .0281 .0097 .0934 .0113 .0043 .0196	.6439
.1789	.0482 .0162 .0837 .0308 .2423 2.0263 .3516 1.0484 1.1105 .6057 .6129 .2135 .3687 .0823 .0273 .0090 .0071 .0162 .0035 .0207	.6911
.1908	.0474 .0113 .0849 .0310 .1605 2.0134 .3269 1.0400 1.0692 .6236 .6121 .1677 .3572 .0985 .0266 .0084 .0114 .0203 .0027 .0217	.7419
.2027	.0463 .0127 .0857 .0316 .0758 1.9997 .3021 1.0326 1.0263 .6362 .6065 .1226 .3437 .1138 .0259 .0080 .0160 .0237 .0020 .0225	.7968

Table 6.19 (Continued)

Time(s)	Mode1 Mode6 Mode11 Mode16	Mode2 Mode7 Mode12 Mode17	Mode3 Mode8 Mode13 Mode18	Mode4 Mode9 Mode14 Mode19	Mode5 Mode10 Mode15 Mode20	Q
.2146	.0448	.0141	.0861	.0324	.0116	.8563
	1.9850	.2772	1.0262	.9824	.6437	
	.5960	.0782	.3281	.1283	.0251	
	.0078	.0206	.0263	.0012	.0232	
.2265	.0432	.0152	.0864	.0334	.0977	.9179
	1.9689	.2529	1.0202	.9383	.6472	
	.5819	.0357	.3110	.1417	.0244	
	.0078	.0257	.0283	.0004	.0237	
.2384	.0412	.0062	.0862	.0323	.1855	.9842
	1.9511	.2287	.5217	.8944	.6456	
	.5634	.2738	.2922	.1541	.0238	
	.0079	.0308	.0296	.0003	.0241	
.2503	.0391	.0098	.0859	.0276	.2722	1.0534
	1.9315	.2049	.5015	.8650	.6404	
	.5415	.2839	.2721	.1652	.0231	
	.0081	.0359	.0302	.0011	.0244	
.2622	.0367	.0129	.0856	.0234	.3556	1.1241
	1.9102	.1821	.4845	.8608	.6322	
	.5169	.2921	.2510	.1752	.0226	
	.0085	.0412	.0302	.0019	.0246	
.2741	.0341	.0156	.0850	.0200	1.4404	1.1987
	1.8866	.1597	.4710	.8550	.6201	
	.4890	.2985	.2286	.1838	.0222	
	.0090	.0465	.0295	.0027	.0247	
.2860	.0312	.0179	.0842	.0173	1.4907	1.2767
	1.8608	.1375	1.0018	.8478	.6049	
	.4589	.3030	.2054	.1910	.0217	
	.0097	.0516	.0282	.0035	.0246	
.2980	.0283	.0198	.0835	.0154	1.5375	1.3547
	1.8333	.1166	.9999	.8395	.5881	
	.4273	.3059	.1819	.1969	.0214	
	.0101	.0568	.0276	.0042	.0245	
.3099	.0250	.0213	.0826	.0142	1.5833	1.4369
	1.8032	.0958	.9990	.8300	.5682	
	.3933	.3070	.1576	.2013	.0218	
	.0096	.0616	.0283	.0050	.0243	

Table 6.19 (Continued)

Time(s)	Mode1	Mode2	Mode3	Mode4	Mode5	Q
	Mode6	Mode7	Mode8	Mode9	Mode10	
	Mode11	Mode12	Mode13	Mode14	Mode15	
	Mode16	Mode17	Mode18	Mode19	Mode20	
.3218	.0216	.0223	.0816	.0139	1.6269	1.5209
	1.7709	.0757	.9986	.8194	.5465	
	.3583	.3064	.1330	.2043	.0222	
	.0093	.0662	.0290	.0057	.0240	
.3337	.0181	.0229	.0805	.0143	1.6675	1.6059
	1.7369	.0562	.9988	.8078	.5233	
	.3224	.3044	.1083	.2058	.0225	
	.0091	.0705	.0293	.0065	.0236	
.3456	.0144	.0232	.0793	.0156	1.7057	1.6927
	1.7009	.0371	.9997	.7952	.4989	
	.2859	.3008	.0836	.2058	.0226	
	.0092	.0744	.0288	.0072	.0231	
.3575	.0135	.0271	.0623	.0177	1.7411	1.7798
	1.6634	.1153	1.0012	.7816	.2494	
	.2331	.3019	.1201	.2044	.0173	
	.0095	.0428	.0275	.0018	.0229	
.3694	.0126	.0275	.0585	.0173	1.7739	1.8676
	1.6245	.1345	1.0034	.7670	.2662	
	.2574	.3055	.1390	.2016	.0174	
	.0100	.0400	.0253	.0011	.0227	
.3813	.0111	.0276	.0540	.0151	1.8035	1.9540
	1.5854	.1538	1.0062	.7514	.2811	
	.2789	.0728	.1569	.1975	.0175	
	.0107	.0372	.0224	.0003	.0225	
.3932	.0100	.0274	.0492	.0133	1.8310	2.0416
	1.5449	.1739	1.0096	.7348	.2950	
	.2980	.0474	.1739	.1919	.0176	
	.0113	.0346	.0190	.0004	.0221	
.4051	.0091	.0268	.0439	.0118	1.8562	2.1283
	1.5040	.1942	1.0136	.7376	.3064	
	.3138	.0195	.1896	.1850	.0177	
	.0113	.0321	.0155	.0011	.0217	
.4170	.0096	.0259	.0382	.0107	1.8792	2.2143
	1.4629	.2150	1.0183	.7557	.3159	
	.3265	.0101	.2042	.1769	.0177	
	.0115	.0298	.0112	.0018	.0212	

Table 6.19 (Continued)

Time(s)	Mode1 Mode2 Mode3 Mode4 Mode5 Mode6 Mode7 Mode8 Mode9 Mode10 Mode11 Mode12 Mode13 Mode14 Mode15 Mode16 Mode17 Mode18 Mode19 Mode20	Q
.4289	.0111 .0247 .0319 .0101 1.9001	2.2981
	1.4226 .2358 1.0236 .7739 .3225	
	.3351 .0414 .2172 .1677 .0178	
	.0119 .0275 .0103 .0024 .0205	
.4408	.0123 .0232 .0254 .0098 1.9190	2.3796
	.3520 .2566 1.0296 .7917 .3264	
	.3400 .0733 .2288 .1573 .0178	
	.0124 .0255 .0102 .0030 .0198	
.4527	.0133 .0214 .0184 .0102 1.9361	2.4560
	.2895 .2772 1.0362 .8082 .3260	
	.3402 .1059 .2387 .1460 .0178	
	.0127 .0235 .0096 .0036 .0189	
.4646	.0140 .0194 .0112 .0109 1.9520	2.5314
	.2276 .2979 1.0435 .8237 .3234	
	.3365 .1391 .2471 .0133 .0179	
	.0123 .0219 .0089 .0041 .0179	
.4765	.0144 .0174 .0039 .0122 1.9669	2.6026
	.1693 .3183 1.0514 .8372 .3171	
	.3281 .1719 .2538 .0009 .0179	
	.0121 .0205 .0077 .0045 .0168	
.4884	.0146 .0153 .0036 .0139 1.9808	2.6693
	.1153 .3381 1.0601 .8480 .3074	
	.0058 .2044 .2587 .0116 .0179	
	.0119 .0193 .0061 .0050 .0156	
.5003	.0144 .0132 .0626 .0163 1.9939	2.7290
	.0682 .3568 1.0696 .8553 .2933	
	.0259 .2349 .2619 .0243 .0179	
	.0119 .0182 .0041 .0053 .0148	
.5122	.0141 .0005 .0585 .0191 2.0068	2.7851
	.0246 .3750 1.0798 .8594 .2763	
	.0462 .2641 .2695 .0371 .0180	
	.0119 .0176 .0018 .0056 .0141	
.5241	.0134 .0018 .0530 .0226 2.0195	2.8324
	.0099 .3915 1.0909 .8585 .2551	
	.0670 .2907 .2784 .0497 .0180	
	.0122 .0169 .0011 .0059 .0132	

Table 6.19 (Continued)

Time(s)	Mode1	Mode2	Mode3	Mode4	Mode5	Q
	Mode6	Mode7	Mode8	Mode9	Mode10	
	Mode11	Mode12	Mode13	Mode14	Mode15	
	Mode16	Mode17	Mode18	Mode19	Mode20	
.5360	.0125	.0045	.0464	.0264	2.0322	2.8755
	.0398	.4072	1.1025	.8535	.2312	
	.0877	.3151	.2858	.0622	.0180	
	.0125	.0166	.0043	.0061	.0123	
.5479	.0114	.0073	.0406	.0307	2.0451	2.9092
	.0598	.4206	1.1153	.8427	.2038	
	.1088	.3355	.2915	.0744	.0180	
	.0129	.0165	.0081	.0125	.0113	
.5598	.0102	.0067	.0474	.0354	2.0583	2.9383
	.0747	.4329	1.1285	.8272	.1742	
	.2929	.3535	.2957	.0862	.0180	
	.0134	.0165	.0120	.0122	.0102	
.5717	.0087	.0068	.0537	.0406	2.0719	2.9564
	.0778	.4425	1.1429	.8051	.1416	
	.1086	.3662	.2983	.0976	.0179	
	.0142	.0166	.0166	.0118	.0091	
.5836	.0072	.0073	.0597	.0460	2.0860	2.9687
	.0748	.4503	1.1577	.7776	.1075	
	.0660	.3760	.2994	.1084	.0080	
	.0150	.0122	.0214	.0113	.0079	
.5955	.0054	.0086	.0652	.0518	2.1004	2.9705
	.0604	.4551	1.1736	.7436	.1117	
	.0216	.3797	.2987	.1187	.0109	
	.0159	.0029	.0266	.0107	.0066	
.6074	.0036	.0105	.0701	.0578	2.1152	2.9635
	.0370	.4573	1.1902	.7034	.1166	
	.0242	.3793	.2965	.1283	.0138	
	.0169	.0065	.0321	.0100	.0053	
.6193	.0018	.0131	.0747	.0639	2.1300	2.9489
	.0058	.4570	1.2073	.6579	.1206	
	.0708	.3740	.2927	.1372	.0151	
	.0181	.0158	.0378	.0093	.0039	

Table 6.20 Nonlinear Index and Q (11gen.)(case II)

Time(s)	Mode1	Mode2	Mode3	Mode4	Mode5	Q
	Mode6	Mode7	Mode8	Mode9	Mode10	
	Mode11	Mode12	Mode13	Mode14	Mode15	
	Mode16	Mode17	Mode18	Mode19	Mode20	
.0000	.0062	.0450	.0064	.1247	2.0504	2.0212
	2.0504	.0915	1.6807	.5407	.0379	
	.0925	.1571	.0155	.1267	.0041	
	.0288	.0123	.0830	.0006	.0001	
.0184	.0089	.0479	.0187	.0831	1.6980	1.3931
	1.2389	.2617	1.6119	.6063	.0545	
	.5183	.2266	.1296	.1487	.0035	
	.0202	.0105	.0897	.0058	.0036	
.0368	.0244	.0552	.0336	.0606	.2768	.7795
	1.2639	.4453	1.4059	.9700	.0834	
	1.1699	.4423	.2552	.1934	.0242	
	.0203	.0120	.0589	.0123	.0069	
.0552	.0435	.0600	.0508	.0347	.4704	.1768
	1.4755	.6375	1.2380	1.4697	.1634	
	1.4940	.7259	.3984	.2506	.0352	
	.0741	.0203	.2208	.0199	.0111	
.0736	.5375	.3614	1.5767	.3204	.6739	-.4156
	1.4440	1.1842	2.7126	.5646	.1607	
	1.1379	1.0743	.7675	.4629	.2585	
	.1151	.5793	.4088	.0424	.0188	
.0920	.1345	.0673	.0602	1.4424	.7643	-1.0017
	.8892	1.2870	.0005	.4028	.0491	
	1.2518	.5172	.7936	1.2891	.0341	
	.1757	.1790	.4681	.1079	.0570	
.1104	.0839	.3944	.3461	1.7033	.8387	-1.5897
	.7282	.4994	2.7766	1.3428	.0548	
	.2922	.3460	.8238	.2740	.3454	
	.0450	.9712	.0637	.0536	.0112	
.1288	.0204	.7530	1.7753	.2329	.8985	-2.1888
	.8615	.3403	.3819	2.1791	.1392	
	.1340	.7763	.4990	1.5768	.0047	
	.1004	.0478	.1891	.0070	.0240	
.1380	.2643	.8072	.9019	.6389	.9455	-2.4962
	.9902	.5407	2.0980	2.8458	.4497	
	.2424	.4428	.8788	.0829	.3150	
	.2282	.8946	.6912	.0482	.0606	

Table 6.20 (Continued)

Time(s)	Mode1 Mode6 Mode11 Mode16	Mode2 Mode7 Mode12 Mode17	Mode3 Mode8 Mode13 Mode18	Mode4 Mode9 Mode14 Mode19	Mode5 Mode10 Mode15 Mode20	Q
.1579	.5271	.5571	.4876	2.2887	.9802	-2.5022
	1.1140	.6867	1.3445	3.2786	.9246	
	1.0954	.5167	.1788	1.7847	.0611	
	.0410	.3343	.0041	.0898	.0730	
.1778	.5364	.2036	.4653	1.8466	1.0061	-2.5153
	1.2356	1.3730	1.0445	3.4998	1.4656	
	1.8062	1.5452	.8930	.0951	.1913	
	.3661	.4234	.9998	.0131	.0022	
.1977	.2309	.0125	1.4877	.4802	1.0241	-2.5375
	1.3556	1.2574	2.3929	3.4677	2.0010	
	1.8423	2.0327	.1150	1.9129	.1706	
	.0506	.7615	.2285	.0302	.0075	
.2177	.2067	.0944	.0914	1.4284	1.0345	-2.5683
	1.4739	1.5331	.2489	3.1999	2.4591	
	1.1110	1.6855	.8379	.2546	.0290	
	.3940	.0024	.8518	.0342	.0885	
.2376	.5751	.4108	.8386	2.7259	1.0416	-2.6076
	1.5950	1.0429	2.9198	2.7363	2.7743	
	.0201	.8165	.4389	1.9453	.2505	
	.1511	.8710	.8052	.0486	.0715	
.2575	.6478	.7271	.5318	1.6430	1.0435	-2.6556
	1.7158	.9162	.1327	2.1347	2.8703	
	.8064	.0395	.7878	.3928	.0835	
	.3262	.0496	.5021	.0393	.0061	
.2774	.4192	.7992	.9263	.5975	1.0429	-2.7100
	1.8397	.1880	2.6716	1.5334	2.7838	
	.8486	.1015	.7389	1.9069	.2339	
	.3084	.4986	1.2888	.0621	.0236	
.2973	.0863	.5648	.7650	1.9274	1.0406	-2.7717
	1.9674	.1354	.7896	.8648	2.4590	
	.2044	.5074	.6881	.4778	.1064	
	.2107	.2654	.4079	.0061	.0906	
.3172	.0846	.1212	1.0840	2.6279	1.0381	-2.8392
	2.1004	.8493	1.7671	.2685	1.9071	
	.6156	1.5153	.9853	1.7608	.1084	
	.4387	.0848	1.3129	.0070	.0434	

Table 6.20 (Continued)

Time(s)	Mode1 Mode2 Mode3 Mode4 Mode5 Mode6 Mode7 Mode8 Mode9 Mode10 Mode11 Mode12 Mode13 Mode14 Mode15 Mode16 Mode17 Mode18 Mode19 Mode20	Q
.3371	.0189 .2699 .4188 1.0485 1.0357	-2.9141
	2.2395 1.0755 1.8399 .1928 1.1624	
	.9893 2.1791 .5904 .5552 .0477	
	.1343 .5119 .7278 .0977 .0278	
.3571	.3620 .3886 .1325 .5736 1.0356	-2.9947
	2.3879 1.4455 .7467 .4726 .3444	
	.5436 2.0881 1.2065 1.5316 .0745	
	.4679 .4645 .9129 .0962 .0151	
.3770	.7116 .2050 1.5616 2.0295 1.0371	-3.0824
	2.5438 1.3618 2.7223 .5538 .6028	
	.4769 1.2806 .4722 .5662 .0199	
	.1353 .3482 1.2075 .0298 .0622	
.3969	.8202 .1017 1.1893 2.0119 1.0418	-3.1799
	2.7102 1.2876 .1526 .4381 1.5500	
	1.4829 .2570 1.3698 1.2695 .2498	
	.3772 .3876 .4960 .0669 .0109	
.4168	.5976 .2624 .2025 .2460 1.0504	-3.2884
	2.8882 .8545 2.9550 .1315 2.4188	
	1.8912 .3559 .3414 .5809 .0340	
	.2102 .2354 1.3749 .1499 .0697	
.4367	.2015 .1515 .6878 .3436 1.0637	-3.4090
	3.0797 .4260 .3390 .3252 3.1396	
	1.4731 .1647 1.4770 .9144 .3367	
	.2022 .1030 .4373 .1218 .0158	
.4566	.1739 .2192 2.0865 1.7187 1.0829	-3.5461
	3.2876 .1336 2.4039 .8736 3.6342	
	.6181 .6079 .2051 .5681 .0561	
	.2853 .8101 1.0344 .0636 .0046	
.4765	.2848 .6268 1.0665 .9534 1.1081	-3.7016
	3.5110 .6429 1.1856 1.3764 3.9310	
	.0508 1.3824 1.5156 .5179 .3226	
	.0293 .0118 .7230 .1190 .0876	
.4965	.0970 .8148 .0653 .7149 1.1406	-3.8795
	3.7532 1.0574 1.3606 1.9027 3.9713	
	.0330 1.5705 .0643 .4883 .2194	
	.2971 .9988 .4058 .1863 .1277	

Table 6.20 (Continued)

Time(s)	Mode1 Mode6 Mode11 Mode16	Mode2 Mode7 Mode12 Mode17	Mode3 Mode8 Mode13 Mode18	Mode4 Mode9 Mode14 Mode19	Mode5 Mode10 Mode15 Mode20	Q
.5164	.2152	.6893	1.4051	.0636	1.1807	-4.0844
	4.0156	1.3651	2.2530	2.3152	3.7630	
	.7118	.9636	1.5061	.1394	.2391	
	.0839	.3731	.9492	.1328	.0685	
.5363	.3807	.3252	2.2700	.9597	1.2303	-4.3207
	4.3017	1.4022	.4410	2.5544	3.3372	
	1.7340	.1704	.0485	.4292	.3963	
	.1897	.7580	.0354	.0869	.0767	
.5562	.2734	.0293	.8105	.4406	1.2877	-4.5945
	4.6127	1.3221	2.9116	2.5778	2.7438	
	2.4044	1.1024	1.4109	.2853	.1640	
	.1115	.9409	.7608	.1546	.1758	
.5761	.0998	.1406	.3250	1.6762	1.3555	-4.9120
	4.9495	.9617	.1267	2.3645	2.1176	
	2.2550	1.3508	.1735	.3536	.4934	
	.0121	.4081	.0589	.1949	.1951	
.5960	.5180	.0487	1.8525	.5709	1.4331	-5.2804
	5.3148	.5609	2.8258	1.9485	1.3887	
	1.4317	.8525	1.2488	.6595	.1592	
	.0812	1.2880	.1213	.1218	.1341	
.6159	.7211	.3556	2.0261	.0571	1.5198	-5.7092
	5.7096	.0099	.6077	1.3130	.6970	
	.4783	.0374	.2502	.2342	.4700	
	.2500	.3731	.1641	.0885	.1685	
.6359	.6097	.5854	.3506	1.7963	1.6159	-6.2088
	6.1360	.5267	2.0181	.5148	.1078	
	.0097	.4687	1.0645	1.0389	.2304	
	.0685	1.0986	.5493	.1594	.2640	
.6558	.2548	.5207	.4404	2.4062	1.7221	-6.7927
	6.5965	.9943	1.5998	.3821	.3248	
	.3406	.1830	.3400	.1472	.3339	
	.4295	.6816	.1847	.1672	.2554	
.6757	.1001	.1700	1.9304	.9958	1.8357	-7.4776
	7.0923	1.3064	.9647	1.3026	.5683	
	1.1844	.7615	.7946	1.3661	.3320	
	.1356	.5643	.8518	.0781	.1986	

manifold is constructed by spanning those selected stable modes. The unstable manifold is corresponding to mode 6.

The critical machines, i.e., generator 3 and generator 5, together with generator 1 are selected for plotting the picture of the stable manifold. The stable manifold and unstable manifold, along with the unstable trajectory are displayed in Figure 6.9.

In the pictures in Figure 6.9, the stable manifold is displayed in blue, the unstable manifold in green and the trajectory in red. The axis tree at lower left describes the Euclidean projection from 6-space. The first three axes (Var1, Var2, Var3) represent three relative angles, i.e., δ_{1-11}, δ_{3-11} and δ_{5-11}. The other three axes (Var4, Var5, Var6) represent three relative speeds, i.e., ω_{1-11}, ω_{3-11} and ω_{5-11}. It is easy to see that in the top picture (the stable case), the trajectory approaches to the stable manifold and comes back without passing through it while in the bottom picture (the unstable case), the trajectory goes to the stable manifold and passes through it and leaves.

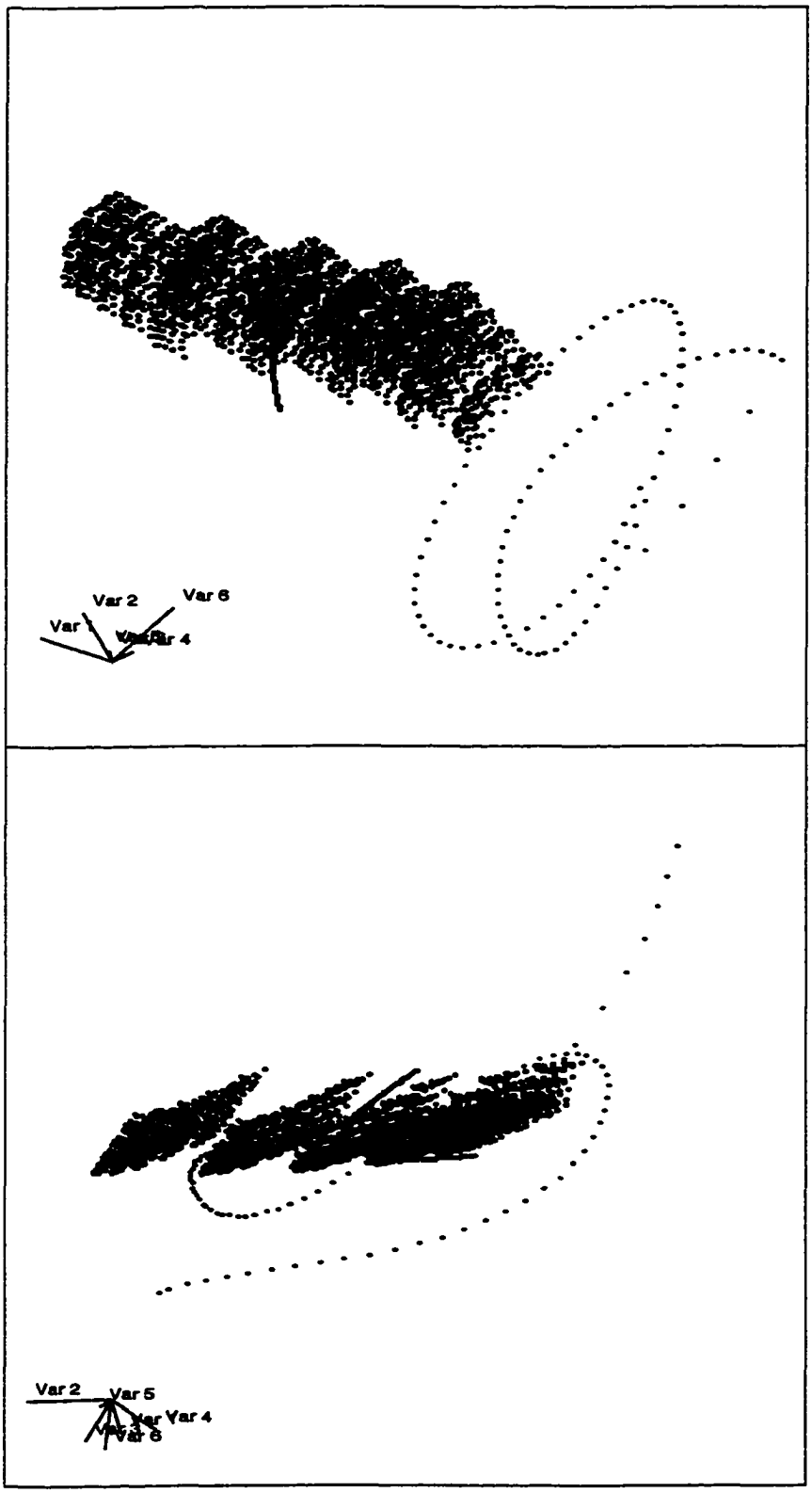

Figure 6.9 Second order approximation (top: stable case and bottom: unstable case) (11 gen.)

Table 6.21 A few big $h2_r$ coefficients for 11gen. system

Mode	Mode	Mode	$h2_r$
5	5	5	.091
5	5	6	.183
5	5	7	-.051
6	5	6	-.183
6	6	6	-.091
6	6	7	.051
7	7	12	-.071
7	8	11	.073
7	9	13	-.098
7	10	14	-.103
8	5	6	-.095
8	7	11	.070
8	8	12	.071
8	9	14	-.105
8	10	13	.106
9	5	10	.080
9	6	10	.080
9	7	13	-.226
9	8	14	-.219
10	5	9	-.087
10	6	9	-.087
10	7	14	-.223
10	8	13	.209
11	5	12	.165
11	6	12	.165
11	7	8	.275
11	7	12	-.059
12	5	11	-.155
12	6	11	-.155
12	7	7	-.136
12	7	11	.067
12	8	8	.142
12	10	11	.061
13	5	14	.054
13	6	14	.054
14	5	13	-.052
14	6	13	-.052

7 CONCLUSIONS AND SCOPE OF FUTURE WORK

7.1 Conclusions and Discussions

This research work aims at analyzing and explaining the nonlinear phenomena in stressed power systems and characterizing the stability boundary of the power system when subjected to large disturbances. It presents the use of real normal forms of vector fields, a comparatively new analysis tool in the area of power systems, combined with the use of XGobi, an effective graphic package for multi-dimensional visualization, to investigate and visualize the stability boundary of the stressed system. It also depicts the structural characteristics for the stressed power system corresponding to specific fault scenarios by computing the nonlinear participation factors and the nonlinear indices along the actual fault trajectory obtained from time simulation of the equations governing system dynamics.

The results on the IEEE 4-generator system and the 11-generator system describe the proposed approaches well and the structural information provided by computing nonlinear participation factors and nonlinear index $I1$ along the fault trajectory is verified by the results from time simulation and the visualization of the stability boundary, together with the fault trajectory.

The results obtained lead to the following conclusions:

- This research work developed a new method to approximate the stability boundary of stressed power systems by computing the second order stable manifold of the controlling UEP using real normal form technique. The stable manifold is

constructed by spanning all the stable directions. This approximation is more accurate than the one approximated merely by some eigen-directions.

- An extended approach allows us to deal with large sized power systems. Some critical stable modes related to large values of $h2_r s$ are selected to construct the stable manifold and the energy surface in order to reduce the computational burden. This extension provides an effective way to study large sized systems, which are the standard situation in practical power system, without losing important nonlinear information.

- The effective graphic tool XGobi allows us to visualize the stability boundary together with the unstable manifold and fault trajectory in all dimensions of the system, which helps to obtain a global structural information of the system. The shape and curvature of the stability boundary approximated by the two approaches, i.e., stable manifold and energy surface, are observed.

- The combination of the nonlinear participation factors and the nonlinear indices of the fault trajectory obtained by ETMSP provides the basis to study the structural characteristics of the system. It allows us to identify the important modes along the fault trajectory, which provides information regarding system dynamic behavior. Once the unstable mode becomes the clearly dominant mode indicated by the value of $I1$ corresponding to this unstable mode becomes large, the system loses synchronism. On the other hand, when the stable mode, usually the real stable mode becomes the dominant mode indicates that the system remains stable. It also allows us to identify the critical machines corresponding to specific contingencies, which sometimes can't be predicted by the time simulation or controlling UEP. This information could be used to develop effective control and special protection schemes which would include generation rejection and the generators leading to lose synchronism.

- The exit points of the fault trajectory from both approximations allow us to check the accuracy of the approximations, whether the approximation is conservative or optimistic, which one is better?

- It has been shown that the energy surface method is more conservative than the stable manifold method according to the comparison of the exit points from these two different approximations, and the trajectory clings close to the stable manifold than it does to the energy surface, from visualization of the two approximations via XGobi.

7.2 Scope of Future Work

Based on the experience of this research work, the following suggestions are made for further research work:

1. Sparse techniques can be used to compute the homological operator La since it is very sparse. By doing so, a lot of computational storage and time can be saved. Therefore, larger systems can be easily handled.

2. Perform the $3rd$ order real normal form transformation to improve the accuracy of the approximation.

3. The mathematical foundation of structural characteristics for stressed power systems needs further study.

APPENDIX A DATA FOR 4-GENERATOR 11-BUS TEST SYSTEM

Table A.1 Dynamic data for 4 generators

Bus#	Machine#	H(MW/MVA)	$x'_d(p.u.)$
1	3	3.01	0.1813
2	2	6.40	0.1198
3	4	6.40	0.1198
4	1	23.64	0.0608

Table A.2 Power flow data for 11 buses

Bus #	Bus name	|V| p.u.	Angle(V) degree	P_{load} MW	Q_{load} MVAR	P_{gen} MW	Q_{gen} MVAR
1	GEN3	1.0350	-.85	.00	.00	100.00	36.15
2	GEN2	1.0350	3.82	.00	.00	160.00	44.14
3	GEN4	1.0350	15.03	.00	.00	160.00	19.66
4	GEN1	1.0400	.00	.00	.00	226.73	83.05
5	STA 'A'	.9692	-11.78	200.00	80.00	.00	.00
6	STA 'B'	.9634	-14.19	230.00	77.00	.00	.00
7	BUS7	1.0129	-1.66	.00	.00	.00	.00
8	STA 'C'	.9960	-3.61	200.00	70.00	.00	.00
9	BUS9	1.0160	-4.04	.00	.00	.00	.00
10	BUS10	1.0277	9.85	.00	.00	.00	.00
11	BUS4	1.0018	-7.21	.00	.00	.00	.00

Table A.3 Power flow data for branches(4gen.)

Bus #	Bus #	R p.u.	X p.u.	B p.u.	off-norminal tap
11	6	.017000	.092000	.03794	.0000
5	11	.010000	.085000	.04226	.0000
6	9	.0390000	.170000	.08596	.0000
7	5	.0320000	.161000	.07347	.0000
7	8	.008500	.072000	.03577	.0000
8	10	.035700	.302400	.15054	.0000
8	10	.035700	.302400	.15054	.0000
9	8	.011900	.100800	.05018	.0000
4	11	.000000	.057600	.00000	1.0000
2	7	.000000	.062500	.00000	1.0000
1	9	.000000	.058600	.00000	1.0000
3	10	.000000	.060000	.00000	1.0000

APPENDIX B POWER FLOW GENERATOR BUS DATA FOR 11-GENERATOR 55-BUS TEST SYSTEM

Table B.1 Dynamic data for 11 generators

Bus#	Machine#	H(MW/MVA)	$x'_d(p.u.)$
54	GEN1	241.000	.00393
458	GEN2	74.400	.01280
733	GEN3	73.850	.01220
784	GEN4	28.140	.06233
968	GEN5	73.850	.01220
975	GEN6	57.520	.04803
991	GEN7	115.040	.02402
1001	GEN8	105.792	.01797
2001	GEN9	109.960	.00848
2018	GEN10	207.230	.00451
2192	GEN11	9344.170	.00010

Table B.2 Power flow data for 55 buses

Bus #	|V| p.u.	Angle(V) degree	P_{load} MW	Q_{load} MVAR	P_{gen} MW	Q_{gen} MVAR
3	1.0643	32.06	-4.85	-90.83	0.00	0.00
5	1.0769	32.45	250.39	480.10	0.00	0.00
7	1.0890	32.44	228.02	77.17	0.00	0.00
8	1.0670	34.67	6.35	221.21	0.00	0.00
24	1.0623	16.00	341.12	244.28	0.00	0.00
30	1.1049	14.78	432.69	111.05	0.00	0.00
33	1.1064	23.04	497.84	-88.98	0.00	0.00
37	1.1276	32.15	235.69	-12.89	0.00	0.00
39	1.1320	34.32	43.70	-6.79	0.00	0.00
40	1.1320	34.29	43.80	-6.88	0.00	0.00
43	1.1118	34.66	45.88	3.64	0.00	0.00
44	1.1131	34.45	45.87	3.64	0.00	0.00
47	1.1040	36.73	945.23	-374.91	0.00	0.00

Table B.2 (Continued)

Bus #	|V| p.u.	Angle(V) degree	P_{load} MW	Q_{load} MVAR	P_{gen} MW	Q_{gen} MVAR
48	1.1255	47.02	71.72	186.88	0.00	0.00
54	1.0909	40.35	4114.20	1365.20	6357.47	2104.43
80	1.0440	30.61	920.78	-75.58	0.00	0.00
140	1.1274	32.46	18.08	10.25	0.00	0.00
141	1.1274	32.46	17.98	10.22	0.00	0.00
142	1.1293	33.72	19.72	13.77	0.00	0.00
143	1.1293	33.72	19.70	13.80	0.00	0.00
144	1.1347	35.19	40.54	30.29	0.00	0.00
145	1.1578	43.57	30.77	-3.79	0.00	0.00
146	1.1578	43.57	30.86	-3.81	0.00	0.00
148	1.1352	32.77	17.18	9.37	0.00	0.00
149	1.1352	32.77	17.18	9.37	0.00	0.00
150	1.1363	32.26	233.50	31.41	0.00	0.00
226	1.1792	49.25	0.00	0.00	0.00	0.00
288	1.1704	46.14	52.18	-3.29	0.00	0.00
297	1.1088	29.30	2049.10	-667.91	0.00	0.00
458	1.0667	37.54	644.56	285.91	1669.37	168.14
617	1.1503	42.46	38.70	2.76	0.00	0.00
618	1.1506	42.49	38.66	2.74	0.00	0.00
644	1.0614	15.71	115.54	-537.09	0.00	0.00
733	1.0000	56.47	31.64	20.00	2499.20	406.92
784	1.0000	28.40	887.73	926.25	500.00	397.65
963	1.0406	32.88	0.00	0.00	0.00	0.00
967	1.0674	48.21	-8.41	-156.82	0.00	0.00
968	1.0000	54.84	31.64	20.00	2499.20	907.55
975	1.0000	51.69	28.00	29.00	300.00	35.27
977	1.1819	48.14	22.10	-7.04	0.00	0.00
989	1.0985	51.70	0.00	0.00	0.00	0.00
991	1.0000	53.84	57.00	59.00	600.00	128.16
992	1.1787	48.88	0.00	0.00	0.00	0.00
993	1.0379	32.72	193.17	378.30	0.00	0.00
994	1.0379	32.72	190.93	374.18	0.00	0.00
996	1.0430	31.96	-7.12	-107.08	0.00	0.00
1000	1.0988	51.75	0.00	0.00	0.00	0.00
1001	1.0000	53.19	360.00	360.00	700.00	440.16
1060	1.1763	49.07	2.73	2.12	0.00	0.00
1106	0.9817	26.99	184.83	199.34	0.00	0.00
2001	0.9664	7.21	2632.00	498.53	2827.60	244.89
2018	1.0895	33.96	4244.60	805.48	5329.50	2022.65

Table B.2 (Continued)

Bus #	|V| p.u.	Angle(V) degree	P_{load} MW	Q_{load} MVAR	P_{gen} MW	Q_{gen} MVAR
2192	1.0340	14.05	235100.00	62413.00	240835.98	63481.63
2317	1.0590	-4.40	8783.70	-517.70	0.00	0.00
2325	1.0695	9.38	471.40	-151.14	0.00	0.00

Table B.3 Power flow data for branches(11gen.)

Bus #	Bus #	R p.u.	X p.u.	B p.u.	off-norminal tap
3	5	0.003520	0.036720	3.45154	0.0000
3	5	0.003390	0.036690	3.45813	0.0000
3	996	0.000960	0.009080	0.85556	0.0000
3	996	0.000960	0.009080	0.85556	0.0000
5	7	0.002280	0.027560	2.62024	0.0000
7	8	0.001730	0.020750	1.96472	0.0000
24	30	0.003380	0.029770	0.00000	0.0000
24	33	-0.052620	1.383430	0.00000	0.0000
24	33	0.012920	0.112030	0.18075	0.0000
24	33	0.012920	0.112050	0.18073	0.0000
24	33	0.005740	0.060520	0.00000	0.0000
30	33	0.016010	0.099370	0.15627	0.0000
30	33	0.016040	0.099390	0.15623	0.0000
33	37	0.008120	0.078180	0.13190	0.0000
33	37	0.008120	0.078180	0.13190	0.0000
33	47	0.010010	0.098760	0.15844	0.0000
33	47	0.003290	0.046510	0.00000	0.0000
37	39	0.005010	0.034670	0.05207	0.0000
37	40	0.005010	0.034660	0.05207	0.0000
37	43	0.002400	0.031800	0.05672	0.0000
37	44	0.002400	0.031800	0.05671	0.0000
37	140	0.001410	0.008720	0.01366	0.0000
37	141	0.001410	0.008720	0.01366	0.0000
39	40	0.030620	0.809460	0.00000	0.0000
39	40	-0.035640	0.543650	0.00000	0.0000
39	617	0.014490	0.113180	0.00000	0.0000
39	618	0.000240	0.870170	0.00000	0.0000
40	617	0.000240	0.870170	0.00000	0.0000
40	618	0.015110	0.115070	0.00000	0.0000
43	44	-0.023140	0.377740	0.00000	0.0000
43	47	0.001800	0.020100	0.03459	0.0000
44	47	0.001800	0.024000	0.04222	0.0000

Table B.3 (Continued)

Bus #	Bus #	R p.u.	X p.u.	B p.u.	off-norminal tap
47	48	0.003500	0.044490	0.07339	0.0000
47	48	0.003500	0.044490	0.07339	0.0000
47	48	0.002700	0.031800	0.11433	0.0000
47	48	0.003520	0.044730	0.07386	0.0000
47	48	0.003520	0.044730	0.07386	0.0000
80	996	0.000530	0.005840	0.60400	0.0000
80	996	0.000530	0.005840	0.60400	0.0000
140	141	-0.062300	0.927530	0.00000	0.0000
140	142	0.004780	0.029280	0.04586	0.0000
141	143	0.004780	0.029280	0.04586	0.0000
142	143	-0.005500	0.383150	0.00000	0.0000
142	144	0.004670	0.028850	0.04519	0.0000
143	144	0.004670	0.028850	0.04519	0.0000
144	145	0.008950	0.077910	0.12311	0.0000
144	146	0.008950	0.077910	0.12311	0.0000
144	148	0.007590	0.048320	0.07128	0.0000
144	149	0.007590	0.048320	0.07128	0.0000
145	146	-0.005010	0.208210	0.00000	0.0000
145	226	0.005640	0.050370	0.07944	0.0000
145	288	0.085750	0.568540	0.00000	0.0000
146	226	0.005640	0.050370	0.07944	0.0000
146	288	0.085500	0.567040	0.00000	0.0000
148	149	-0.002830	0.382420	0.00000	0.0000
148	150	0.001880	0.011980	0.01769	0.0000
149	150	0.001880	0.011980	0.01769	0.0000
150	288	0.066340	0.555860	0.00000	0.0000
150	297	0.028270	0.247970	0.00000	0.0000
226	288	0.009950	0.063350	0.11046	0.0000
226	617	0.007650	0.071990	0.10050	0.0000
226	618	0.007650	0.072000	0.10050	0.0000
226	977	0.009950	0.070690	0.11169	0.0000
226	992	0.000200	0.021800	0.00000	0.0000
226	992	0.000200	0.022000	0.00000	0.0000
226	992	0.000180	0.022150	0.00000	0.0000
226	1060	0.000000	0.158000	0.00000	0.0000
288	977	-0.005660	0.325930	0.00000	0.0000
617	618	-0.034810	0.934120	0.00000	0.0000

Table B.3 (Continued)

Bus #	Bus #	R p.u.	X p.u.	B p.u.	off-norminal tap
617	618	0.012240	0.597670	0.00000	0.0000
784	1106	0.000790	0.178760	0.00000	0.0000
963	967	0.001290	0.013850	1.46527	0.0000
963	993	0.000160	0.001680	0.17525	0.0000
963	994	0.000160	0.001680	0.17529	0.0000
963	996	0.000190	0.002030	0.87993	0.0000
963	996	0.000190	0.002030	0.87993	0.0000
989	1000	0.000030	0.000580	0.06315	0.0000
989	1000	0.000030	0.000580	0.06315	0.0000
993	994	-0.009390	0.109190	0.00000	0.0000
3	150	0.000300	0.018200	0.00000	0.9259
3	150	0.000300	0.020300	0.00000	0.9259
5	458	0.000640	0.034460	0.00000	1.0000
7	458	0.041050	0.393870	0.00000	1.0000
8	458	0.001280	0.026470	0.00000	1.0000
24	644	0.000100	0.005460	0.00000	1.0000
30	644	-0.001620	0.077330	0.00000	1.0000
33	644	0.028260	0.461480	0.00000	1.0000
47	54	0.001540	0.023400	0.00000	1.0000
47	80	0.021770	0.479680	0.00000	1.0000
47	297	0.004330	0.039990	0.00000	1.0000
47	458	0.032940	0.771160	0.00000	1.0000
47	644	-0.168360	2.246910	0.00000	1.0000
47	784	0.157880	1.518370	0.00000	1.0000
47	784	0.059910	0.936860	0.00000	1.0000
47	784	0.109310	1.701790	0.00000	1.0000
47	993	0.000580	0.078940	0.00000	1.0000
47	994	0.000560	0.079840	0.00000	1.0000
47	1106	0.157990	1.520600	0.00000	1.0000
47	2018	-0.017990	0.445020	0.00000	1.0000
47	2317	-1.056490	4.386920	0.00000	1.0000
48	733	0.000600	0.025700	0.00000	1.1435
48	733	0.000600	0.026500	0.00000	1.1435
48	733	0.000600	0.026500	0.00000	1.1435
48	733	0.000600	0.026500	0.00000	1.1435
967	48	0.000300	0.018100	0.00000	0.9167
967	48	0.000300	0.016300	0.00000	0.9167
54	80	-0.000780	0.076070	0.00000	1.0000

Table B.3 (Continued)

Bus #	Bus #	R p.u.	X p.u.	B p.u.	off-norminal tap
54	297	0.005750	0.157510	0.00000	1.0000
54	458	0.005910	0.739670	0.00000	1.0000
54	644	-0.014740	0.096690	0.00000	1.0000
54	784	0.002430	0.812190	0.00000	1.0000
54	784	-0.002370	0.751970	0.00000	1.0000
54	784	0.001210	0.447110	0.00000	1.0000
54	993	-0.025040	0.528020	0.00000	1.0000
54	994	-0.025450	0.534040	0.00000	1.0000
54	1106	-0.002430	0.753070	0.00000	1.0000
54	2001	-0.096710	0.419510	0.00000	1.0000
54	2018	-0.002990	0.025740	0.00000	1.0000
54	2192	-0.188400	0.877980	0.00000	1.0000
54	2317	-0.115110	0.331850	0.00000	1.0000
80	297	-0.000800	0.040080	0.00000	1.0000
80	458	-0.031240	0.478100	0.00000	1.0000
80	784	-0.004440	0.106330	0.00000	1.0000
80	784	-0.004600	0.094580	0.00000	1.0000
80	784	-0.002460	0.058540	0.00000	1.0000
80	993	-0.031210	0.659410	0.00000	1.0000
80	994	-0.031730	0.666930	0.00000	1.0000
80	1106	-0.004610	0.094720	0.00000	1.0000
80	2018	-0.056810	0.548510	0.00000	1.0000
150	458	0.014190	0.155890	0.00000	1.0000
226	975	0.000240	0.015630	0.00000	1.1801
989	226	0.000300	0.017900	0.00000	0.9259
989	226	0.000300	0.017900	0.00000	0.9259
989	226	0.000300	0.017900	0.00000	0.9259
297	458	-0.000120	0.050630	0.00000	1.0000
297	784	0.004860	0.127190	0.00000	1.0000
297	784	-0.000120	0.078270	0.00000	1.0000
297	784	-0.000180	0.142180	0.00000	1.0000
297	993	0.000830	0.055210	0.00000	1.0000
297	994	0.000820	0.055840	0.00000	1.0000
996	297	0.000300	0.019200	0.00000	0.9167
996	297	0.000300	0.018800	0.00000	0.9167
996	297	0.000300	0.019200	0.00000	0.9167
297	1106	0.004860	0.127370	0.00000	1.0000
297	2018	-0.266020	2.781220	0.00000	1.0000

Table B.3 (Continued)

Bus #	Bus #	R p.u.	X p.u.	B p.u.	off-norminal tap
458	784	-0.026010	1.432810	0.00000	1.0000
458	784	-0.072710	2.173670	0.00000	1.0000
458	784	-0.014540	0.788760	0.00000	1.0000
458	993	-0.053110	1.057950	0.00000	1.0000
458	994	-0.053970	1.070020	0.00000	1.0000
458	1106	-0.072990	2.176840	0.00000	1.0000
644	2001	-0.414030	1.712200	0.00000	1.0000
644	2018	-0.050240	0.272610	0.00000	1.0000
644	2192	-0.000560	0.005790	0.00000	1.0000
644	2317	-0.057280	0.242950	0.00000	1.0000
784	993	0.022650	2.095820	0.00000	1.0000
784	993	-0.037310	1.288360	0.00000	1.0000
993	784	-0.067110	2.340360	0.00000	1.0000
784	994	0.022410	2.119770	0.00000	1.0000
784	994	-0.038040	1.303070	0.00000	1.0000
994	784	-0.068440	2.367080	0.00000	1.0000
784	1106	-0.079710	0.777450	0.00000	1.0000
784	1106	-0.144390	1.412310	0.00000	1.0000
967	968	0.000100	0.018100	0.00000	1.1053
967	968	0.000100	0.018100	0.00000	1.1053
967	968	0.000100	0.018100	0.00000	1.1053
967	968	0.000100	0.018100	0.00000	1.1053
989	991	0.000240	0.013740	0.00000	1.1037
989	991	0.000240	0.013680	0.00000	1.1037
989	992	-0.008600	-0.165790	0.00000	0.9259
989	992	-0.008700	-0.167400	0.00000	0.9259
989	992	-0.008990	-0.171790	0.00000	0.9259
993	1106	0.022530	2.098890	0.00000	1.0000
994	1106	0.022280	2.122870	0.00000	1.0000
1001	3	0.014770	0.00000	0.	0.00
1001	3	0.014770	0.00000	0.	0.00
2018	1	0.070820	0.00000	0.	0.00
2192	2	0.650650	0.00000	0.	0.00
2317	4	0.021160	0.00000	0.	0.00
2192	2	2.050080	0.00000	0.	0.00
2317	4	0.064670	0.00000	0.	0.00
2317	4	0.005620	0.00000	0.	0.00
2325	5	0.019870	0.00000	0.	0.00

BIBLIOGRAPHY

[1] Arrowsmith, D. K. and C. M. Place, *An Introduction to Dynamical Systems.* Cambridge: Cambridge University Press, 1990.

[2] Arnold, V. I., *Geometrical Methods in the Theory of Ordinary Differential Equations.* New York: Springer-Verlag, 1983.

[3] Lin, C.M., Vittal, V., Kliemann, W. and Fouad, A.A., "Investigation of modal interaction and its effects on control performance in stressed power systems using normal forms of vector fields", *IEEE/PES Summer Meeting*, paper#95SM522-3, 1995.

[4] Saha, S., "Approximation of stability boundary of a power system using the real normal form of vector fields". Ph.D. Thesis, Iowa State University, Ames, Iowa, 1996.

[5] Saha, S., Fouad, A. A., Kliemann, W. and Vittal, V., "Stability boundary approximation of a power system using the real normal form of vector fields", *IEEE-Transactions-on-Power-Systems.*, v. 12, p. 797-802, May 1997

[6] Cook, D., Buja, A. and Cabrera, J. "Direction and motion control in the grand tour," *Proceedings of the 23rd Symposium on the Interface,* Springer-Verlag, 1991.

[7] Swayne, D. F., Cook, D. and Buja, A., *User's Manual for XGOBI: A Dynamic Graphics Program for Data Analysis Implemented in the X Window System (Release 2)*, Bell core, 1991.

[8] Fouad, A. A. and Vittal, V., "Power System Transient Stability Assessment Using the Transient Energy Function Method." *Control and Dynamic Systems, 43, Academic Press, San Diego,* 1991, 115-184.

[9] Fouad, A. A. and Vittal, V., *Power System Transient Stability Analysis Using the Transient Energy Function Method.* Englewood Cliffs, New Jersey: Prentice hall Inc., 1992.

[10] Pai, M., *Energy Function Analysis for Power System Stability.* Kluwer Academic Publishers, Boston: 1989.

[11] Kakimoto, N., Ohsawa, Y. and Hayashi, M. "Transient Stability Analysis of Electric Power Systems Via Lure Type Lyapunov Functions." *Trans. IEE of Japan, (May/June 1978)*: 98, 5/6

[12] Athay, T., Podmore, R., and Virmani, S., "A practical Method for Direct Analysis of Transient Stability," *IEEE Trans. Power Appar. Syst.*, PAS-98, 2, Mar./Apr., pp. 573–584, 1979.

[13] Chiang, H. D., Wu, F.F. and Variya, P.P.,"Foundations of the potential energy boundary surface method for power system transient stability analysis." *IEEE Transactions on Circuits and systems(June 1988)*: 712-728

[14] Chiang, H. D., Wu, F.F. and Variya, P.P.,"Foundations of the director methods for power system transient stability analysis." *IEEE Transactions on Circuits and systems(Feb. 1987)*: 160-172.

[15] Treinen, R., Vittal, V. and Kliemann, W., "An improved technique to determine the controlling UEP in a power system." *IEEE Transactions on CAS-I(April 1996)*: Vol. 43, No.4.

[16] Zaborsky, J., Huang, G., Zheng, B. and Leung, T.C., "On the phase portrait of a class of large nonlinear dynamic systems such as the power system." *IEEE Transactions on Automatic Control(Jan. 1988)*: 4-15

[17] Lyapunov, A.M., *The general Problem of the Stability of Motion.* London: Taylor and Francis Ltd., 1992.

[18] Yee, H. and Spalding, B.D., "Transient stability analysis of multi-machine power systems by method of hyper-plane." *IEEE Transactions on Power Apparatus and Systems(Jan./Feb. 1977)*: 276-284

[19] Cook, P.A. and Eskicioglu, A.M., "Transient stability analysis of electric power systems by the method of tangent hypersurfaces." *IEE Proceedings(July 1983)*: 183-193

[20] Wiggins, S., *Introduction to applied nonlinear dynamical systems and chaos*, New York: Springer-Verlag, 1990

[21] Guckenheimer, J., *Nonlinear oscillations, dynamical systems and bifurcations of vector fields*, New York: Springer-Verlag, 1983

[22] Katok, A. and Hasselblatt, B., *Introduction to the modern theory of dynamical systems*, New York, NY: Cambridge University Press, 1995

[23] Pliss, V.A., "The reduction principle in the theory of stability of motion", *Soviet Math.*, v. 5, 247-250, 1964

[24] S̃oš̃itaĩs̃vili, A.N., "Bifurcations of topological type of a vector field near a singular point", *Trudy Sem. Petrovsk.*, v. 1, 279-309. 1975

[25] Poincaré, H., "Sur les propriétés des fonctions définies par les équations aux différences partielles", *Oeuvres*, Gauthier-Villars: Paris, pp. XCIX-CX, 1929

[26] Bryuno, A. D., *Local Methods in Nonlinear Differential Equations. Part I. The Local Method of Nonlinear Analysis of Differential Equations. Part II. The sets of Analyticity of a Normalizing Transformation.* Springer-verlag: New York, Heidelberg, Berlin. 1989

[27] Sell, G.R., "The structure of a flow in the vicinity of an almost periodic motion", *Journals of Differential Equations*,v. 27, p. 359-393. 1978.

[28] Fouad, A.A., et. al.,"Analysis of Stressed Interconnected Power Networks", Electric Power Research Institute ReportTR-103704, March 1994.

[29] Starrett, S.K.,"Application of normal forms of vector fields to stressed power systems". PhD dissertation, Iowa State University, 1994.

[30] Ni, Y., Vittal, V., Kliemann, W. and Fouad, A.A., "Nonlinear modal interaction in HVDC/AC power systems with DC power modulation", *IEEE-Transactions-on-Power-Systems.* v. 11, p. 2011-17, Nov. 1996.

[31] Thapar, J., Vittal, V., Kliemann, W. and Fouad, A.A., "Application of the Normal Form of Vector Fields to predict Interarea Separation In Power Systems", *IEEE-Transactions-on-Power-Systems.* v. 12, p. 844-50, May 1997.

[32] Jang, G., Vittal, V. and Kliemann, W., "Effect of Nonlinear Modal Interaction On Control Performance: Use of Normal Forms Technique In Control Design. Part I", *IEEE-Transactions-on-Power-Systems.* v. 13 no2, p. 401-7, May 1998.

[33] Jang, G., Vittal, V. and Kliemann, W., "Effect of Nonlinear Modal Interaction On Control Performance: Use of Normal Forms Technique In Control Design. Part II", *IEEE-Transactions-on-Power-Systems.* v. 13 no2, p. 408-13, May 1998.

[34] Anderson, P. M. and Fouad, A.A., *Power System Control and Stability.* New York: IEEE Press, 1994.

[35] Ni, E. Y., Vittal, V. and Kliemann, W., "System separation mechanism in the neighbourhood of a relevant type-n UEP using the normal form of vector fields", *IEE Proc. -Gen. Trans. Distrib.* Vol. 145, No. 2, Mar. 1998.

[36] Ruelle, D., *Elements of Differentiable Dynamics and Bifurcation Theory.* Boston: Academic Press, 1988.

[37] Sauer, P.W. and Pai, M.A. *Power System Dynamics and Stability.* Prentice Hall, Upper Saddle River, New Jersey 07458, 1998

[38] Fouad, A.A., Kruempel, K.C., Mamandur, K.R.C., Stanton, S.E., Vittal, V., and Pai, M.A. "Transient Stability Margin as a Tool for Dynamic Security Assessment", EPRI Project Report, EL-1755, March 1981.

[39] Buja, A., Cook, D., Asimov, D. and Hurley, C. "Theory and Computational Methods for Dynamic Projections in High-Dimensional Data Visualization", Draft submitted to Journal of computational and Graphical Statistics, 1997.

[40] Qi, R., Cook, D., Kliemann, W. and Vittal, V., "Visualization of Stable Manifolds and Multidimensional Surfaces in the Analysis of Power System Dynamics". Draft submitted to *Journal of Nonlinear Science, 1998.*

[41] Asimov, D. "The Grand Tour: A Tool for Viewing Multidimensional Data." *SIAM Journal of Scientific and Statistical Computing(1985)*:128–143, Vol. 6, No.1.

[42] Buja, A. and Asimov, D. "Grand Tour Methods: An Outline." *Computing Science and Statistics(1985)*:63–67, Vol. 17.

[43] Hurley, C. and Buja, A., "Analyzing High-Dimensional Data with Motion Graphics." *SIAM Journal on Scientific and Statistical Computing (1990)*:1193–1211, Vol. 11, No.6.

[44] Qi, R. and Vittal, V., "Computation and Visualization of the Stability boundary for the Stressed Power System". EPRC Report: 221-231, 1998.

[45] Cook, D. and Buja, A., Manual Controls For High-Dimensional Data Projections. *Journal of Computational and Graphical Statistics(1997)*:464–480, Vol. 4, No. 6.

[46] Chen, C. T. *Linear System Theory and Design.* Holt, Rinehart and Winston, New York, 1970.

[47] Kundur, P., Wong, D. Y., Rogers, G. J., Arabi, S., and Wang, L., "Extended transient-midterm stability program(ETMSP): Version 3.1.", EPRI TR-102004-V2R1 projects 1208,-11,1212,1213, Palo Alto, California, May 1994.

[48] Perez-Arriaga, I. J.,Verghese, G. C., and Schweppe, F. C., "Selective Modal Analysis with Applications to Electric Power Systems. Part 1: Heuristic Introduction." *IEEE Transactions on PAS* v.101, Sept.1982: 3117-3125

[49] Thapar, J., "Application of normal form of vector fields to predict interarea split following large disturbances in power systems," M.S. Thesis, Iowa State University, Ames, Iowa, 1996.

[50] Jang, G., "Nonlinear control design for stressed power systems using normal forms of vector fields," Ph.D. Thesis, Iowa State University, Ames, Iowa, 1997.

IMAGE EVALUATION TEST TARGET (QA-3)

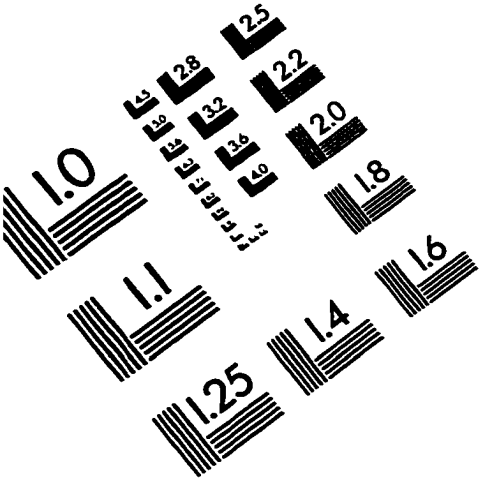

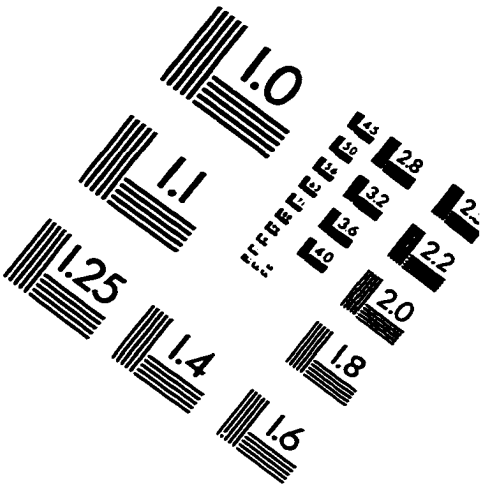

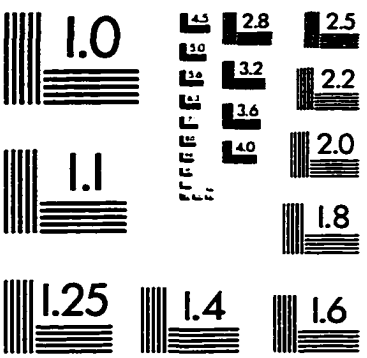

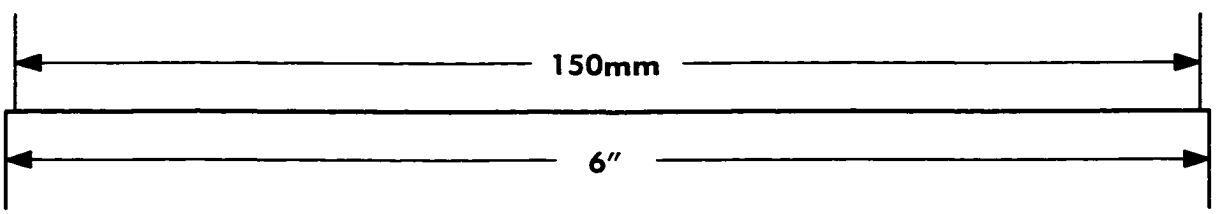

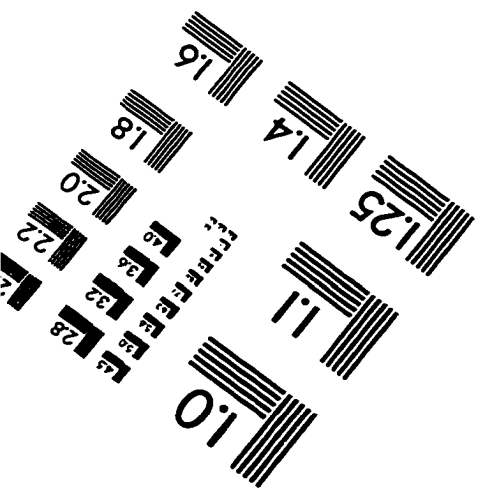

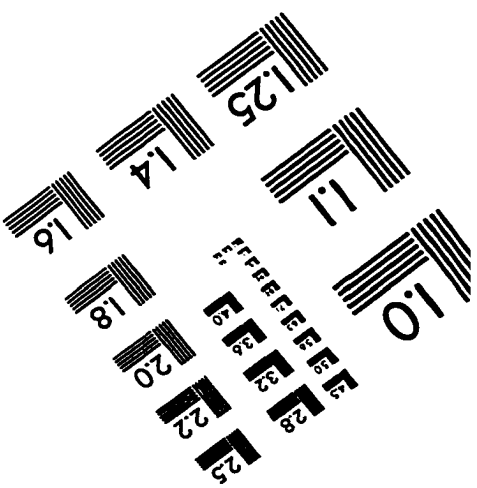

APPLIED IMAGE, Inc
1653 East Main Street
Rochester, NY 14609 USA
Phone: 716/482-0300
Fax: 716/288-5989